NAVAL POSTGRADUATE SCHOOL
MONTEREY, CALIFORNIA

THESIS

A COMPARISON OF MODEL PERFORMANCE BETWEEN THE NESTED GRID AND ETA MODELS

by

Jay W. Colucci

December, 1994

Thesis Advisor: Patricia M. Pauley

Approved for public release; distribution is unlimited.

REPORT DOCUMENTATION PAGE

Form Approved OMB No. 0704-0188

1. AGENCY USE ONLY *(Leave blank)*	2. REPORT DATE	3. REPORT TYPE AND DATES COVERED
	December 1994.	Master's Thesis

4. TITLE AND SUBTITLE A COMPARISON OF MODEL PERFORMANCE BETWEEN THE NESTED GRID AND ETA MODELS	5. FUNDING NUMBERS
6. AUTHOR(S) Jay W. Colucci, LT, USN	
7 PERFORMING ORGANIZATION NAME(S) AND ADDRESS(ES) Naval Postgraduate School Monterey CA 93943-5000	8. PERFORMING ORGANIZATION REPORT NUMBER
9. SPONSORING/MONITORING AGENCY NAME(S) AND ADDRESS(ES)	10. SPONSORING/MONITORING AGENCY REPORT NUMBER

11. SUPPLEMENTARY NOTES The views expressed in this thesis are those of the author and do not reflect the official policy or position of the Department of Defense or the U.S. Government.

12a. DISTRIBUTION/AVAILABILITY STATEMENT	12b. DISTRIBUTION CODE
Approved for public release; distribution is unlimited.	

13. ABSTRACT *(maximum 200 words)*

Assessment of the performance of the National Meteorological Center's (NMC) new Eta numerical weather prediction model requires objective evaluation through direct comparison of model forecast output to its own analysis and to the analysis of other numerical models. The ultimate goal of the Eta Model is to provide accurate mesoscale weather forecasts through the late 1990's which are superior to those currently provided by the older NGM. To accurately evaluate the Eta Model, several model forecast output fields were compared to the NGM for a common population of extratropical cyclones over a period of five months. The separate model forecasts were also evaluated against their own analysis. Selected fields included central sea level pressure, 12h central pressure change, 1000 - 500 mb thickness at the cyclone center, and both convective and total precipitation at the cyclone center. Results indicated a consistent negative bias in forecast central pressure values for the NGM, and a positive bias for the Eta Model. Mean forecast position errors were nearly identical for both models through 36h with the Eta forecast position errors only slightly larger at 48h. Both models exhibited a slight cold bias in 1000 - 500 mb thickness fields at the cyclone centers with the NGM being greater. The Eta Model tended to forecast more precipitation in general and in particular the precipitation was higher for stable precipitation.

14. SUBJECT TERMS Eta Model, Numerical Weather Prediction, Nested Grid Model	15. NUMBER OF PAGES * 130
	16. PRICE CODE

17. SECURITY CLASSIFICATION OF REPORT	18. SECURITY CLASSIFICATION OF THIS PAGE	19. SECURITY CLASSIFICATION OF ABSTRACT	20. LIMITATION OF ABSTRACT
Unclassified	Unclassified	Unclassified	UL

NSN 7540-01-280-5500

Standard Form 298 (Rev. 2-89)

Prescribed by ANSI Std. 239-18 298-102

Approved for public release; distribution is unlimited.

A COMPARISON OF MODEL PERFORMANCE BETWEEN THE NESTED GRID AND ETA MODELS

by

Jay W. Colucci
Lieutenant, United States Navy
B.S., The State University of New York, Maritime College, 1985

Submitted in partial fulfillment
of the requirements for the degree of

MASTER OF SCIENCE IN METEOROLOGY AND PHYSICAL OCEANOGRAPHY

from the

NAVAL POSTGRADUATE SCHOOL
December 1994

Author: Jay W. Colucci
Jay W. Colucci

Approved by: Patricia M. Pauley
Patricia M. Pauley, Thesis Advisor

Wendell A. Nuss
Wendell A. Nuss, Second Reader

Robert L. Haney
Robert L. Haney, Chairman
Department of Meteorology

ABSTRACT

Assessment of the performance of the National Meteorological Center's (NMC) new Eta numerical weather prediction model requires objective evaluation through direct comparison of model forecast output to its own analysis and to the analysis of other numerical models. The ultimate goal of the Eta Model is to provide accurate mesoscale weather forecasts through the late 1990's which are superior to those currently provided by the older NGM. To accurately evaluate the Eta Model, several model forecast output fields were compared to the NGM for a common population of extratropical cyclones over a period of five months. The separate model forecasts were also evaluated against their own analysis. Selected fields included central sea level pressure, 12h central pressure change, 1000 - 500 mb thickness at the cyclone center, and both convective and total precipitation at the cyclone center. Results indicated a consistent negative bias in forecast central pressure values for the NGM, and a positive bias for the Eta Model. Mean forecast position errors were nearly identical for both models through 36h with the Eta forecast position errors only slightly larger at 48h. Both models exhibited a slight cold bias in 1000 - 500 mb thickness fields at the cyclone centers with the NGM being greater. The Eta Model tended to forecast more precipitation in general with and in particular the precipitation was higher for stable precipitation.

TABLE OF CONTENTS

ACKNOWLEDGEMENTS

First, I want to thank my family and friends for all of their support during my tour at NPS, especially my parents, Joseph and Dorothy Colucci. Second, I want to thank my thesis advisor, Dr Patricia M. Pauley for her patience and thorough guidance throughout the thick and thin of putting this thesis together. Third, I want to thank my Second Reader, Dr Wendell A. Nuss for his support and assistance with the graphics portions of my research. I also want to thank Jim Cowie, Russ Schwanz, and the rest of the idea lab staff for their support and navigation through some of the more abstract realms of the computer world. Lastly, I want to extend special thanks and appreciation to my shipmate and friend, Lcdr Christopoher Butler for his support and assistance with many of the more challenging topics in our curriculum.

I. INTRODUCTION

Assessment of the performance of the National Meteorological Center's (NMC) new Eta numerical weather prediction model requires objective evaluation through direct comparison of model forecast output to its own analysis and to the analysis and forecasts of other numerical models. The ultimate goal of the Eta model is to provide accurate mesoscale weather forecasts through the late 1990's that are demonstrably better than the forecasts provided by the older Nested Grid Model, especially for quantitative precipitation. The Eta model differs significantly from current operational models in terms of its structure, numerics, and some physical parameterizations. The most significant difference is that the Eta vertical coordinate system is normalized with respect to mean sea-level pressure while the sigma coordinate, which is employed by the NGM and most other models, is normalized with respect to surface pressure (Black 1994).

In order to best identify and quantify any particular systematic biases inherent in the Eta Model, several model forecast output fields must be compared to those of another well established forecast model for a common population of synoptic-scale weather systems, and over a sufficiently large time span. The Nested Grid Model was selected for this comparison because it is the primary forecast model for the continental United States. The NGM and Eta models are also both available on a common output grid, the 190.5 km resolution LFM grid. Finally, the NGM is also the model that the Eta Model will eventually replace.

With this in mind, the primary objective of this thesis is to undertake a direct comparison of the NGM and the Eta models using several selected parameters related to extratropical cyclones. These include central sea-level pressure and 12-h central pressure change, 1000 - 500 mb thickness at the cyclone center, and both convective and total precipitation averaged over the immediate vicinity of the cyclone. In order to meet this objective, Chapter II will first provide background information on previous model verification studies and other research. Chapter III will then

present thorough descriptions of the two forecast models used, NMC's Nested Grid and Eta Models. Detailed information on the methodology employed in the processing of data, the generation of graphics, and the computation of the statistics are addressed as well. The results, discussed in Chapter IV, identify systematic model forecast errors, biases, and trends in the models separately and also compare the performance of the two models. Finally, Chapter V contains conclusions, summarizes results, and provides recommendations for future research.

II. BACKGROUND

For about the last twenty years, numerous model verification studies and statistical comparisons have been conducted on synoptic-scale cyclones and their prediction. The studies referred to in this chapter may be sub-divided into three general categories. The first includes general case studies, such as those by Whittaker and Horn (1991) and by Roebber (1984). The second type are, like this paper, studies of specific model performance. Studies such as those by Smith and Mullen (1993), Oravec and Grumm (1991), and Harr and Elsberry (1992) also fall into this category. The third type are model sensitivity studies, such as that by Kuo and Low-Nam (1990).

In one general study case, Whittaker and Horn (1991), examined a very lengthy data set extending from 1958-1977 in which NMC cyclone track charts were generated from successive NMC surface analyses. Geographical, seasonal, and longer term statistics on cyclone formation frequency and position over North America and adjacent ocean areas were generated. Results identified cold season areas of most frequent cyclogenesis as the Colorado and Great Basin area, the U.S. East and Gulf Coasts, and Alberta and the Northwest Territories. A notable decrease in summer-time activity is noted in the Colorado area with other, less dramatic changes identified by month, season, and geographical location. Results also indicated that over this long-term data set, a decreasing trend in overall cyclone formation frequency over the North American continent was identified.

Another general study by Roebber (1984), focused on the climatology of explosive cyclogenesis. A statistical analysis of 12 and 24 hour deepening rates for all surface lows analyzed on at least two successive NMC 12 hourly hemispheric charts was performed for one year of data. Results of the statistical analysis indicated that the preferred regions for explosive cyclogenesis are baroclinic zones with the climatological and statistical evidence indicating that the explosive mechanism is a combination of

baroclinic processes and of additional physical mechanisms distinct from ordinary baroclinic instability. The climatology of explosive cyclones, Sanders and Gyakum (1980), was also updated and a new climatology of formation positions, maximum deepening positions, and dissipations for all cyclones in this one-year sample was compiled.

In a very recent paper on model performance, Smith and Mullen (1993) examined sea level cyclone forecasts produced by NMC'S Nested Grid Model (NGM) and the Aviation run (AVN) of the Global Spectral Model over two separate cold seasons with all 24h and 48h forecast lows over North America and adjacent coastal regions included. Forecast errors in position, pressure, and thickness near the cyclone center are computed for each model and arranged according to geographical region. Results indicated that the NGM tended to forecast central cyclone pressure too low but with less variability while the AVN Model tended to forecast central pressures too high. Mean absolute and mean vector displacement errors were smaller for the AVN with the NGM exhibiting a bias toward moving cyclones too slow and placing them too far into the cold air. Both models also exhibited a weak cold bias in the 1000-500-mb thickness field. In addition, results indicated that ensemble averaging of the two model forecasts using an equally weighted average often verified better when forecast differences between the two separate models increased significantly.

In another model performance study, Oravec and Grumm (1993) evaluated a single model, the NGM, and focused on a selected topic, the prediction of rapidly deepening cyclones. Data from three full years (Winter 1989 to Autumn 1991), subdivided into seasons, were examined. Results indicated that one primary axis of rapid deepening cyclones was located over the Western Atlantic from the mid-Atlantic coast northeastward to the Southern part of Greenland with a secondary axis defined over the Gulf of Alaska. Results from this study also highlight the fact that the NGM was slow in deepening rapidly deepening cyclones at all forecast periods and also, as has been previously noted, exhibited a cold bias in the

1000-500 mb thickness fields. The NGM exhibited a slow bias over the western Atlantic but very rarely mis-forecast the sign of the 12-hour pressure change and also exhibited forecast position errors that were approximately 10% smaller than those for all cyclones in the NGM at all forecast periods. Two specific cases of rapidly deepening east coast cyclogenesis were also examined. In one case, the ERICA IOP 4 cyclone, the NGM performed very well, only exhibiting a slow bias in forecast eastward movement. In the second case, a 4 Jan 1992 cyclone off the Carolina coast, the NGM performed much poorer, exhibiting significant problems in resolving the small-scale processes as the system rapidly intensified over the Gulf Stream.

Harr and Elsberry (1992), elected to survey longer range model predictions, examining 72-h forecasts of sea level cyclones in the climatological areas of maximum cyclone formation over the western and central North Pacific Ocean. Only one model, the U.S. Navy's Operational Global Atmospheric Prediction System (NOGAPS) was employed in this study. It had been observed that specific patterns of systematic central-pressure and position errors were present in forecasts generated by NOGAPS in the North Pacific basin. Results indicate that maximum under-forecasting and maximum position errors occur over the central North Pacific climatological region of maximum cyclone deepening, and that maximum over-forecasting errors occur over the region of maximum cyclone dissipation. These systematic model forecast error distributions indicate that there are diagnostic relationships between model performance and cyclone track type and pressure change at forecast verification time. Results also indicate that when cyclones are separated according to the pressure tendencies of deepening, filling or mixed pressure tendency, different forecast pressure errors tend to occur depending on cyclone track type.

Specifically, when the category of intensity change was correctly forecast, cyclones forecast to follow a western Pacific track tendto be over-forecast while those forecast to follow a central Pacific track tend to be under-forecast.

It was also noted that position errors are more sensitive to forecast track type rather than forecast central pressure profile.

In a model sensitivity study, Kuo and Low-Nam (1990) conducted a series of numerical experiments using the Pennsylvania State University/National Center for Atmospheric Research mesoscale model on nine specific cases of explosive cyclogenesis. The purpose of their research was to identify and to rank by order of importance, those key factors which are important to the short-range prediction of explosive cyclones. Results indicated, as had been expected, that the structure of simulated cyclones was sensitive to precipitation parameterization, with the grid-scale-resolvable precipitation associated with mesoscale ascent in the vicinity of the warm front being a crucial element for rapid development. The upright convective precipitation played a far lesser role, and surface energy fluxes had little effect on development during the 24 hour period of rapid development. In summary, the most crucial model components for accurate short range prediction of rapidly deepening cyclogenesis averaged over the nine study cases were found to be initial conditions, followed by horizontal grid resolution, then precipitation parameterization and finally lateral boundary conditions. The parameterization of surface energy fluxes and vertical resolution were found to have a far lesser impact.

This thesis will serve as a comparison of the forecast accuracy of the Nested Grid and Eta models. All statistics have been compiled and evaluated in a storm relative sense, whereby individual cyclones have been identified for the Nested Grid Model and the Eta model separately, and followed throughout their entire life cycle. Cyclones tracked separately by either model were employed in the generation of statistics whereby model forecast output was verified against that particular model's own analysis and cyclones commonly forecast by both models were also compared in order to examine forecast accuracy of the two models against each other for all times from 00h through 48h. Grid point data was employed in this thesis instead of charts which allowed the authors to view and evaluate more parameters such as convective and stable

precipitation separately when compared to 12-hour sea-level pressure change. Additionally, because gridded data were employed, the identification of the cyclone's lowest central pressure, central thickness, 12-hour central pressure change, forecast central pressure error, and mean precipitation values for a finite number of grid point locations surrounding each cyclone was automated. This process also helped eliminate possible human error in the measurement or interpolation of the values of the parameters listed above.

III. METHODOLOGY AND DATA

The statistics presented in this thesis were generated from forecast model output and analyses from the National Meteorological Center's (NMC) Nested Grid and Eta models. This chapter describes the methodology employed in the verification of model output for both models. A brief physical description and some background information for both models is presented. Some additional information on the data sets employed and specific data availability is also provided.

A. MODEL DESCRIPTIONS

1. Nested Grid Model

The Nested Grid Model (NGM) is the forecast component of NMC'S Regional Analysis and Forecast System (RAFS). First developed as a research model at NMC in 1978, the NGM became operational in a three-grid version in 1985 (Hoke et al. 1989). Several model changes and upgrades, including the implementation of the Regional Data Assimilation System (RDAS) and improving the horizontal resolution in a two-grid version, (Fig. 3.1), were undertaken between 1986 and 1991, when the model was finally frozen (Petersen et al. 1991).

The NGM gains its name from the nested structure of the model's grids. This nesting allows the NGM to be a stand-alone model because the boundaries of the NGM'S outer grid extend to the equator, and thus a separate larger-scale model is not required to provide boundary conditions.

The first of the three major components of the RAFS is the Regional Optimum Interpolation analysis (ROI). According to Petersen et al. (1991), the ROI, is performed over the entire Northern Hemisphere on a thinned latitude-longitude grid with a resolution of 1° longitude by 0.75° latitude at midlatitudes. Observations used in the ROI include conventional surface, marine,

and rawinsonde data, ACARS aircraft winds, profiler winds, satellite cloud drift winds, and satellite soundings (Hoke et al. 1989, Petersen et al. 1991). Error checks are performed by comparing observations against the first-guess field and against each other. A field of observed corrections is then generated by subtracting the first-guess field from the observations at observation sites. Next, in the actual analysis portion of the ROI, corrections for each grid point are generated, statistically weighted based on the properties of the observational and first-guess fields using the optimum interpolation technique, and added to the first-guess field to yield the analyzed field. The ROI analyzes height, pressure, specific humidity, and wind components on the sigma surfaces used by the forecast model. The analysis of height and wind components is mulitvariate, while the analysis of specific humidity is univariate.

In its currently operational form, the ROI is incorporated in the Regional Data Assimilation System (RDAS), which was developed to improve the resolution of the first-guess field and also to allow the incorporation of newer, high-frequency data sets available over the U.S. into the RAFS.

According to Petersen et al. (1991) and DiMego et al. (1992), the RDAS begins with a ROI analysis and initialization using data from 12 hours before the forecast initialization time (T-12). In its current operational version, RDAS obtains its first-guess field and one-way boundary conditions for the inner-grid forecasts from the Global Data Assimilation System (GDAS). This coupling between the GDAS and RDAS is designed to take advantage of the GDAS'S current and future improvements in defining the global-scale circulation. Essentially, a series of 3h forecasts produced by the NGM on its inner grid are sequentially corrected and updated by a series of high-resolution ROI analyses. This process, repeated for a 12h time period prior to model initialization, allows the inclusion of newer asynoptic data types into the analysis, allows gradients in the analysis to become more fully developed, and

improves the uniformity of precipitation rates in the early period of the model forecast itself.

The second component of RAFS is the initialization. According to Bonner et al. (1989), the purpose of initialization is to remove meteorologically insignificant gravity waves which produce "noise" in the forecast output. The currently operational procedure, derived from a method developed by Temperton (1988), performs the initialization only upon the corrections derived from observations rather than the full analysis field as was previously done. It is designed to retain a major share of the divergence associated with mountains and ageostrophic flow and permits better modeling of precipitation during the very early portions of the forecast period. The Temperton (1988) initialization is a vertical-mode, grid-point scheme, but is functionally equivalent to the previously used normal-mode spectral scheme. Following the results of Carr et al. (1989), only the lowest two modes are initialized.

The third major component of the RAFS is the NGM itself. Like the previous two components, it employs the terrain following sigma coordinate of Phillips (1957) in the vertical. As illustrated in Fig. 3.2, vertical resolution in the RAFS changes relatively smoothly with height with the finest resolution at lower levels designed to accurately capture and model boundary layer processes (Hoke et al. 1989). The NGM is currently run in a two-grid configuration (Fig. 3.1), with the outermost grid being hemispheric and the inner grid having twice the resolution of the outer grid (DiMego et al. 1992) These grids use a polar stereographic projection with a mesh length of 84 km at 45°N on the inner "C-grid". Symmetry is imposed as the equatorial boundary condition for the outer "B-grid", but two-way interactive boundary conditions are used between the B and C grids.

The Arakawa-D system of staggering forecast variables is employed in the NGM, whereby the u and v wind components are offset one-half grid interval from the mass forecast points in both the y and x directions. Fourth-order finite differencing is used in the horizontal, with second-order used in the vertical (Hoke 1992). A

Lax-Wendroff time differencing scheme provides superior performance in terms of computational modes. According to Hoke (1992), in a comparison between the fourth and second order methods, forecast fields for several layers and variables were quite similar. Average daily anomaly correlation coefficients showed slight, consistent improvement in all layers with the fourth order method. Averaged mean and rms errors for height and wind at several layers also showed slight improvement when the fourth order method was employed.

The NGM is a primitive equation model, meaning that the model equations are maintained in or near to their original form, as opposed to forms modified by geostrophic assumptions. Explicit variables forecast are those of wind velocity, potential temperature, and specific humidity, all weighted by surface pressure at the middle of the model layers. Heights and vertical motion are diagnosed at layer interfaces.

The effects of the physical processes of precipitation, radiation, and heat, momentum and moisture exchanges between the atmosphere and the oceans are also modeled, as well as boundary layer mixing, and dry convection and turbulent energy transport in the vertical. According to Hoke et al. (1989), moist convection is parameterized using a modified Kuo (1965) scheme and so occurs at a model grid point when there is significant convergence of moisture in the lowest six layers of the model, when a parcel originating in any one of the four lowest layers would become buoyant if lifted, and also if total moisture convergence into the column below the cloud top is positive. Moisture available from this convergence below cloud top, including evaporation from the land and sea surface is subsequently redistributed in the vertical in the form of latent heating and moistening. Grid-scale precipitation occurs when the relative humidity at a grid point exceeds 95%. The precipitation is allowed to fall and re-evaporate in lower layers in which the relative humidity is less than 95%. This process is continued downward through each subsequent model layer with any net precipitation accumulating at the surface.

According to Hoke et al. (1989) the effects of longwave radiation on the modeled atmosphere and land surface are computed as a function of ground temperature, atmospheric temperature, specific humidity, and cloud amount. Formulations of cloud amount for both longwave and shortwave radiation computations are computed solely from relative humidity, patterned after a method developed by Slingo (1984). Cloud amount is zero for relative humidity below 80% and increases to 100% as humidity approaches 100%. Longwave radiation usually produces cooling with average values for a tropical clear sky on the order of 1° to 3°C per day. Shortwave radiative heating of the atmosphere and earth's surface is computed as a function of the specific humidity of the modeled atmosphere, cloud cover, surface albedo, and solar zenith angle. Typical values are on the order of 1° to 2°C per day for a tropical clear sky. In the NGM in general, as cloud amounts increase, both the longwave cooling and the shortwave warming of the air increase. At the earth's surface, as cloud amount increases, incident solar radiation decreases and thus net longwave radiative flux at the earth's surface decreases.

Heat, moisture, and momentum are exchanged between atmospheric and the land and water surfaces of the earth in the NGM. The sensible heat flux is proportional to the surface exchange "drag" coefficient, wind speed in the lowest layer of the model, and the difference between the ground and air temperatures. Latent heat flux is proportional to the drag coefficient, moisture availability, bottom layer wind speed, and the difference between the saturation specific humidity of the ground and the specific humidity of the bottom layer. Finally, surface drag for each horizontal wind component is proportional to the drag coefficient, the magnitude of the wind, and the wind speed in the lowest layer. Drag coefficient values increase with increasing bottom layer wind speed, surface roughness, and decreasing boundary layer stability.

A surface energy budget, which includes the processes of shortwave radiation, longwave radiation, sensible and latent heating, and exchange of heat with the subsoil, is used to forecast

the surface temperature over land. This surface temperature is needed to compute the sensible and latent heat fluxes at ground level and also the longwave radiative flux. Over a water surface a surface energy budget is unnecessary as sea surface temperature is assumed to be constant during a forecast cycle. The NMC sea surface temperature analysis, which is updated daily, serves as the skin temperature for longwave radiation, sensible heat fluxes, and latent heat flux for the NGM. Snow and ice cover fields, which affect the surface albedo in the radiation calculations and the sensible and latent heat fluxes at the surface, are reanalyzed weekly by NESDIS (Hoke et al. 1989).

The boundary-layer mixing process, described by Phillips (1986), develops a mixed layer near the earth's surface in the model in response to buoyancy produced by heating and moistening from the surface and in response to mechanical stirring by the wind. A mixed layer that is adiabatic with uniform specific humidity is generated by these effects. Surface mixing in the NGM is supplemented by vertical turbulent mixing of momentum throughout the entire model atmosphere. A third type of mixing in the NGM is a dry convective adjustment. In the case where a superadiabatic layer develops, the temperature profile is adjusted to be adiabatic in a way that conserves the enthalpy of the column (Hoke et al. 1989).

Recent modifications (7 November 1990) to the NGM include a modification of the moisture extrapolation procedure at upper levels and inclusion of a zonal mean ozone climatology, both of which serve to lessen a systematic cold bias in the upper layers of the NGM. Modifications in orography were also undertaken in order to lessen the tendency for leeside cyclogenesis and to more accurately predict orographic precipitation. A revised interpolation procedure was adopted to correct a local problem of erroneously large surface wetness over coastal land points. This problem was caused when large oceanic wetness values were allowed to affect adjacent coastal land points. Stability dependent surface fluxes over water, designed to reduce fluxes into warm air

masses over cold currents and to increase evaporation into cold air masses over the Great Lakes and Gulf Stream as well as improve the forecast intensity of oceanic cyclones, were added also. RAFS subsoil temperature specifications were also added in order to lessen the erroneously large variability from cycle to cycle at a fixed location which resulted in a net cold bias in low-level air temperature. By setting subsoil temperature to a 15-day running average of the RAFS analyzed air temperature at the models lowest sigma layer the lagged dependence of subsoil temperature was simulated. The cycle to cycle variability in subsoil temperature was thus eliminated and mean and random temperature forecast errors in the models lowest forecast layer were improved (Petersen et al. 1991).

2. Eta Model

The newer of the two forecast models evaluated in this thesis is the Eta model. According to Black et al. (1993), the model was given the name of the coordinate it employs in the vertical, namely the Greek letter eta. Eta is a generalization of the commonly used sigma coordinate and yields essentially horizontal coordinate surfaces. According to Black et al. (1993), the most significant difference in the two models is that the Eta coordinate system is normalized with respect to mean sea level pressure while the sigma coordinate is normalized with respect to surface pressure. The eta coordinate was first defined in 1984 by Mesinger in order to greatly reduce the magnitude of errors inherent in the computation of the pressure gradient force, advection, and horizontal diffusion along the relatively steeply inclined sigma coordinate surfaces. The current version of the Eta model, with a mesh length of 80 km and with 38 vertical levels, replaced the Limited-Area Fine Mesh Model (LFM) as NMC'S "early run" in July of 1993 (Black 1994).

The current version of the Eta model receives its first-guess field from a GDAS 6h forecast. This first guess is then interpolated onto the Eta levels and an optimal interpolation is

done on the Eta surfaces in a manner similar to the NGM'S ROI. No initialization is performed. According to Black et al. (1993), the Eta model employs second-order finite differencing and is semi-staggered in the horizontal, with wind components predicted on alternate points to those of the mass variables. The mesh length between mass points of the Eta model is 80 km. The grid's central point is located at 52°N and 111°W, and is in effect a re-positioning of the equator and prime meridian which serves to minimize the distortion of features across the grid (Fig 3.3). Numerically, this repositioning also minimizes the difference in delta-x and delta-y across the grid.

Vertically, the Eta model's 38 levels have maximum resolution at the lowest levels of the atmosphere with a secondary maximum in resolution at 250 mb designed to improve modeling of the jet stream. Figure 3.4 illustrates the vertical structure of the Eta model.

According to Black et al. (1993), Eta model equations employ the split-explicit approach to integration. Physically this means that processes such as advection and convection are computed in sequence, whereby each primary prognostic variable is updated to reflect the influence of a particular process. The fundamental time step of the Eta model is 200 seconds, which is associated with geostrophic adjustment. The advective time step is twice that of adjustment, while that of processes such as convection and turbulence is four times that of geostrophic adjustment. Like the NGM, the Eta model is a primitive equation model. Explicit forecast variables are wind velocity, potential temperature, and specific humidity.

According to Black (1994) both grid-scale and convective precipitation are predicted in the Eta Model. Grid-scale precipitation is formed after every two adjustment time steps if the relative humidity in a grid box exceeds 95%; it is subsequently evaporated if it falls through layers where the relative humidity is less then 95%. Convective precipitation, which is based on the Betts-Miller cumulus parameterization scheme (Betts 1986; Betts and

Miller 1986) with some modifications described by Janjic (1986), is calculated every four time steps. The calculation of vertical turbulent exchange is carried out every fourth adjustment time step and is exchanged between model layers in the free atmosphere based on the Mellor-Yamada Level 2.5 Model (Black 1994). Turbulent kinetic energy (TKE) in this scheme, is a fully prognostic variable that is carried on layer interfaces in the Eta Model. When updated, TKE is used to compute exchange coefficients for the transfer of heat, moisture, and momentum between adjacent model layers. Exchange between the earth's surface and the lowest model layer uses the Mellor-Yamada Level 2 Model in which TKE is held constant.

Surface fluxes are also calculated using the Monin-Obukov fluctuations generated from the Mellor-Yamada Level 2 Model. A viscous sublayer is located over water surfaces in order to model the differences in temperature, moisture, and momentum at the surface and what the bulk atmosphere itself feels. Only one prognostic ground layer currently exists but more layers are to be included in the future. Temperature and moisture at the ground surface are updated every four time steps with these quantities being held constant over water. Surface soil temperatures are computed using a force-restore relation (Black 1994).

The radiation package employed by the Eta model is nearly identical to that of the MRF. Both the shortwave and the longwave radiation schemes are executed every two forecast hours with the shortwave calculation soon to be changed to hourly to better resolve the position of the sun. Ozone and carbon dioxide distributions are taken from climatology. Surface albedo is also taken from climatology but is allowed to evolve during the forecast. Stratiform and cumuliform interactive clouds are diagnosed based upon model relative humidity and convective rainfall rates. Atmospheric temperature tendencies arising from the radiative effects are applied after each adjustment time step (Black 1994).

B. DATA

All data from the NGM and Eta models employed in this research were obtained from the National Meteorological Center (NMC) in GRIB format in near real time via ftp over the Internet. Data availability averaged 83.8% over a five month period beginning 11 January 1994 and ending 11 May 1994.

Only selected fields were unpacked from the GRIB files, specifically sea level pressure, surface pressure, 700mb vertical motion, 500 mb and 300 mb winds, 1000 mb and 500 mb heights, parameterized and total accumulated precipitation, the "Best-four" lifted index, .9823 sigma-level temperature and specific humidity, and 1000 mb to 300 mb mean relative humidity. From these basic fields, 1000-500mb thickness, stable precipitation, and .9823 sigma-level equivalent potential temperature were also computed. All gridded data for both models had been stored in 45 point (Y-direction) by 53 point (X-direction) arrays on the Limited Area Fine Mesh (LFM) forecast grid (Fig. 3.5), a polar-stereographic projection with a mesh length of 190.5 km. Initialized fields (00h) as well as 6, 12, 18, 24, 30, 36, 42, and 48h forecasts were obtained and unpacked.

C. METHODOLOGY

In this study of extratropical cyclones, the sea level pressure field was employed in the model comparison to the largest extent. All high and low pressure centers and cols (saddle points) were identified through the use of a derivative test applied for each grid point against surrounding adjacent grid points in the field. Specifically, low centers were identified in the case where directional derivatives calculated from a given point to the eight surrounding points were all positive, and high centers were identified where all directional derivatives were negative. Cols were identified as points where the directional derivatives

alternated between positive and negative values four times. A comparison of the absolute values of the sums of the directional derivatives for each col was made when another col was identified at any one of the eight adjacent grid points. The col with the lowest absolute sum was retained, because this point in the sea level pressure field had the weakest mean gradient and so was most representative of the center of the col. The pressure values at highs, lows, and cols were also retained.

Subsequently each low pressure center identified was paired with the nearest col in the sea level pressure field. By comparing pressures and locations for a low center and its nearest col, a pressure deficit and radius were calculated for each low center. All lows and their nearest cols were plotted and numbered on the sea level pressure analysis for each analysis and forecast time. Latitude and longitude values and grid coordinates were also calculated and retained for every low and col identified.

A second program, with a small degree of manual interaction, was employed to pair forecast with analyzed lows for 12, 24, 36, and 48h forecasts through the calculation of distances and thickness differences. Initially, each observed low was compared sequentially to every forecast low and distances as well as thickness differences were calculated. If the closest forecast low also had the lowest thickness difference, then a match was declared. If, during this comparison, for any subsequently observed low, a better distance/thickness combination was found with the same forecast low, then this observed low was declared as a match instead of the earlier observed low in the analysis sequence. Also, a match was declared if the nearest forecast cyclone to the observed cyclone did not have the smallest thickness difference but was within a thickness difference limit threshold of 150 m and a distance limit of 990 km. Again, if this matched low was previously matched to an observed low, a logic step was employed to determine which combination of distance and thickness error was best, with that combination being retained as the optimum combination of analyzed vs forecast lows. For all observed lows as

well as forecast lows which were not matched by the computer program, a manual intervention was allowed where visual comparisons could be made in the case where program thresholds, designed to prevent erroneous matches, may not have allowed actual correct matches. Program output indicated which observed and forecast lows were matched as well as which lows were forecast but not observed and which ones were observed but not forecast. Visual comparison was made of each forecast-analysis match in order to assure accuracy and to later manually correct any miss-matches. New cyclones were also identified through later manual comparison. Systems located to the south of 25°N were not considered in the comparison because this study is focused on extra-tropical systems. All cyclones considered in the analysis were required to have been analyzed for at least 24 hours, and be identified by at least one closed isobar for at least two analyses 12 hours apart. Heat lows were also not considered. In order to track individual cyclones through their life cycle, a manual inspection was conducted for each cyclone meeting the above thresholds from the first time a cyclone was analyzed, until it was no longer identifiable on the chart. A cyclone number was assigned for each cyclone up to a total of 227. Computer assigned cyclone numbers for each cyclone were recorded for each analysis time as well as computer matched forecast vs analyzed low numbers for the 12, 24, 36, and 48h forecasts for each analysis time.

Resultant forecast errors in position and central pressure were retained for each low for each of the 12, 24, 36, and 48h forecasts available for each model. Subsequent forecast error statistics on cyclone development, movement, central pressure and position for all cyclones analyzed for both models were generated and analyzed. Systematic biases were identified and are presented in the conclusions.

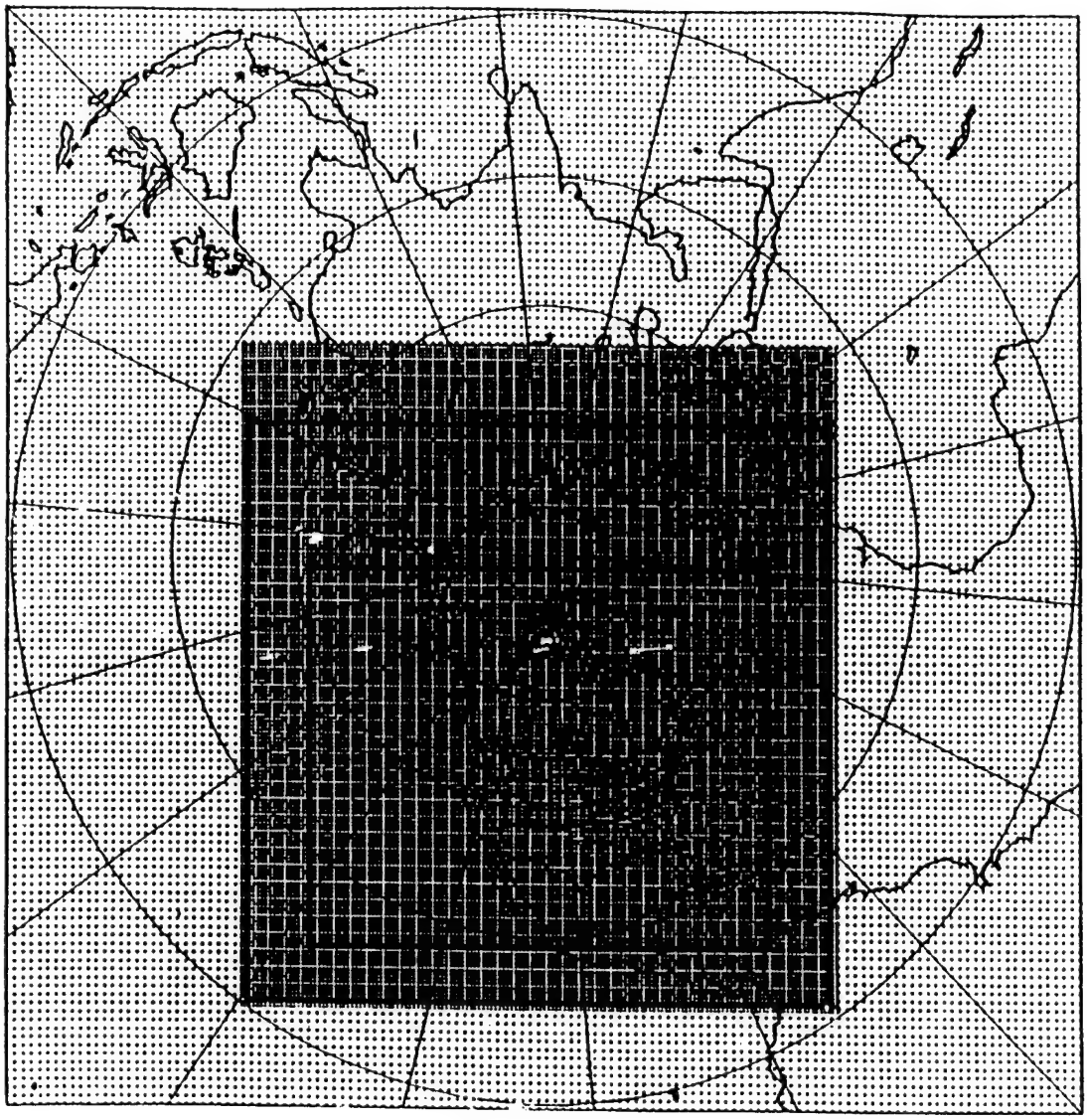

Figure 3.1: The current nested grid model structure, showing the expanded northern hemispheric domain of grid B and the new super grid C. heavy solid lines outline the approximate boundaries of grids B and C of the original NGM "From Dimego *et al.* 1992".

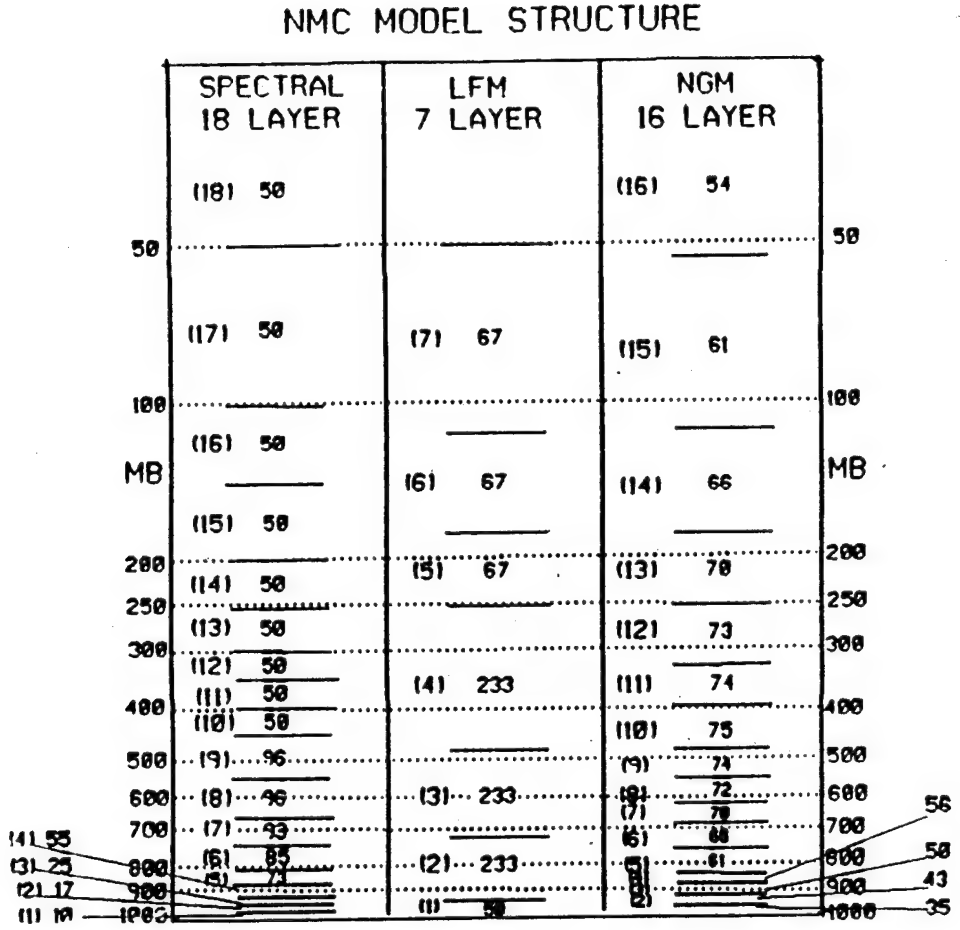

FIG. 3 Vertical structure of NMC's regularly scheduled forecast models. Depth of sigma layers (in millibars) and locations of layer interfaces shown for a surface pressure of 1000 mb.

Figure 3.2: Vertical structure of three of NMC's regularly scheduled forecast models. Depth of sigma layers (in millibars) and locations of layer interfaces shown for a surface pressure of 1000 mb "From Petersen *et at.* 1989".

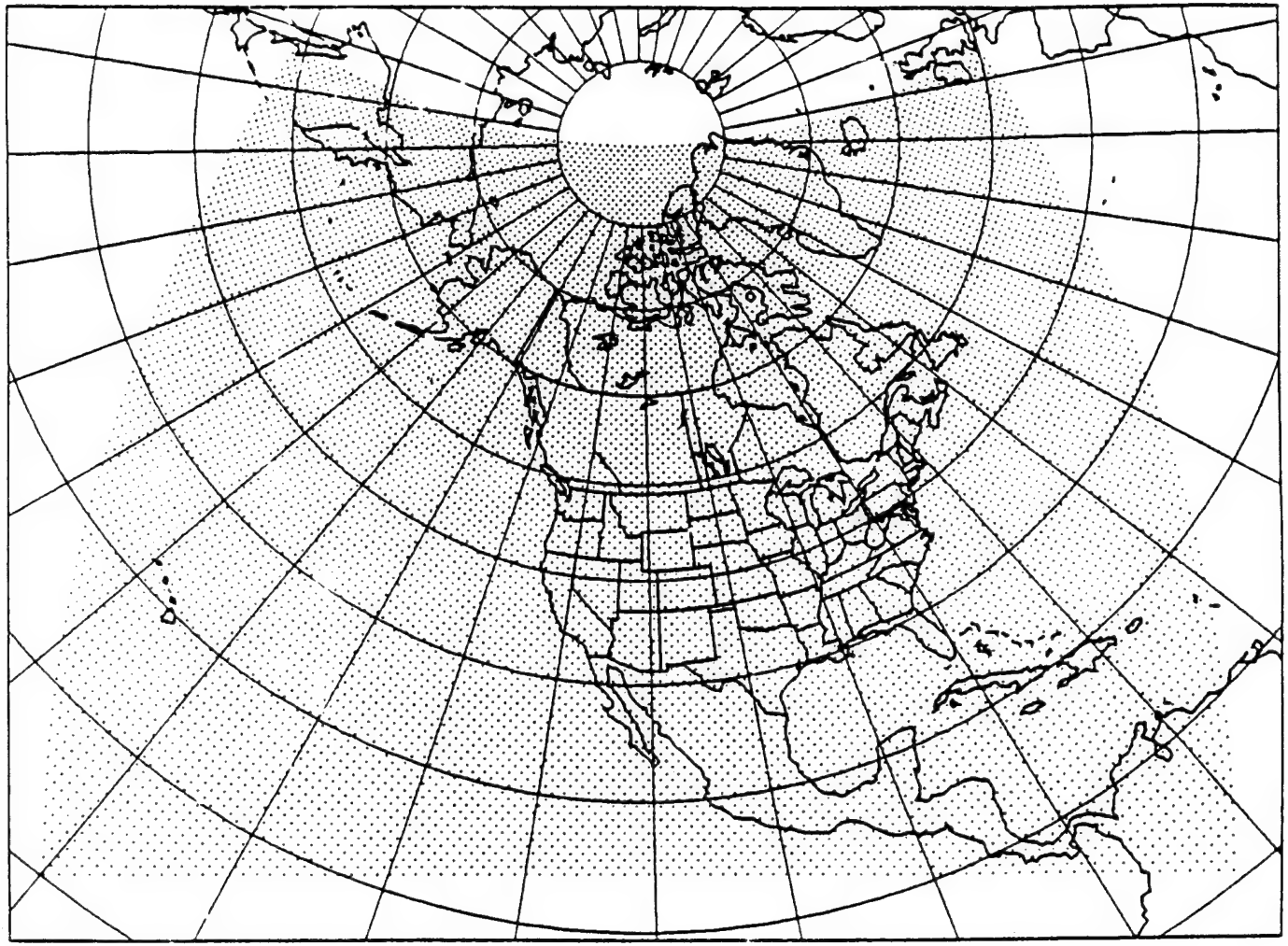

Figure 3.3: The horizontal area (and grid points) covered by the 80-km Eta Model forecasts "From Black *et al.* 1993".

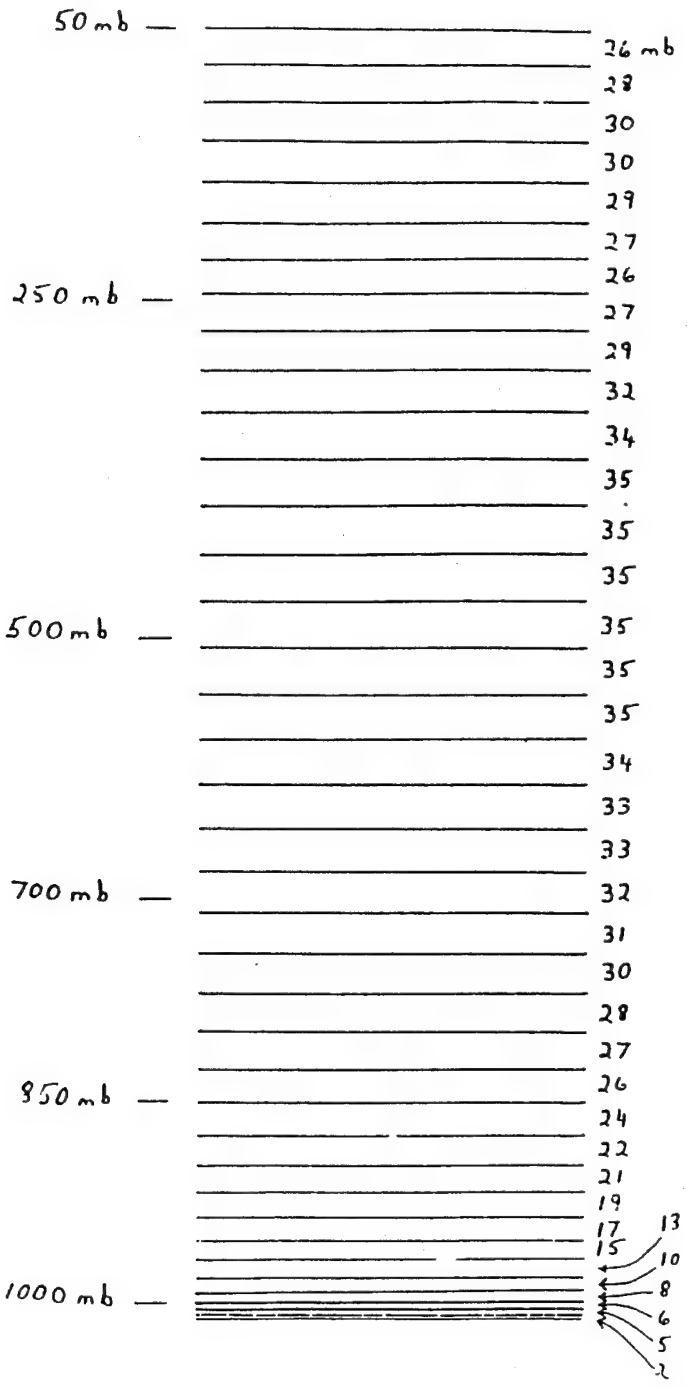

Figure 3.4: The 38 layers of the Eta Model, drawn proportional to their thickness in mass (mb) for the standard atmosphere "From Black *et al.* 1993".

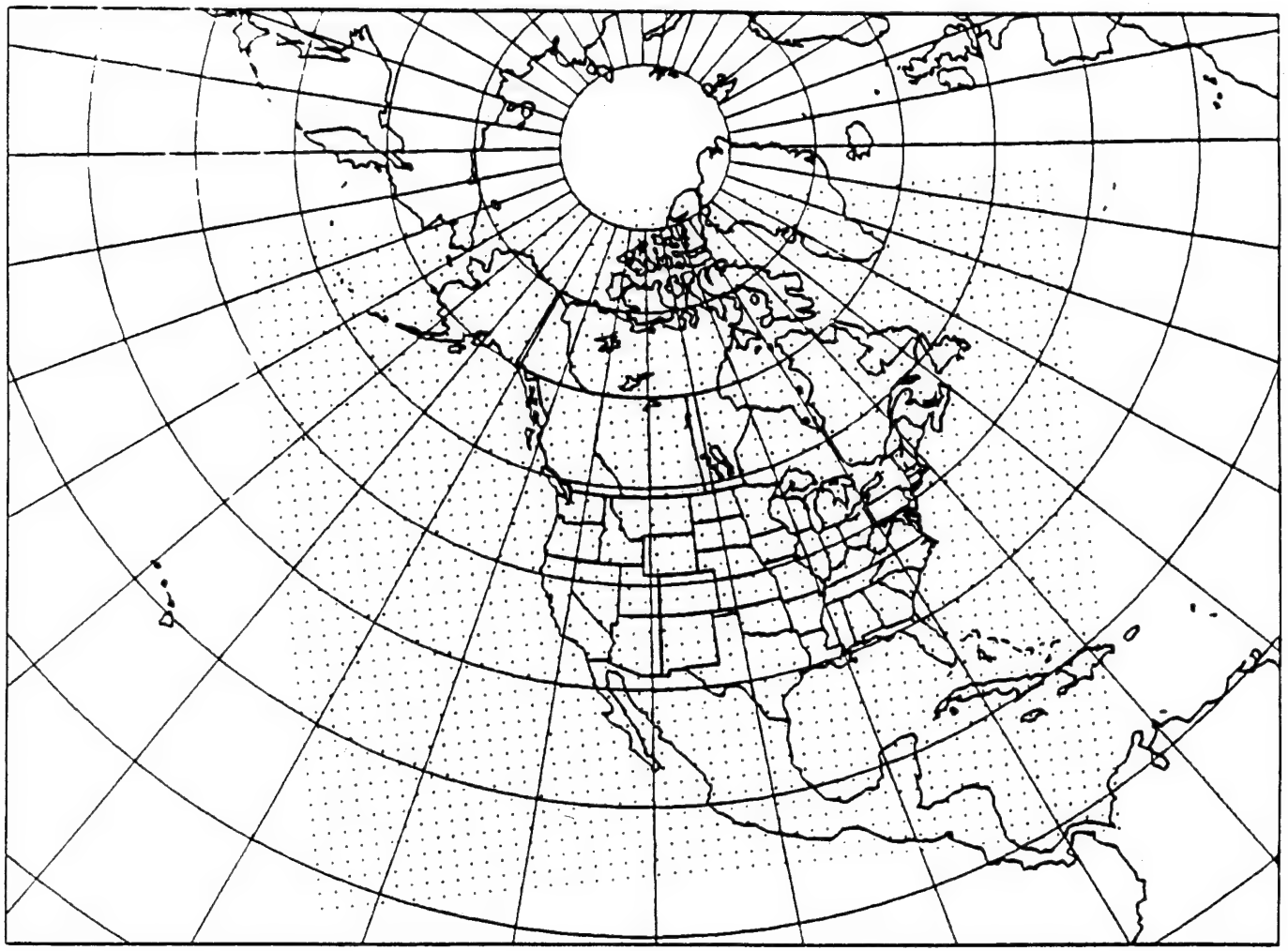

Figure 3.5: The horizontal area (and grid points) covered by the 190.5-km LFM "From Black *et al.* 1993".

IV. RESULTS

A. SEA LEVEL PRESSURE ERRORS

Forecast sea-level pressure errors and statistics are listed in Tables 4.1 and 4.2 for the Nested Grid Model (NGM) and Eta model, respectively. Table 4.3 contains statistics on cyclones which were analyzed and/or forecast by both models. Mean sea-level pressure errors at the analysis, and all forecast times are also listed, along with additional information on the data base from which they were derived. Forecast pressure errors are defined as positive in the case where forecast pressure values are higher than analyzed values, and are negative when analyzed pressure values are higher than forecast pressure values. In the case where the two models are compared, errors are negative when Eta model forecast values are lower than NGM values, and positive when higher than NGM values. Standard deviation (SD) values for mean forecast and analyzed mean sea-level pressure values, and for forecast error values are also calculated and examined. Correlation coefficients (R) are also presented to help quantify the linear fit between forecast vs analyzed data groups, and between NGM and Eta Model data groups when they are directly compared. A total of 227 cyclones were employed in the generation of this statistical data base, with all comparisons of forecast vs analyzed data available included.

In some instances data were missing for one, or several model runs for one model or the other. Consequently, some individual cyclones were analyzed by only one model. In other instances, one model carried a cyclone for more forecast cycles than the other model. These factors helped contribute to some of the differences in forecast and analyzed values when statistics on the two models are viewed separately.

1. Nested Grid Model

As shown in Table 4.1 NGM forecast pressure errors exhibited a consistent negative bias with error magnitudes increasing from a minimum of -.23 mb at the 12h forecast to a maximum of -.8 mb at 48h indicating that the model predicted slightly stronger cyclones than analyzed. With increased forecast range, the forecast error standard deviation increased steadily as would be expected, from 2.33 mb at 12h to 6.01 mb at 48h. Correlation coefficients exhibited their best linear fit at the 12h forecast time with a value of .986, then very steadily eroded to a minimum value of .908 by 48h. The standard deviation of forecast error values exhibited a similar steady trend toward a wider variability with increased forecast range. Figure 4.1 indicates the same decrease in linear fit over the four forecast ranges. With the exception of the NGM tending to over-forecast the central pressure of the very few deepest cyclones, a trend can easily be observed wherein cyclones analyzed at the higher end of the mean sea-level pressure spectrum tended to be over-forecast, and cyclones analyzed at the lower end of the mean sea-level pressure spectrum tended to be under-forecast.

2. Eta Model

Fewer forecast to analysis comparisons are available for the Eta model, primarily due to data availability. Forecast pressure errors illustrated a consistent, positive bias in the Eta model, with absolute forecast error magnitudes being consistently larger than those of the NGM (Table 4.2). Mean errors began with a minimum value of .68 mb at 12h and rapidly increased to slightly over 1 mb by 24h, remaining there through 48h. Both correlation coefficients, and error standard deviations were remarkably close in magnitude and character to those of the NGM, with no significant differences identifiable. Inspection of Figure 4.2, illustrates the consistent, positive pressure error noted above at all forecast ranges for the

Eta model through the decreasing slope and leftward shift of the best linear fit (R) curves through the model forecast cycle.

3. Eta and NGM Comparison

For the population of cyclone analyses and forecasts common to both models the number of comparisons began at over 1000 at analysis time and dropped rapidly to 699 at the 12h forecast time, remained nearly steady at 24h, then dropped sharply again to 581 for the 36h and 48h forecast times (Table 4.3), The sharp reduction in number for the 12h forecast reflects a large number of missing 12h Eta forecasts at the beginning of the period examined. Initially, at 00h, the mean Eta model analysis was deeper than the NGM by .54 mb, but rapidly changed to a positive value of .39 mb by 12h and to 1.11 mb at 24h, with further increases to over 1.3 mb at 36h and 48h. This observed pressure error pattern is in good agreement with trends identified in the separate model comparisons showing that the Eta model's error is of the same magnitude as the difference between the two models. A noteworthy observation in this common comparison is the close fit of correlation coefficients and forecast error standard deviation values between the two models over the range of forecast times. The two separate models were in very good agreement in cyclone analysis solutions with a correlation coefficient of .99 and a standard deviation of only 1.94 mb. The agreement decreased at a steady rate through 48h, yet still remained better than the agreement between the individual model forecasts and analyses with a maximum Eta standard deviation of 4.70 mb and minimum correlation coefficient of .945 at 48h. Importantly, this observation illustrates no radical difference in model performance of forecast sea-level pressure values over the range of forecast times with the exception of the consistently higher central pressure values forecast by the Eta model.

Inspection of Figures 4.3 and 4.4 illustrates that for the very few deepest cyclones, the Eta model tended to forecast higher central pressure values for all forecast times with the bias

increasing as forecast time increased. The linear fit curves further illustrate this bias rather well. This observation is consistent with the aforementioned comments, although is somewhat more notable when the deepest few cyclones in the data base are examined separately.

4. Large Error Analysis

For a very few cyclones, model forecast solutions differed significantly between the two models. Investigation of these cases revealed that these cyclones were almost exclusively located in data sparse oceanic locations. These occasional significant differences in model forecast or analysis solution, rather than any dramatic model bias helps explain some of the previously discussed model differences. Several cases revealed that one common cause was a differing model solution of cyclone formation in the vicinity of Cape Farewell, Greenland. In this situation a given model may have under-predicted a cyclone deepening rate, or may have analyzed or forecast a different sea level pressure pattern, dividing energy differently between the Southeast Coast and Western Coast of Greenland. In another situation, one model may have analyzed or forecast a cyclone with a single center, while the other model analyzed the same system with a dual center or with a significantly differing surface pattern, such as troughing, both of which served to increase the minimum cyclone central pressure. In a third situation, one model may have analyzed the deepest cyclonic center in a complex system very close, yet inside the model's forecast grid while the other model may have positioned the deepest center of the same complex cyclonic system just outside its forecast grid with a weaker secondary center co-located with the strongest center of the first model. This would cause a comparison leading to radically differing central pressures for a single given cyclone at a specific forecast or analysis time.

Comparisons of sea level pressure vs longitude and of sea level pressure vs latitude were also made for both models

(Fig. 4.5). Beginning with longitude, the deepest cyclones were exclusively of oceanic origin, with the very few deepest cyclones located in the Atlantic Ocean. The highest mean central sea level pressures for both models were observed to be located primarily over the inter-mountain west, although this pattern was not nearly as well defined as that over oceanic areas. Comparisons of latitude vs central pressure illustrate that the cyclones, as expected, lie predominately in the mid-latitudes between 30°N and 65°N. The population of cyclones analyzed at lower latitudes indicated far less variation in central pressure than those at middle or high latitudes, with those at middle latitudes exhibiting the greatest degree of variability.

B. FORECAST POSITION ERRORS

Forecast position errors along with statistics on the relevant populations of cyclone forecast comparisons are listed in Tables 4.4 and 4.5 for the NGM and Eta models separately. Table 4.6 lists the same information for the population of cyclones common to both models. Statistics on cyclone position and pressure in this table are referred to as forecast differences, as it is incorrect to arbitrarily label one model's forecast solution more accurate than the other.

1. Nested Grid Model

Forecast position errors for the NGM verified against its own analysis illustrated a very uniform increase in magnitude as forecast length increased with the mean position error of 146.4 km at 12h increasing gradually to 322 km at 48h (Table 4.4). Note that the position errors were calculated from model output interpolated to the LFM grid, with its 190.5 km spacing (at 60° N). Therefore, the mean distance errors are less than one grid length out to 36h. This also implies that the distance errors may be somewhat overestimated by using the model output on the LFM grid compared to

the original model resolutions closer to 80 km. Standard deviation values for the forecast distance error showed a similar uniform trend in increase with lengthening forecast range, beginning with a minimum value of 169 km at 12h and increasing to a maximum of 246 at 48h. Graphic representation of pressure error vs distance error for each forecast time through 48h, (Fig 4.6), illustrates very little bias or correlation between the sign or magnitude of the pressure error and the magnitude of the distance error. The largest errors in forecast position were nearly evenly divided between positive and negative pressure errors for each forecast time. Graphic depiction of longitude vs forecast position error (Fig 4.7) illustrates no identifiable bias toward oceanic locations for 12h and 24h, with some bias present at 36h and 48h toward larger forecast position errors in oceanic regions especially for Pacific Ocean locations.

2. Eta Model

Eta model forecast position errors, like those of the NGM, exhibited a very uniform increase in magnitude as forecast time progressed through 48h. Initial mean position error values were very close to those of the NGM, at 143 km and increased almost perfectly in step through 36h, when both models reached a mean error magnitude of 275-276 km. Only at 48h did the models show any difference in mean forecast position error, with the difference being only 8 km with the Eta model having the larger mean error value of 330 km. Position error standard deviation values were initially less than the NGM at 12h with a value of 157.3 km, then increased rapidly to 205 km at 24h, but eventually became nearly identical to the NGM at 245.8 km at 48h.

Inspection of graphs (Fig. 4.8) of pressure error vs forecast position error, like those for the NGM, indicates no distinct correlation between the sign of the forecast pressure error and the largest few distance errors, but does indicate a slight bias for the very few cyclones with the largest position error to be under-

forecast in central pressure values. Forecast position error plotted vs longitude for the Eta model illustrated no bias toward the location of larger error values over ocean areas through 24h and only slightly indicated a bias toward locating larger forecast position errors over oceanic regions at 36h and 48h (Fig. 4.9).

In summary, for both models individually, the largest forecast position errors showed far less sensitivity to geographic location than did the largest forecast central pressure errors (not depicted in this paper), which indicated a strong bias toward oceanic locations, especially the Atlantic. A similar distribution to Figure 4.5 was observed, with the largest differences in mean error values over oceanic regions, and a much smaller range of error variance over the Continental United States.

3. Eta and NGM Forecast Position Comparisons.

In a final examination of forecast position errors the Eta model is compared with the NGM. The population of cyclone analyses and forecasts common to both models is presented from 00h through 48h (Table 4.6). A total of 1035 common cyclone comparisons in the analyses rapidly dropped to below 700 by 12h and continued to decline to 579 at 48h. At analysis time the two models agreed to within 141 km. Although this value appears rather large for an analysis comparison of a common population of cyclones, it is important to recall that the coarse 190.5 LFM grid was employed in this research, and also that, as earlier mentioned on page 30, occasionally large differing model analysis solutions also helped to bias the mean analysis distance difference toward a higher numerical value. Forecast position differences between the two models were very similar to the individual model position errors, increasing slightly to 167 km by 12h, then jumping markedly to 233 km at 24h, and continuing to increase to a maximum of 325 km at 48h. Values of standard deviation of forecast position difference between the two models followed a similar trend, as expected, increasing from a minimum of 144 km at analysis to 293 km at 48h,

slightly larger than the standard deviations of the individual model position errors.

Figures 4.10 and 4.11 compare the analyzed and forecast pressure and position differences and indicate no particular bias at all for positive or negative pressure error values in the case of the most radically differing position forecasts. Similarly, the largest deviations in cyclone forecast position between the two models also indicated no bias for geographical location at all (Figs. 4.12 and 4.13).

C. FORECAST THICKNESS ERRORS

Statistics on the thickness between the 1000 mb to 500 mb layers at the center of the cyclone (Tables 4.7, 4.8, and 4.9) were also generated, and presented in the same manner as those for the sea- level pressure fields for both the Eta model and the NGM separately, and then for the models compared against each other.

1. Nested Grid Model

The NGM exhibited a slight, consistent cold bias for all forecast times from 12h through 48h (Table 4.7). Forecast thickness errors ranged from -0.4 m at 12h, to a maximum of -7 m at 48h. Thickness error standard deviation values had a similar trend, increasing from a minimum of 31.3 m at 12h to a maximum of 54.2 m at 48h. Correlation coefficients for the NGM demonstrated a very good correlation of forecast to observed thickness values throughout the forecast cycle, beginning at nearly .99 at 12h, and decreasing very slightly to only .96 by 48h.

Figure 4.14, graphically depicts forecast vs analyzed central thickness values. A trend toward the NGM under-forecasting the thickness of the warmest few cyclones and over-forecasting the thickness of the coldest few cyclones is apparent in each of the four comparisons. This trend becomes more distinct as time progresses out to 48h. A brief inspection of forecast central

thickness errors vs longitude (Fig. 4.15) indicates that the largest variation in thickness error occurred, as expected over the continental United States and Western Atlantic with far less variation over the Eastern Pacific due to the more moderate character of oceanic air masses. No particular bias of positive or negative errors toward geographical locations can be firmly identified.

2. Eta Model

The Eta model exhibited much less bias in the central thickness errors than the NGM (Table 4.8). The Eta Model began with a positive thickness error of 1 m at 12h which soon reversed to a negative error of -.5 m at 24h, and increased to -1.84 by 48h compared to -7 m for the NGM. Even so, both standard deviation values and correlation coefficients for the Eta model forecast vs analyzed central thickness are little different from those of the NGM with the values being nearly identical most of the time. Another interesting similarity in the two models is that the Eta Model, like the NGM, exhibited a consistent bias which increased with forecast time toward under-forecasting the thickness of the warmest few cyclones (Fig.4.16). However, the coldest few cyclones are more evenly split between predicted thickness too cold and too warm than was the case for the NGM. In a similar manner as described for the NGM, inspection of forecast central thickness error vs longitude (Fig. 4.17) indicates that the largest magnitude of thickness errors, both positive and negative occurred over the continental United States and Western Atlantic with no particular bias in negative of positive values toward geographical location.

3. Eta Model and NGM Compared

Like the comparison of cyclone position errors, the number of cyclone comparisons common to both models decreases rapidly from over 1000 at analysis time, to very close to 700 for 12h and 24h,

and then takes another rapid drop to just under 600 at 36h and 48h (Table 4.9). In this comparison, Eta analyzed and forecast values are subtracted from those of the NGM with differences noted as positive when Eta thickness values are lower than those of the NGM, and negative when Eta thickness values are higher than those of the NGM. Close examination of Table 4.9 indicated a very slight cold bias in Eta Model thickness values at analysis time which rapidly changes to a warm bias of 2 to 3 m at 12h and 24h, which is consistent with information presented in the previous two sections. This warm bias illustrates a marked increase to 8.5 m at 36h and 48h, primarily a result of the NGM's cold bias (Table 4.7). Forecast thickness difference standard deviation values remained relatively low at 29.5 m at analysis and at 32.8 m at 12h, but then increased markedly to 44 m by 24h and then showed a slower, steady increase through 36h, reaching a maximum value of 51 m at 48h. The linear correlation of the forecast thickness values exhibited a very good fit through 48h. Correlation coefficients diminished from .99 at analysis to a still rather good fit of nearly .96 at 48h.

Inspection of Figs. 4.18 and 4.19 reveals that the majority of positive central thickness differences in the model comparison result from the Eta Model forecasting higher central thickness values for cyclones in the mid to lower thickness value range that were commonly forecast by both models. As a slight aberration, at 36h and 48h the very few coldest cyclones had actually been forecast at lower thickness values by the Eta model.

D. PRECIPITATION AND PRESSURE ERRORS.

Convective and total precipitation statistics for the total population of cyclones included in this data base are listed in Tables 4.10 through 4.16 for the NGM and Eta Models along with mean 12h pressure change values. The Precipitation values are generated/averaged from the 25 grid points surrounding the center position of the pressure minimum of each cyclone in the data base.

Precipitation values are listed in mm/12h. Total precipitation values represent the sum of the convective (parameterized) listed here and the stable (grid-scale) precipitation values which are not listed.

1. Nested Grid Model

For the Nested Grid Model, mean cyclone-average convective precipitation ranged consistently between .5 mm and .6 mm, while the mean cyclone total precipitation ranged consistently between 2.0 and 2.4 mm. Mean central pressure change statistics for all cyclones, both with and without measurable precipitation, (Table 4.10), indicate very little relationship overall with mean precipitation values in the NGM, with mean pressure changes of less than .4 mb at 12h and 24h and virtually no mean pressure change at 36h and 48h. This is due to the fact that both filling and deepening cyclones are included in this evaluation resulting in a near-zero mean central pressure change. Inspection of Table 4.10 also indicates that mean forecast convective precipitation values tended to decrease with forecast range, yet total precipitation values remained nearly constant at 2.3 mm to 2.4 mm. One exception is the slightly lower value of the 12h forecast, which can be attributed to model forecast spin-up error.

Figure 4.20 and Figure 4.21 depict NGM 12h pressure change vs convective and total precipitation for all forecast periods respectively. In both cases for all four forecast times, cyclones with a positive pressure change (those on a filling trend), exhibited a skewness toward lower mean precipitation values, while those few cyclones with the largest precipitation values tended to favor a mean negative pressure change value. When statistics generated for all cyclones, with and without measurable precipitation and only those with measurable precipitation are viewed separately (Table 4.10 and Table 4.11) the correlation between moister cyclones being on a net deepening trend and drier

cyclones tending to be on filling trend becomes more apparent at all forecast times.

2. Eta Model

The Eta Model precipitation statistics, (Table 4.12), exhibited higher mean values than the NGM throughout all four forecast periods with mean cyclone-average convective precipitation averaging in the .6 to .7 mm range and total cyclone-average precipitation ranging between 2.6 and 3.1 mm. An increase in stable precipitation in the Eta Model over the NGM accounts for most of the difference. However, it is also important to note that the NGM tended to have a greater percentage of cyclones forecast without any precipitation at all, thereby affecting mean precipitation quantities for the two separately analyzed groups of cyclones. Unlike the NGM, mean Eta Model pressure change statistics exhibited a net negative value throughout all four forecast cycles. These values are very small in magnitude, and like those of the NGM and are also simply the result of how pressure change values, both positive and negative, averaged out when all cyclones, both deepening and filling are included.

In a similar pattern to that observed for the NGM, for both types of precipitation and for all four forecast times, Figure 4.22 and Figure 4.23 illustrate that those cyclones observed to be filling, (exhibiting a positive pressure change), had markedly lower values in both precipitation categories. Those cyclones with the greater values in both precipitation categories tended to have a distinct bias toward a negative pressure change (deepening trend). In the same manner as observed in the NGM, when moist cyclone population statistics (Table 4.13) are analyzed separately from the total population of cyclones, (Table 4.12) the greater negative mean pressure change values indicate a clear correlation with higher mean forecast precipitation totals.

3. NGM and Eta Models Compared

Table 4.14 illustrates statistics, and Figures 4.24 and 4.25 illustrate forecast differences on the population of cyclones in this study in which precipitation is commonly forecast by both models. Inspection of the convective precipitation category of Table 4.14 indicates consistently higher forecast values by the NGM for these cyclones at all forecast ranges. Of particular interest is the rapid increase in convective precipitation values at 24h in both models, followed by a decrease of similar magnitude at 36h. Correlation coefficients were relatively low in this precipitation category with the best fit of .83 at 12h and the least fit of .76 at 48h. The total precipitation category indicates an opposite trend, with the Eta Model consistently forecasting higher values at all forecast ranges. This indicates that the Eta Model is forecasting stable precipitation values at a significantly higher rate than the NGM. The total precipitation category also indicates a significantly closer fit between the two models at all forecast ranges with the closest fit of .945 at 12h decreasing to .94 at 24h, then to .89 by 48h.

Table 4.15 and Figures 4.26 and 4.27 depict the differences in 12h forecast pressure change and in both precipitation types for the same population of cyclones noted above. Statistics indicate a consistently more positive mean pressure change in the Eta model associated with lower mean convective, yet higher mean total precipitation values than the NGM as noted in the previous paragraph.

As a final note, Table 4.16, and Figure 4.28 illustrate 12h deepening rate statistics on those cyclones commonly forecast by both models in which precipitation had been forecast by at least one of the models, not exclusively by both as in the preceding paragraph. Table 4.16 illustrates a notable bias toward the NGM forecasting higher deepening rates for cyclones in which precipitation had been forecast by either model. Figure 4.28 illustrates the fact that the NGM tended to forecast greater

pressure change values for both deepening and filling cyclones. The largest values notably occurred in the 24h range for both models. This matches an interesting trend in Table 4.14 in which convective precipitation values also indicated a rapid increase over those forecast at 12h followed by large decrease at 36h. The significant difference in sample sizes may have effected these forecast mean precipitation value differences.

SEA LEVEL PRESSURE STATISTICS (mb)

	NGM Forecast	NGM Analysis	Fcst - Analysis
12-h Forecast			
Size	1031	1031	1031
Mean	998.09	998.33	-.23
Maximum	1030.50	1029.00	9.60
Minimum	947.90	947.80	-17.10
SD	13.97	13.67	2.33
R	.986		
24-h Forecast			
Size	914	914	914
Mean	997.53	998.11	-.58
Maximum	1029.50	1029.00	12.30
Minimum	949.60	947.80	-19.60
SD	14.06	13.83	3.78
R	.961		
36-h Forecast			
Size	864	864	864
Mean	996.78	997.43	-.65
Maximum	1027.70	1029.00	17.60
Minimum	948.80	955.50	-22.3
SD	13.94	13.68	4.88
R	.937		
48-h Forecast			
Size	815	815	815
Mean	996.49	997.26	-.808
Maximum	1039.30	1029.00	20.00
Minimum	945.70	955.50	-24.50
SD	14.25	13.65	6.01
R	.908		

TABLE 4.1: Sea level pressure statistics for the Nested Grid Model. Statistics are organized by forecast, analyzed and error groups. Size indicates the total number of cyclone forecast to analysis comparisons for any given forecast time. Mean is simply the average numerical value for any given analysis or forecast group. Maximum and minimum values indicate the extreme values in any specific group of forecast or analyzed cyclones. SD values represent the standard deviation for any group of forecast or analyzed cyclones. R values represent correlation coefficients between the compared forecast and analyzed groups.

SEA-LEVEL PRESSURE STATISTICS (mb)

	Eta Forecast	Eta Analysis	Fcst - Analysis
12-h Forecast			
Size	807	807	807
Mean	997.81	997.13	.68
Maximum	1029.30	1029.90	12.10
Minimum	952.30	941.10	-7.40
SD	13.68	13.73	2.39
R	.965		
24-h Forecast			
Size	831	831	831
Mean	998.39	997.27	1.22
Maximum	1029.60	1029.90	15.20
Minimum	950.80	941.10	-17.70
SD	14.00	13.92	3.69
R	.965		
36-h Forecast			
Size	703	703	703
Mean	997.70	996.37	1.33
Maximum	1029.20	1029.90	21.30
Minimum	946.60	941.10	-17.30
SD	14.09	13.91	4.78
R	.942		
48-h Forecast			
Size	704	704	704
Mean	997.38	996.12	1.26
Maximum	1034.30	1029.90	21.70
Minimum	948.00	941.10	-18.40
SD	14.14	13.85	5.84
R	.913		

TABLE 4.2: As in Table 4.1, except for the Eta Model.

NGM/ETA SEA LEVEL PRESSURE STATISTICS (mb)

	Eta	NGM	Eta - NGM
00-h Forecast			
Size	1035	1035	1035
Mean	997.87	998.41	-.54
Maximum	1029.90	1029.00	6.90
Minimum	941.10	947.80	-11.80
SD	13.87	13.64	1.94
R	.990		
12-h Forecast			
Size	699	699	699
Mean	997.04	996.66	.39
Maximum	1028.80	1030.50	11.00
Minimum	952.30	947.90	-12.00
SD	13.54	13.70	2.40
R	.984		
24-h Forecast			
Size	691	691	691
Mean	997.42	996.29	1.11
Maximum	1028.50	1029.50	13.60
Minimum	950.80	950.30	-14.00
SD	14.03	13.88	3.37
R	.971		
36-h Forecast			
Size	581	581	581
Mean	996.66	995.19	1.36
Maximum	1029.20	1025.90	16.00
Minimum	954.80	948.80	-14.20
SD	13.95	13.77	4.07
R	.957		
48-h Forecast			
Size	579	579	579
Mean	996.58	995.24	1.34
Maximum	1034.30	1030.90	22.90
Minimum	948.00	945.70	-13.90
SD	14.15	14.14	4.70
R	.945		

TABLE 4.3: As in Table 4.1, except for the population of cyclones commonly analyzed and forecast by both models.

NGM FORECAST DISTANCE ERRORS

Distance Error (km)

12-h Forecast

Size	1031
Mean	146.38
Maximum	1637.70
Minimum	0.00
SD	169.15

24-h Forecast

Size	914
Mean	215.80
Maximum	1637.71
Minimum	0.00
SD	193.89

36-h Forecast

Size	864
Mean	272.086
Maximum	1562.95
Minimum	0.00
SD	226.13

48-h Forecast

Size	815
Mean	322.12
Maximum	2032.49
Minimum	0.00
SD	246.61

TABLE 4.4: As in Table 4.1, except for forecast distance error only.

ETA FORECAST DISTANCE ERRORS

Distance Error (km)

12-h Forecast

Size	807
Mean	143.98
Maximum	995.44
Minimum	0.00
SD	157.34

24-h Forecast

Size	831
Mean	216.68
Maximum	1594.20
Minimum	0.00
SD	205.09

36-h Forecast

Size	703
Mean	276.55
Maximum	1698.96
Min	0.00
SD	215.17

48-h Forecast

Size	704
Mean	330.09
Maximum	1709.56
Minimum	0.00
SD	245.78

TABLE 4.5: As in Table 4.4, except for the Eta Model.

ETA/NGM FORECAST PRESSURE AND DISTANCE DIFFERENCES (ETA - NGM)

	Pressure Difference (mb)	Distance Difference (km)
00-h Forecast		
Size	1035	1035
Mean	-.53	141.03
Maximum	6.90	827.06
Minimum	-11.80	0.00
SD	1.94	144.87
12-h Forecast		
Size	699	699
Mean	.39	167.01
Maximum	11.00	1281.45
Minimum	-12.00	0.00
SD	2.40	170.42
24-h Forecast		
Size	691	691
Mean	1.11	233.79
Maximum	13.60	1698.97
Minimum	-14.00	0.00
SD	3.37	220.43
36-h Forecast		
Size	581	581
Mean	1.36	275.18
Maximum	16.40	1698.90
Minimum	-14.20	0.00
SD	4.07	240.41
48-h Forecast		
Size	579	579
Mean	1.34	325.20
Maximum	22.90	1991.60
Minimum	-12.30	0.00
SD	4.70	293.14

TABLE 4.6: As in table 4.4, except for the population of cyclones commonly analyzed and forecast by both models.

NGM THICKNESS STATISTICS (m)

	NGM Forecast	NGM Analysis	Fcst - Analysis
12-h Forecast			
Size	1031	1031	1031
Mean	5308.97	5309.34	-.37
Maximum	5801.00	5799.00	129.00
Minimum	4757.00	4738.00	-137.00
SD	195.18	197.82	31.29
R	.997		
24-h Forecast			
Size	918	918	918
Mean	5301.64	5303.56	-1.91
Maximum	5792.00	5799.00	152.00
Minimum	4769.00	4736.00	-188.00
SD	190.45	196.85	41.39
R	.988		
36-h Forecast			
Size	870	870	870
Mean	5297.79	5303.13	-5.34
Maximum	5798.00	5799.00	164.00
Minimum	4752.00	4736.00	-193.00
SD	188.91	196.28	47.94
R	.970		
48-h			
Size	817	817	817
Mean	5294.25	5301.33	-7.08
Maximum	5774.00	5747.00	158.00
Minimum	4759.00	4736.00	-213.00
SD	184.02	192.15	54.21
R	.960		

TABLE 4.7: As in Table 4.1, except for cyclone central thickness.

ETA THICKNESS STATISTICS (m)

	Eta Forecast	Eta Analysis	Fcst - Analysis
12-h Forecast			
Size	803	803	803
Mean	5324.30	5323.24	1.06
Maximum	5771.00	5782.00	141.00
Minimum	4759.00	4763.00	-128.00
SD	186.45	187.54	31.05
R	.986		
24-h Forecast			
Size	835	835	835
Mean	5314.48	5314.96	-.48
Maximum	5792.00	5786.00	138.00
Minimum	4753.00	4741.00	-173.00
SD	191.41	192.34	39.81
R	.978		
36-h Forecast			
Size	704	704	704
Mean	5316.79	5318.05	-1.25
Maximum	5770.00	5786.00	180.00
Minimum	4784.00	4763.00	-151.00
SD	181.53	184.03	46.12
R	.968		
48-h			
Size	708	708	708
Mean	5309.01	5310.86	-1.84
Maximum	5717.00	5719.00	179.00
Minimum	4772.00	4763.00	-182.00
SD	177.46	4.86	53.70
R	.957		

TABLE 4.8: As in Table 4.1, except for cyclone central thickness, and for the Eta Model.

NGM/ETA THICKNESS STATISTICS (m)

	Eta Forecast	NGM Analysis	Eta - NGM
00-h Forecast			
Size	1032	1032	1032
Mean	5317.34	5317.75	-.40
Maximum	5786.00	5799.00	129.00
Minimum	4741.00	4763.00	-136.00
SD	190.07	191.00	29.50
R	.988		
12-h Forecast			
Size	702	702	702
Mean	5324.57	5321.22	3.35
Maximum	5771.00	5776.00	166.00
Minimum	4759.00	4790.00	-137.00
SD	181.85	181.90	32.75
R	.984		
24-h Forecast			
Size	697	697	697
Mean	5309.25	5306.65	2.60
Maximum	5792.00	5792.00	253.00
Minimum	4753.00	4770.00	-257.00
SD	188.29	186.64	43.92
R	.973		
36-h Forecast			
Size	584	584	584
Mean	5313.28	5304.65	8.56
Maximum	5770.00	5798.00	266.00
Minimum	4784.00	4785.00	-211.00
SD	179.86	175.51	47.57
R	.964		
48-h			
Size	584	584	584
Mean	5305.47	5296.97	8.50
Maximum	5696.00	5680.00	267.00
Minimum	4772.00	4759.00	-150.00
SD	174.72	175.29	51.07
R	.957		

TABLE 4.9: As in Table 4.1, except for cyclone central thickness, and for the population of cyclones commonly forecast and analyzed by both models.

NGM PRECIPITATION STATISTICS

	NGM Pres change (mb)	Conv Precip (mm)	Total Precip (mm)
12-h Forecast			
Size	736	736	736
Mean	-.38	.63	2.01
Maximum	21.90	13.16	16.04
Minimum	-23.00	0.00	0.00
SD	5.84	1.29	2.65
24-h Forecast			
Size	606	606	606
Mean	-.27	.58	2.34
Maximum	25.00	9.24	19.84
Minimum	-20.10	0.00	0.00
SD	5.96	1.13	3.02
36-h Forecast			
Size	552	552	552
Mean	.07	.59	2.38
Maximum	16.00	6.44	16.80
Minimum	-28.40	0.00	0.00
SD	6.06	1.05	2.94
48-h Forecast			
Size	518	518	518
Mean	-.06	.553	2.31
Maximum	20.20	5.36	17.64
Min	-30.30	0.00	0.00
SD	6.52	.94	2.91

TABLE 4.10: Precipitation statistics for the Nested Grid Model. Statistics are organized by cyclone pressure change, and total and convective precipitation groups. Size indicates the total number of cyclones for any specific time. Mean is simply the average numerical value for any category of values. Maximum and minimum values indicate the extreme numerical values in any specific data category. SD values represent the standard deviation for any group of forecast or analyzed cyclones. R values represent correlation coefficients between the compared forecast and analyzed groups.

NGM PRECIPITATION STATISTICS (MOIST CYCLONES)

	NGM Pres change (mb)	**Total Precip (mm)**
12-h Forecast		
Size	631	631
Mean	-.85	2.35
Maximum	21.90	16.04
Minimum	-23.00	.04
SD	5.92	2.72
24-h Forecast		
Size	531	531
Mean	-.69	2.67
Maximum	25.00	19.84
Minimum	-20.10	.04
SD	5.98	3.08
36-h Forecast		
Size	485	485
Mean	-.26	2.71
Maximum	16.00	16.80
Minimum	-28.40	.04
SD	6.14	2.99
48-h Forecast		
Size	459	459
Mean	-.43	2.61
Maximum	20.30	17.64
Minimum	-30.30	.04
SD	6.55	2.96

TABLE 4.11: As in Table 4.10, except only for cyclones with precipitation forecast.

ETA PRECIPITATION STATISTICS

	Eta Pres change (mb)	Conv Precip (mm)	Total Precip (mm)
12-h Forecast			
Size	529	529	529
Mean	-.52	.61	2.59
Maximum	24.50	11.32	18.44
Minimum	-29.70	0.00	0.00
SD	6.33	1.41	3.05
24-h Forecast			
Size	444	444	444
Mean	-.63	.64	3.03
Maximum	25.50	9.40	26.12
Minimum	-20.60	0.00	0.00
SD	6.18	1.46	3.66
36-h Forecast			
Size	386	386	386
Mean	-.40	.69	3.05
Maximum	22.70	13.60	22.00
Minimum	-25.70	0.00	0.00
SD	6.63	1.53	3.63
48-h Forecast			
Size	368	368	368
Mean	-.34	.61	3.0
Maximum	23.70	9.76	24.76
Minimum	-21.40	0.00	0.00
SD	7.09	1.24	3.56

TABLE 4.12: As in Table 4.10, except for the Eta Model.

ETA PRECIPITATION STATISTICS (MOIST CYCLONES)

	Eta Pres change (mb)	Eta Total Precip (mm)
12-h Forecast		
Size	481	481
Mean	-.88	2.86
Maximum	24.50	18.44
Minimum	-29.70	.04
SD	6.24	3.08
24-h Forecast		
Size	417	417
Mean	-.82	3.22
Maximum	25.50	26.12
Minimum	-20.60	.04
SD	6.19	3.69
36-h Forecast		
Size	362	362
Mean	-.66	3.26
Maximum	22.30	22.00
Minimum	-25.70	.04
SD	6.59	3.66
48-h Forecast		
Size	346	346
Mean	-.49	3.21
Maximum	23.70	24.76
Min	-21.40	.04
SD	7.22	3.59

TABLE 4.13: As in Table 4.10, except for the Eta Model, and only for cyclones in which precipitation is forecast.

COMPARED MODEL PRECIPITATION STATISTICS

	Conv Precip (mm)		Total Precip (mm)	
	NGM	**Eta**	**NGM**	**Eta**
12-h Forecast				
Size	416	416	416	416
Mean	.70	.58	2.41	2.78
Maximum	13.16	10.88	16.04	18.44
Minimum	0.00	0.00	0.00	0.00
SD	1.24	1.30	2.71	3.03
R	.83		.945	
24-h Forecast				
Size	330	330	330	330
Mean	1.25	1.18	2.90	3.03
Maximum	9.24	9.16	19.84	18.80
Minimum	0.00	0.00	0.00	0.00
SD	1.69	1.86	3.24	3.41
R	.82		.94	
36-h Forecast				
Size	284	284	284	284
Mean	.70	.67	2.84	3.24
Maximum	6.44	13.60	16.80	22.0
Minimum	0.00	0.00	0.00	0.00
SD	1.15	1.55	3.10	3.66
R	.79		.90	
48-h Forecast				
Size	275	275	275	275
Mean	.63	.58	2.73	2.98
Max	5.36	9.76	17.64	24.76
Min	0.00	0.00	0.00	0.00
SD	.96	1.21	2.98	3.37
R	.76		.89	

TABLE 4.14: As in Table 4.10, except for the population of cyclones commonly forecast by both models in which precipitation was forecast. Statistics on cyclone sea level pressure change are also not included.

NGM/ETA PRESSURE CHANGE/PRECIP STATISTICS (Eta -NGM)

	Pchg Diff (mb)	Conv pcp Diff (mm)	Total Pcp Diff (mm)
12-h Forecast			
Size	416	416	416
Mean	.23	-.13	.37
Maximum	16.70	6.12	6.92
Minimum	-10.70	-2.96	-2.28
SD	2.81	.75	.99
24-h Forecast			
Size	330	330	330
Mean	.19	-.13	.29
Maximum	20.90	4.28	8.92
Minimum	-23.30	-3.88	-4.04
SD	3.63	.81	1.16
36-h Forecast			
Size	284	284	284
Mean	.05	-.03	.40
Maximum	18.00	7.56	12.60
Min	-17.40	-2.56	-5.12
SD	4.30	.95	1.61
48-h Forecast			
Size	275	275	275
Mean	.30	-.05	.25
Maximum	20.60	5.52	8.20
Minimum	-16.30	-2.80	-6.68
SD	4.77	.79	1.56

TABLE 4.15: Statistics on the forecast pressure change difference, and forecast convective and total precipitation differences between the two models. Specific definitions are as in Table 4.10.

ETA/NGM DEEPENING RATE COMPARISON STATISTICS (MOIST CYCLONES)

	NGM (mb/12h)	Eta (mb/12h)
12-h Forecast		
Size	423	423
Mean	-.75	-.53
Maximum	18.20	23.10
Minimum	-18.90	-26.90
SD	5.90	6.13
R	.89	
24-h Forecast		
Size	345	345
Mean	-.98	-.79
Maximum	20.60	19.10
Minimum	-20.10	-19.50
SD	6.09	6.64
R	.83	
36-h Forecast		
Size	293	293
Mean	-.47	-.38
Maximum	16.00	22.30
Minimum	-28.40	-25.70
SD	6.40	6.90
R	.79	
48-h Forecast		
Size	281	281
Mean	-.61	-.36
Maximum	15.90	21.10
Minimum	-30.30	-26.30
SD	6.65	7.48
R	.76	

TABLE 4.16: Statistics on cyclone deepening rates for both models in which precipitation was forecast by at least one model. Specific definitions are as in Table 4.10.

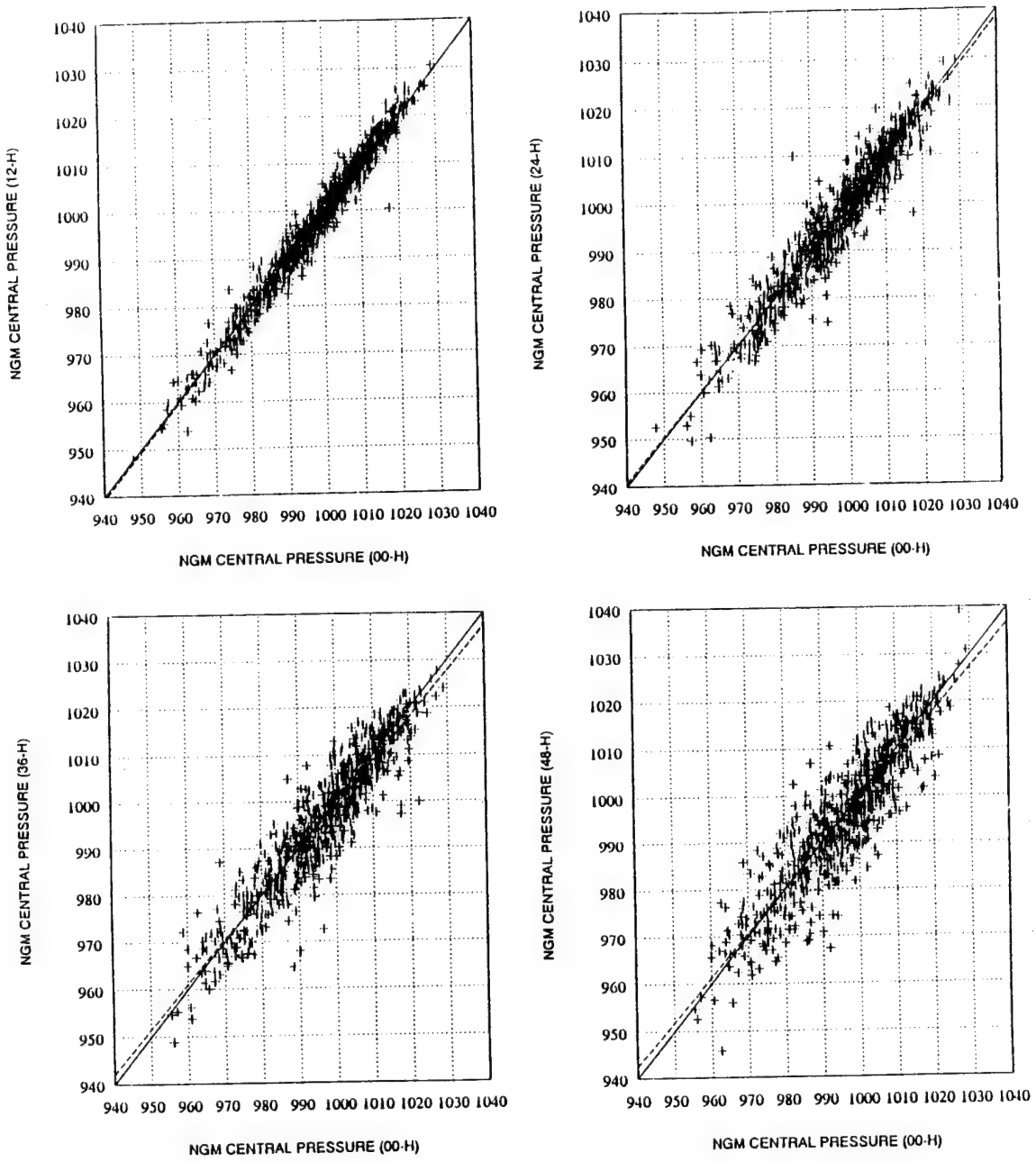

Figures 4.1a-d: Scatter diagrams depicting NGM forecast vs NGM analyzed cyclone sea level pressure values for forecast ranges 12, 24, 36, and 48h.

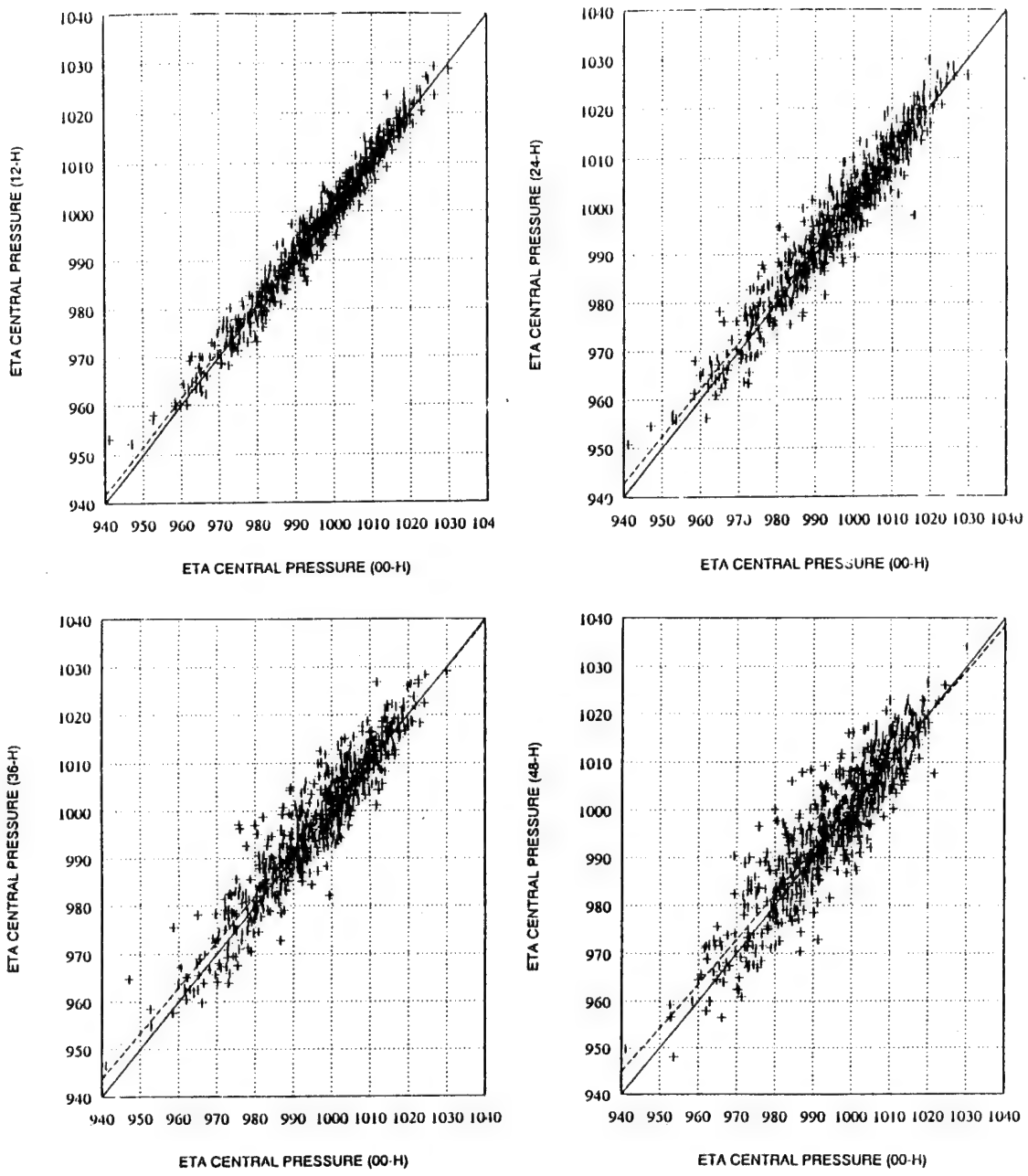

Figures 4.2a-d: As in Figures 4.1a-d, except for the Eta Model.

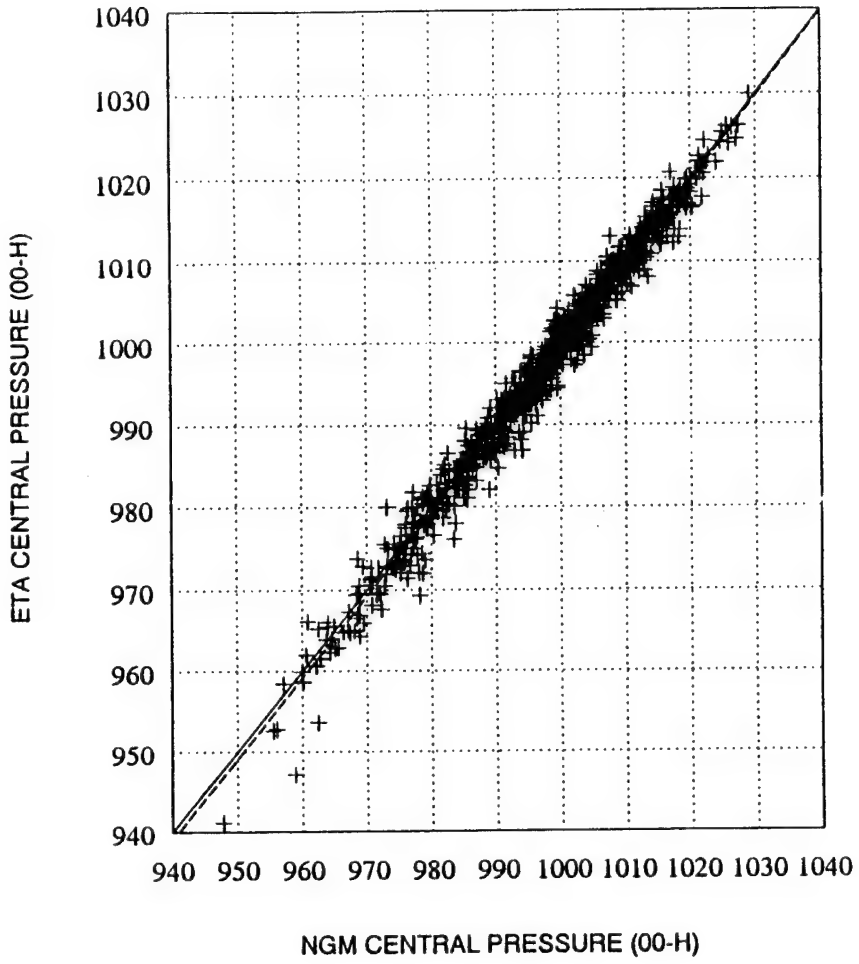

Figure 4.3: Scatter diagram depicting NGM vs Eta Model analyzed sea level pressure values for population of cyclones commonly analyzed by both models.

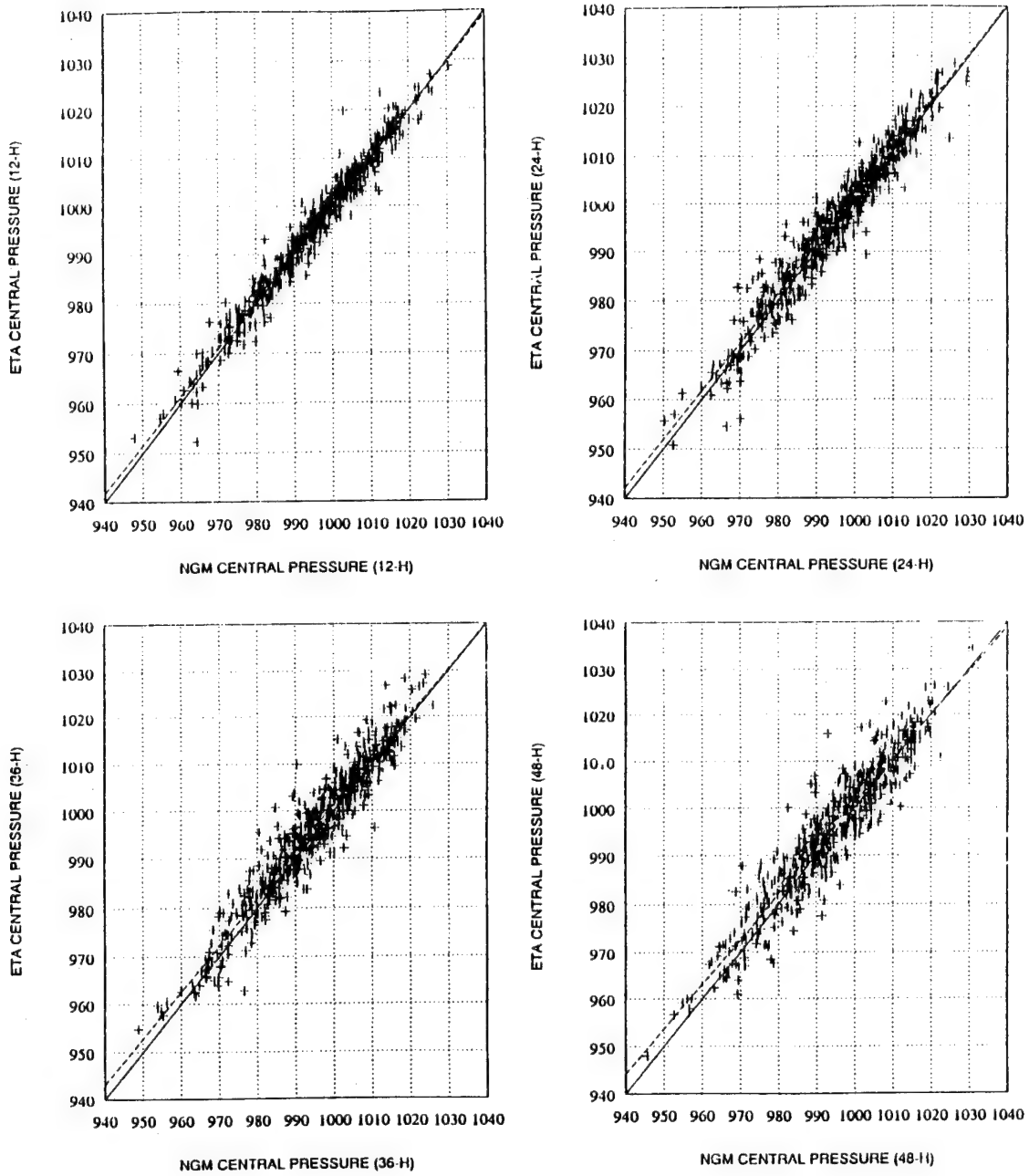

Figures 4.4a-d: Scatter diagrams depicting NGM vs Eta forecast sea level pressure values for forecast ranges 12, 24, 36, and 48h.

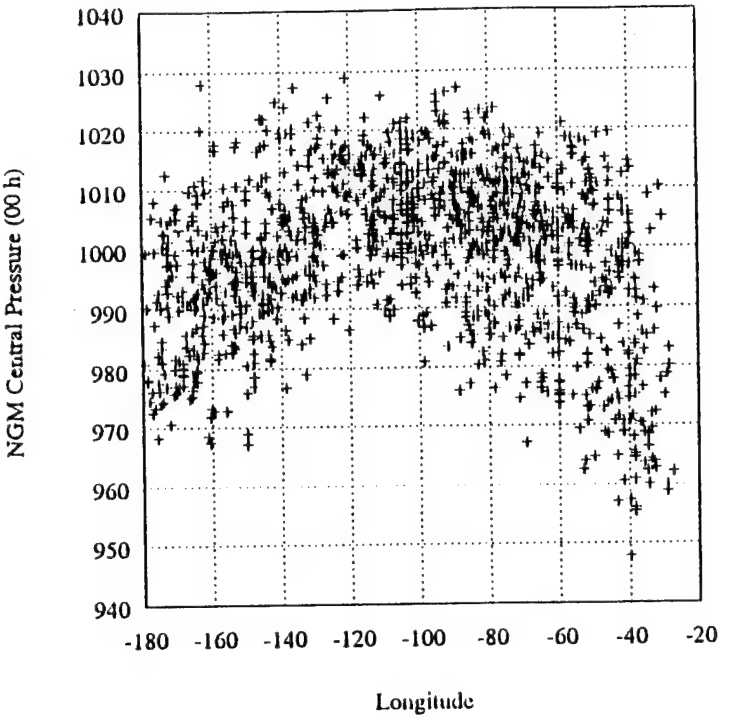

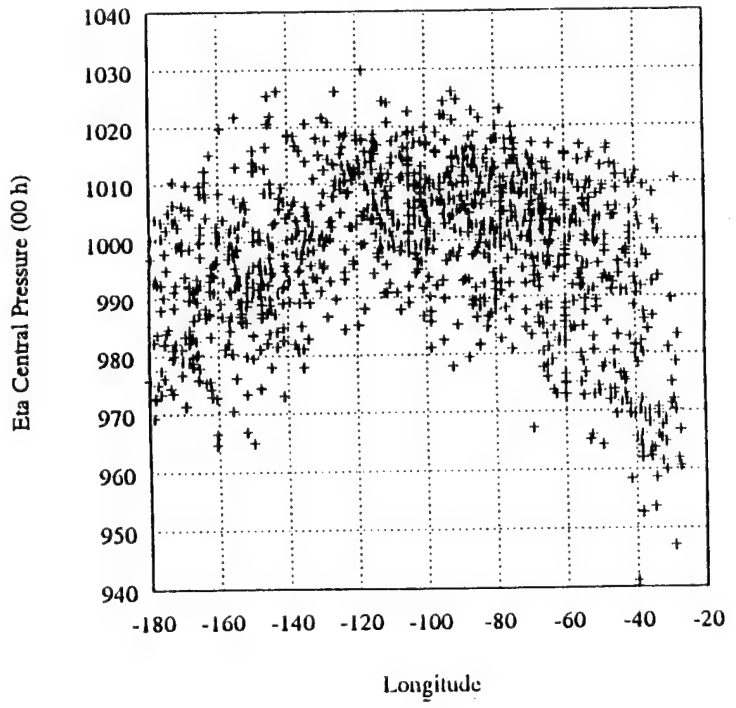

Figures 4.5a-b: Scatter diagrams depicting analyzed sea level pressure values vs longitude for NGM and Eta Model.

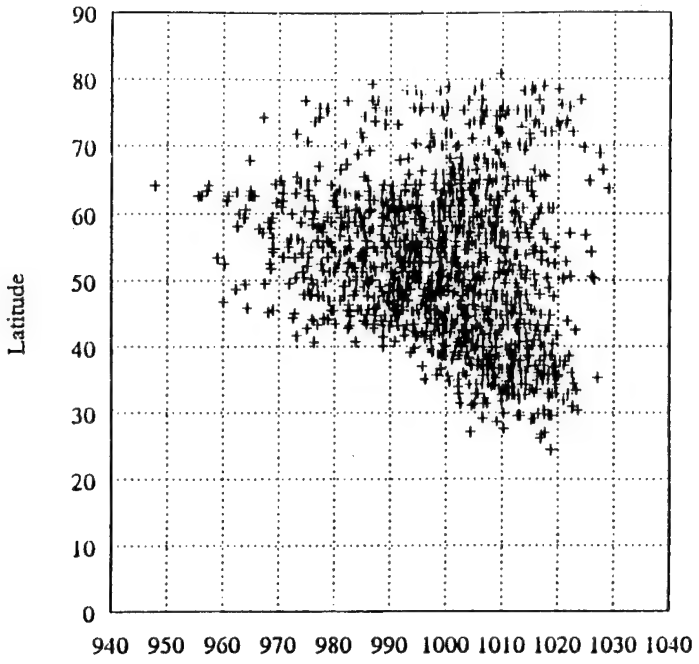

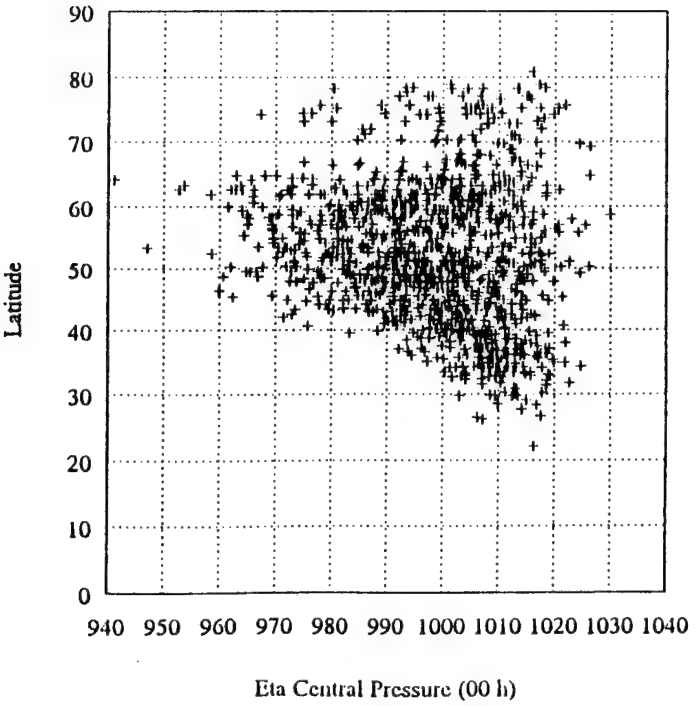

Figures 4.5c-d: As in Figures 4.5a-b, except for latitude,

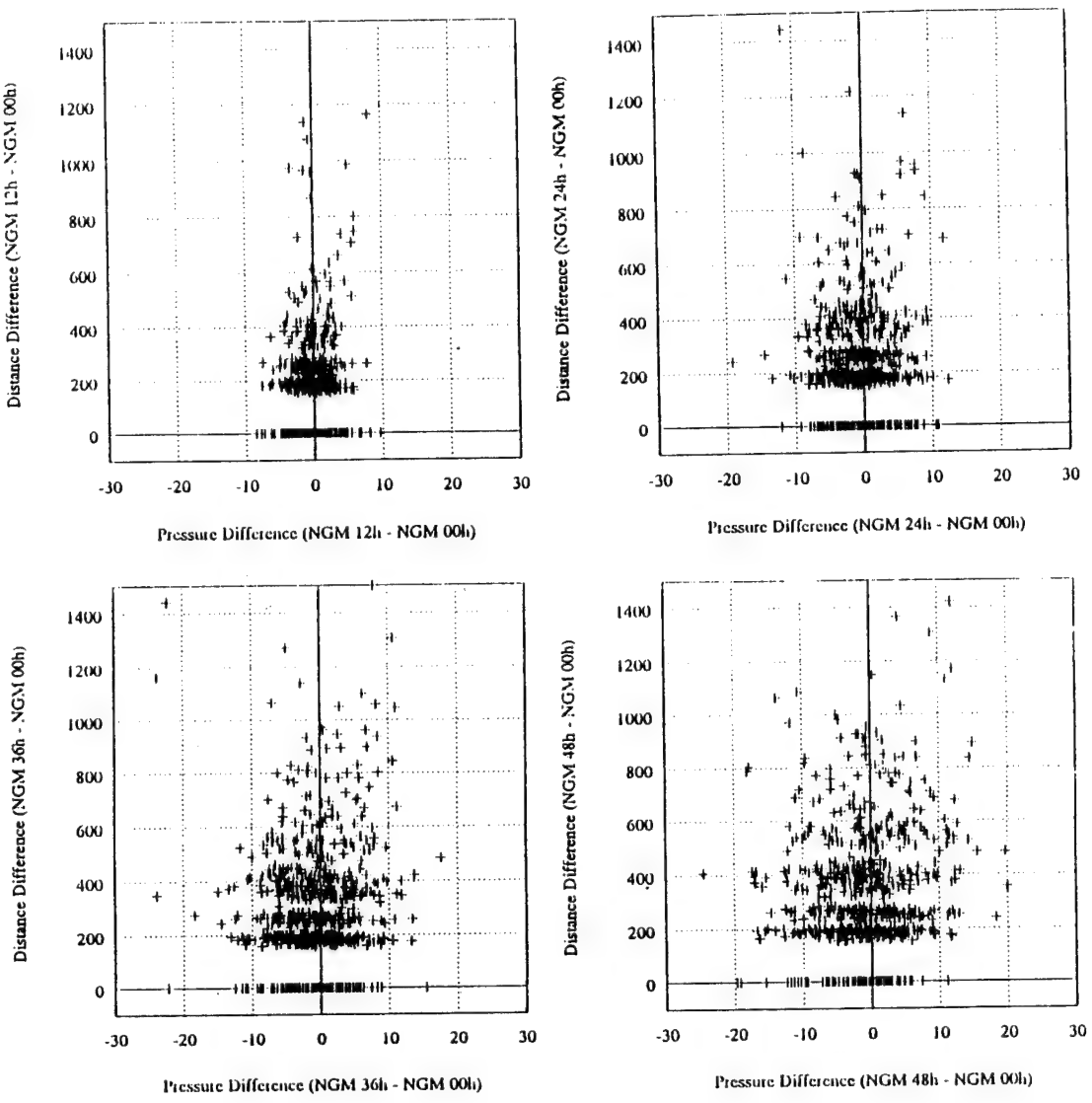

Figures 4.6a-d: Scatter diagrams depicting (forecast - analyzed) position vs (forecast - analyzed) sea level pressure values for forecast ranges 12, 24, 36, and 48h for NGM.

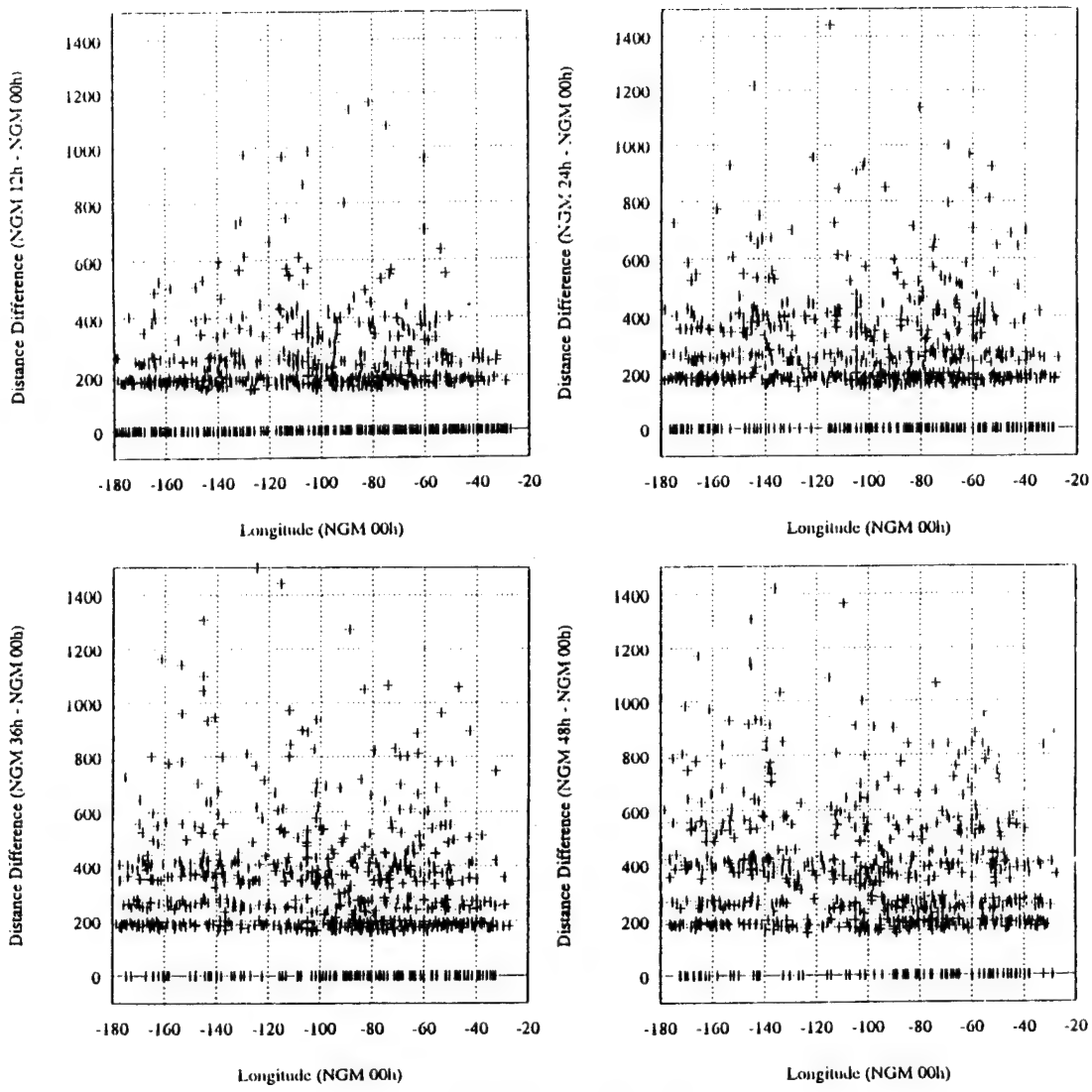

Figures 4.7a-d: Scatter diagrams depicting (forecast - analyzed) position vs longitude for forecast ranges 12, 24, 36, and 48h for NGM.

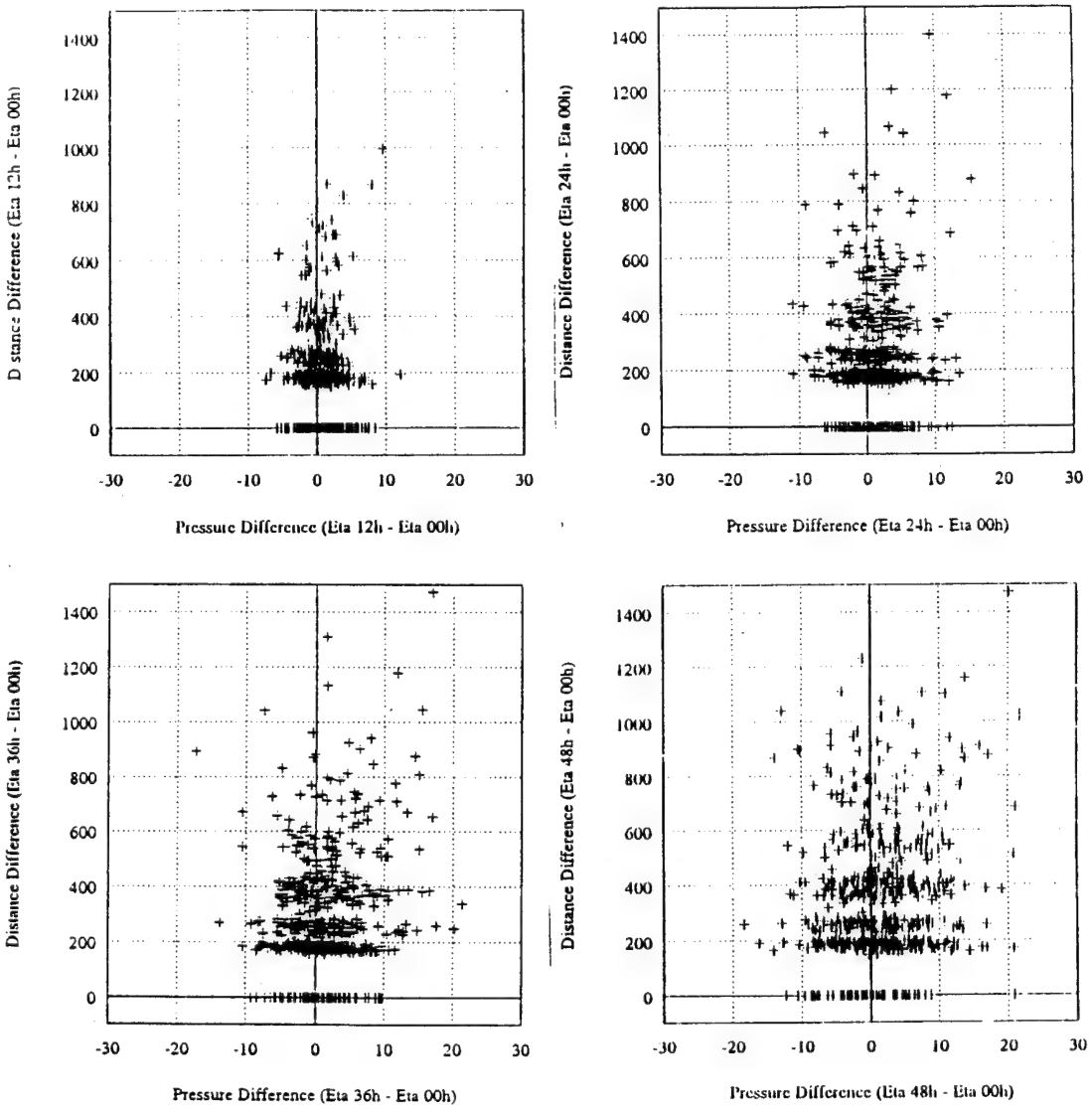

Figures 4.8a-d: As in Figures 4.6a-d, except for Eta Model.

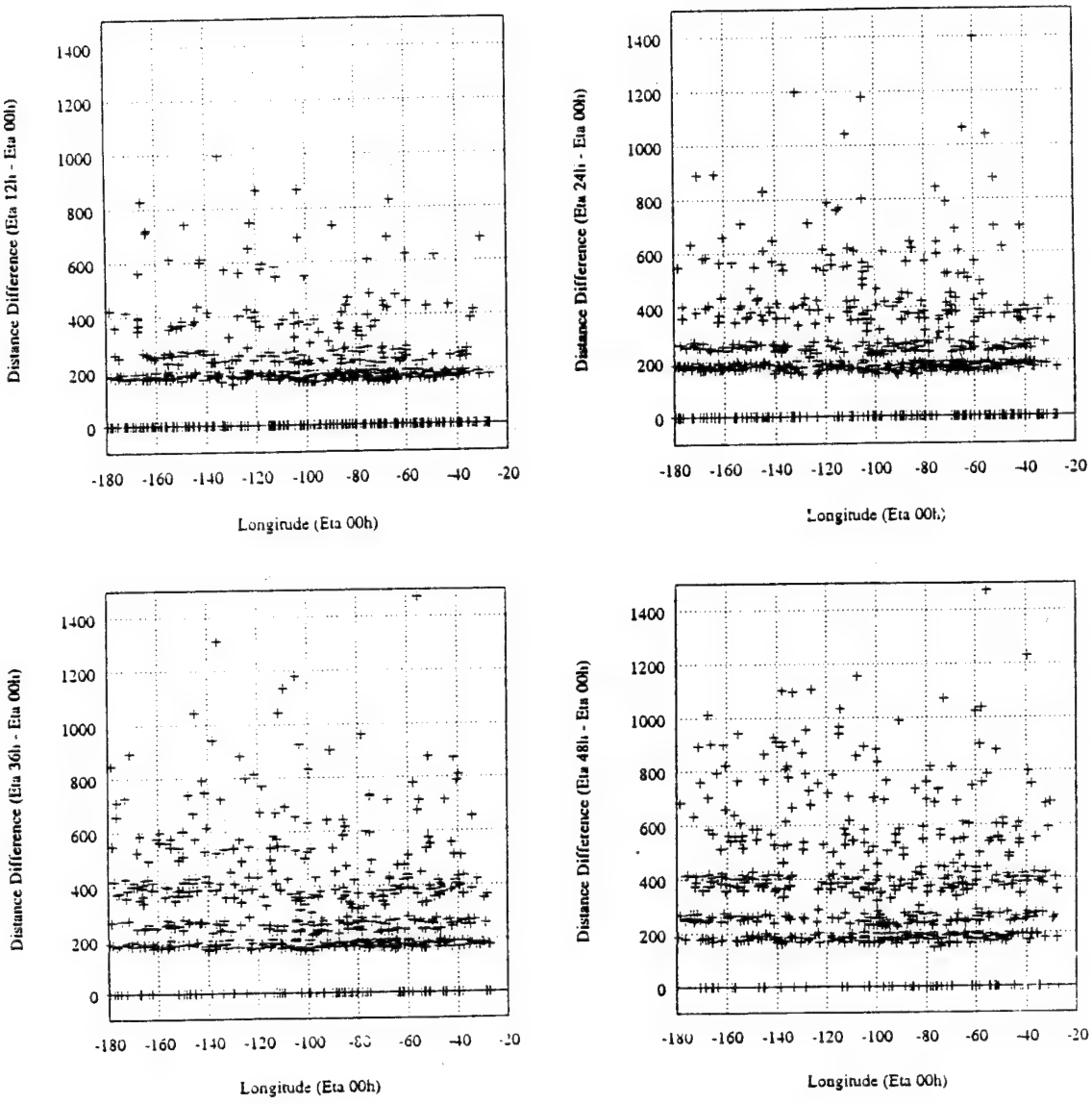

Figures 4.9a-d: As in Figures 4.7a-d, except for Eta Model.

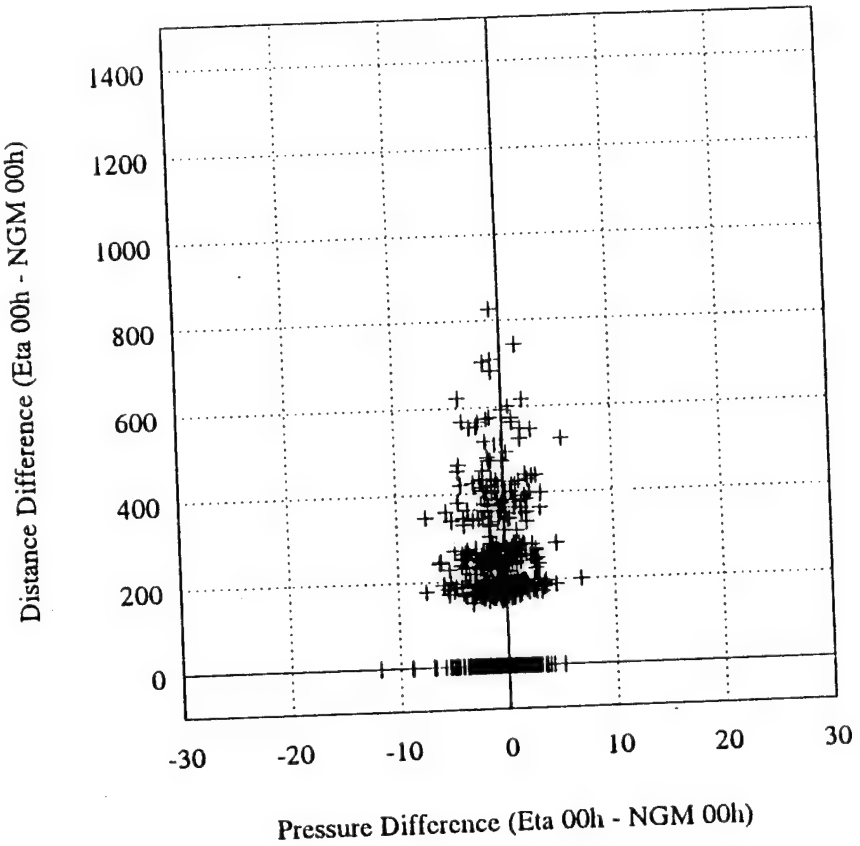

Figure 4.10: Scatter diagram depicting analyzed position differences (Eta - NGM) vs analyzed sea level pressure differences (Eta - NGM).

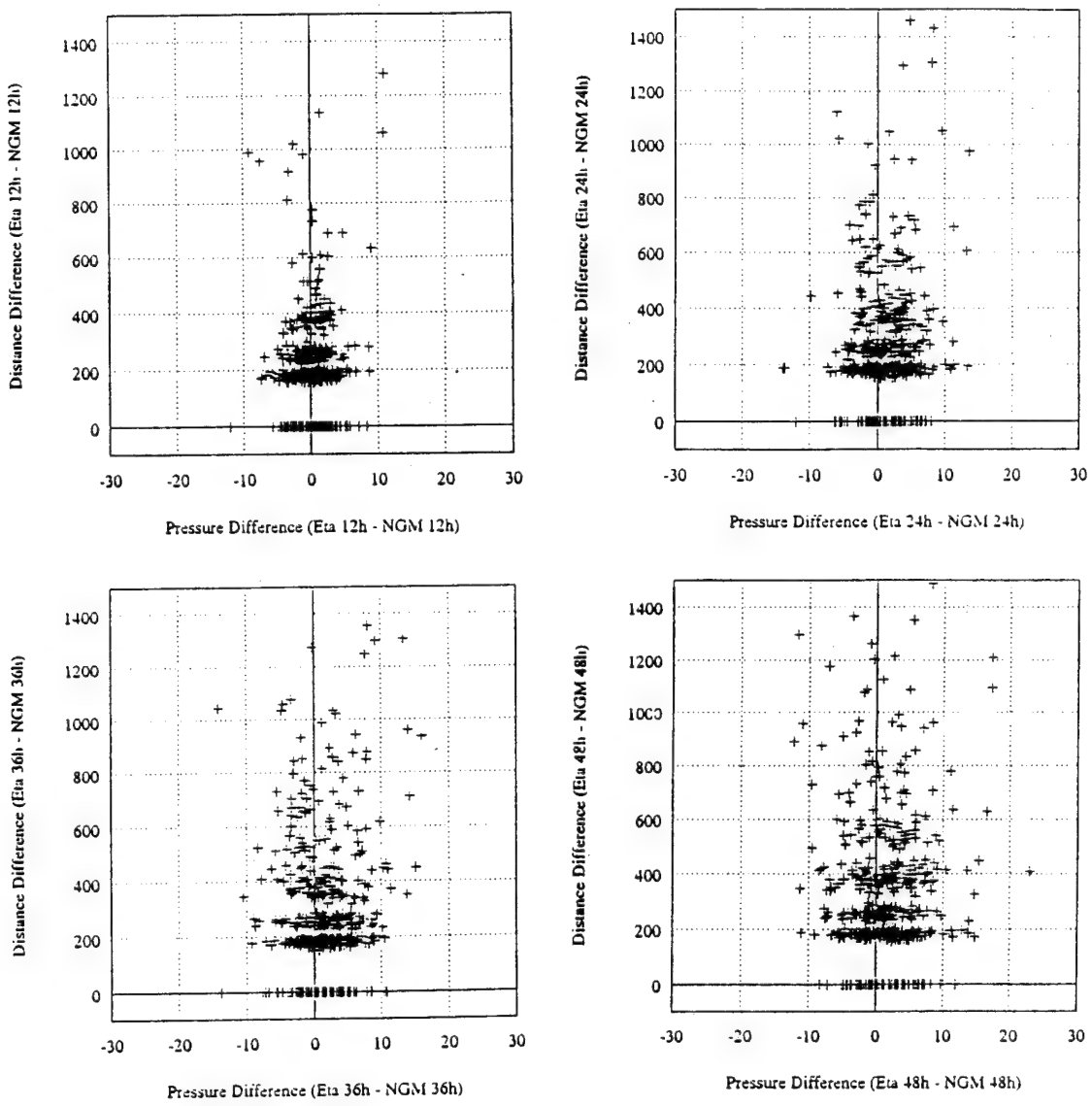

Figures 4.11a-d: As in Figure 4.10, except for forecast ranges 12, 24, 36, and 48h.

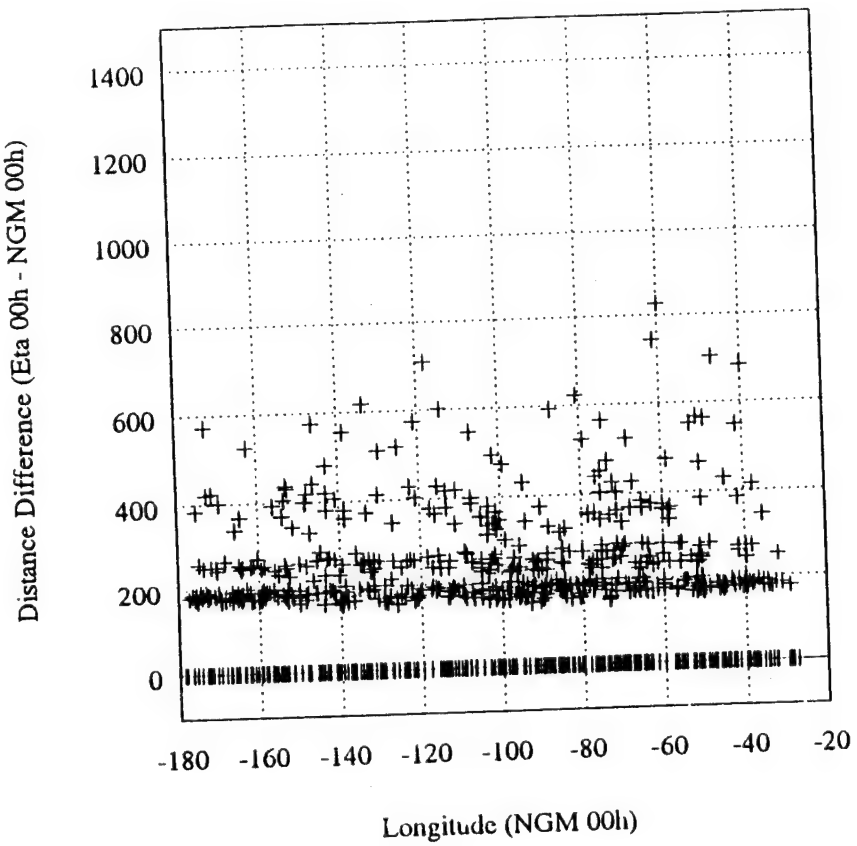

Figure 4.12: Scatter diagram depicting analyzed position differences (Eta - NGM) vs longitude.

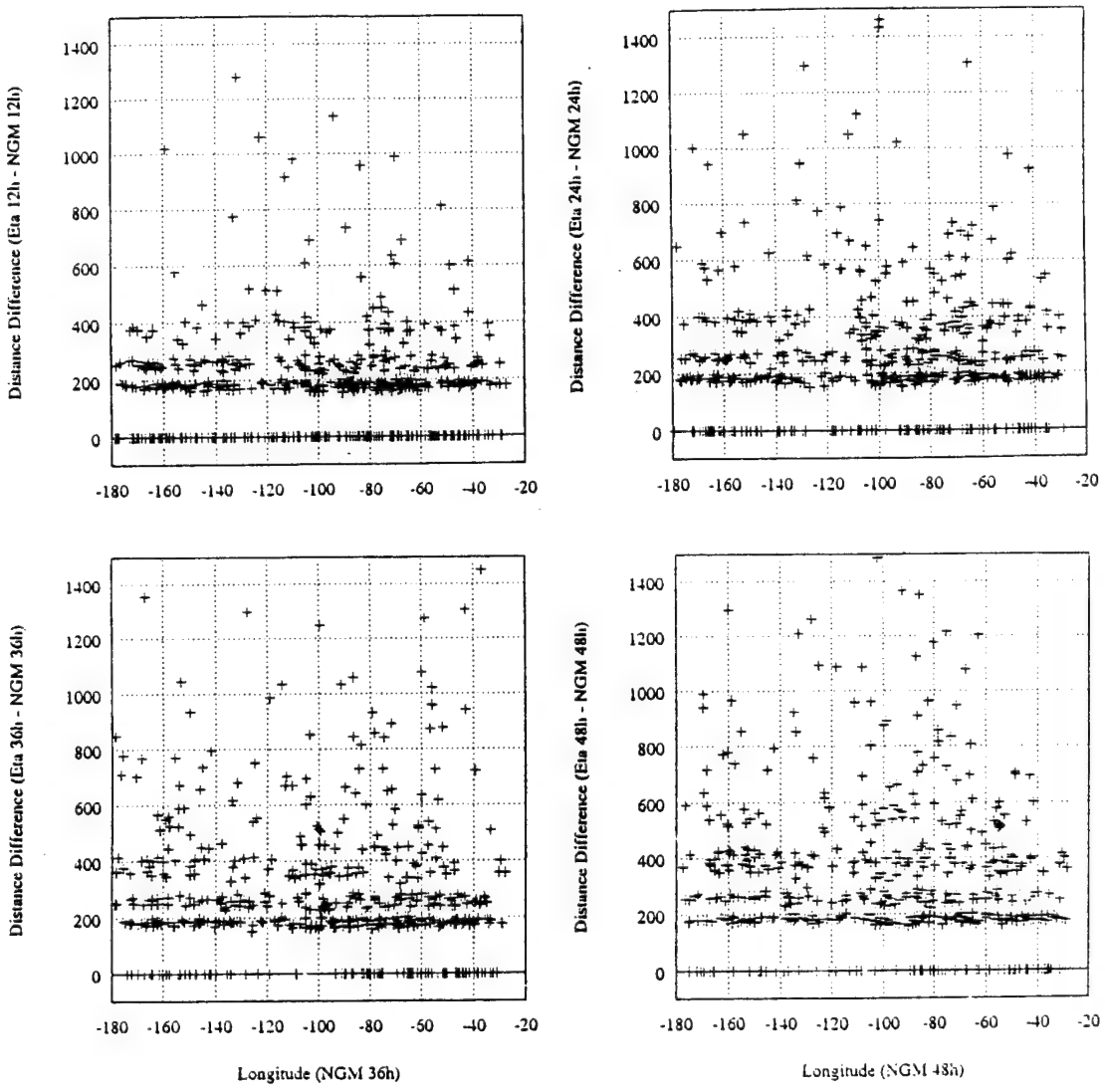

Figures 4.13a-d: As in Figure 4.12, except for forecast ranges 12, 24, 36, and 48h.

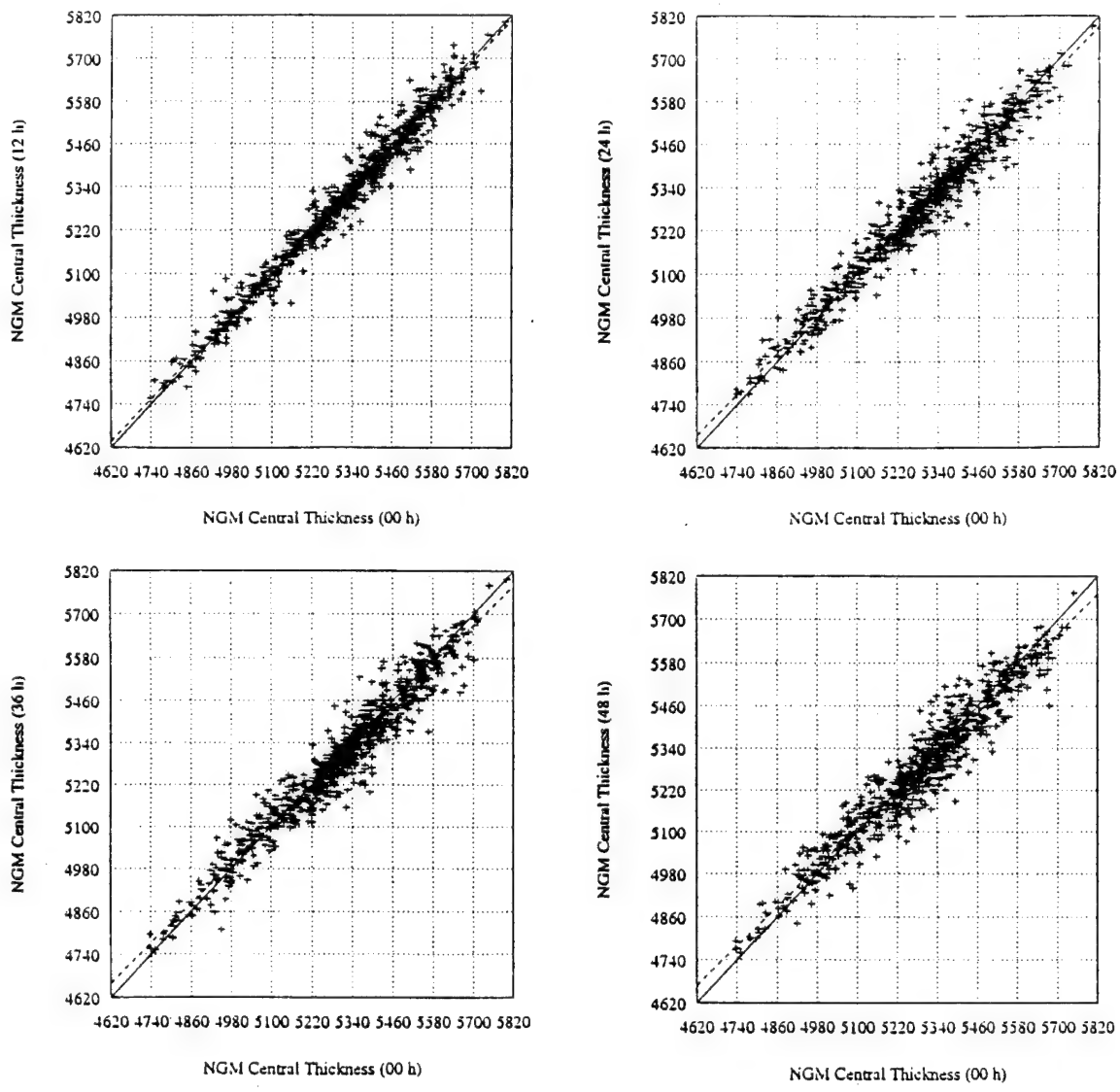

Figures 4.14a-d: Scatter diagrams depicting analyzed cyclone central 1000 - 500 mb thickness values vs forecast cyclone central 1000 - 500 mb thickness values for forecast ranges 12, 24, 36, and 48h for the NGM.

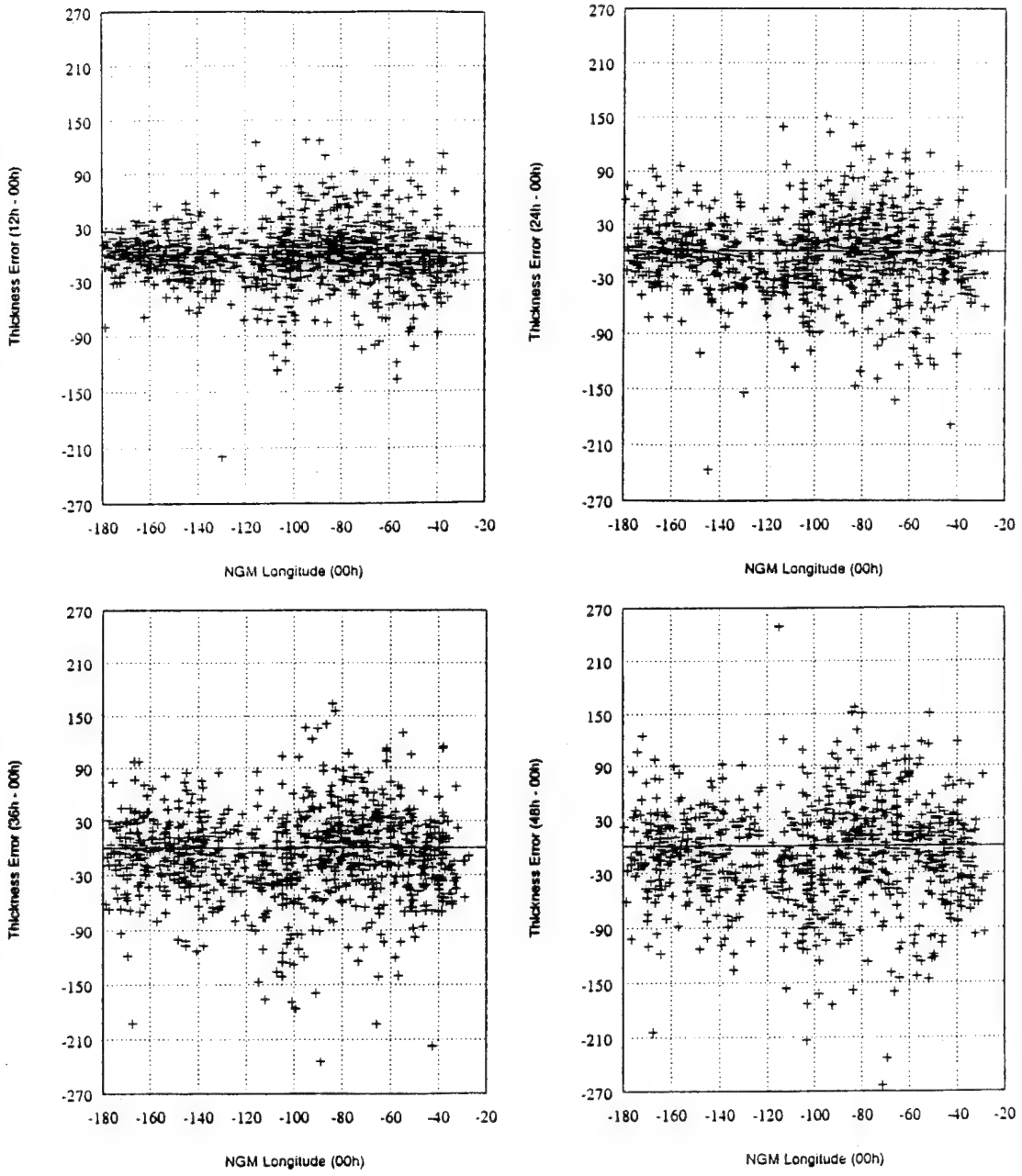

Figures 4.15a-d: Scatter diagrams depicting forecast cyclone central 1000 - 500 mb thickness errors vs longitude (00h) for forecast ranges 12, 24, 36, and 48h for the NGM.

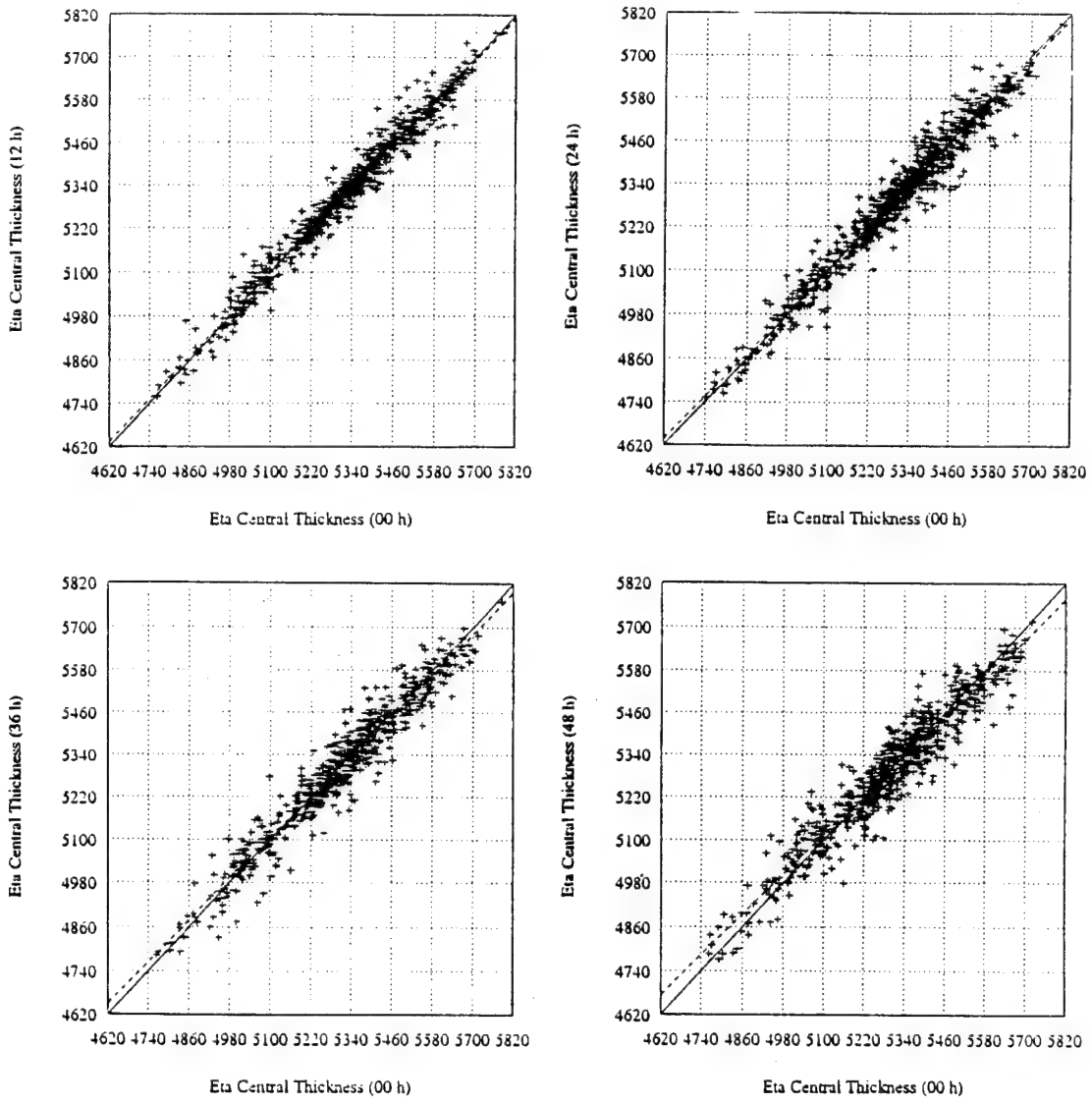

Figures 4.16a-d: As in Figures 4.14a-d, except for the Eta Model.

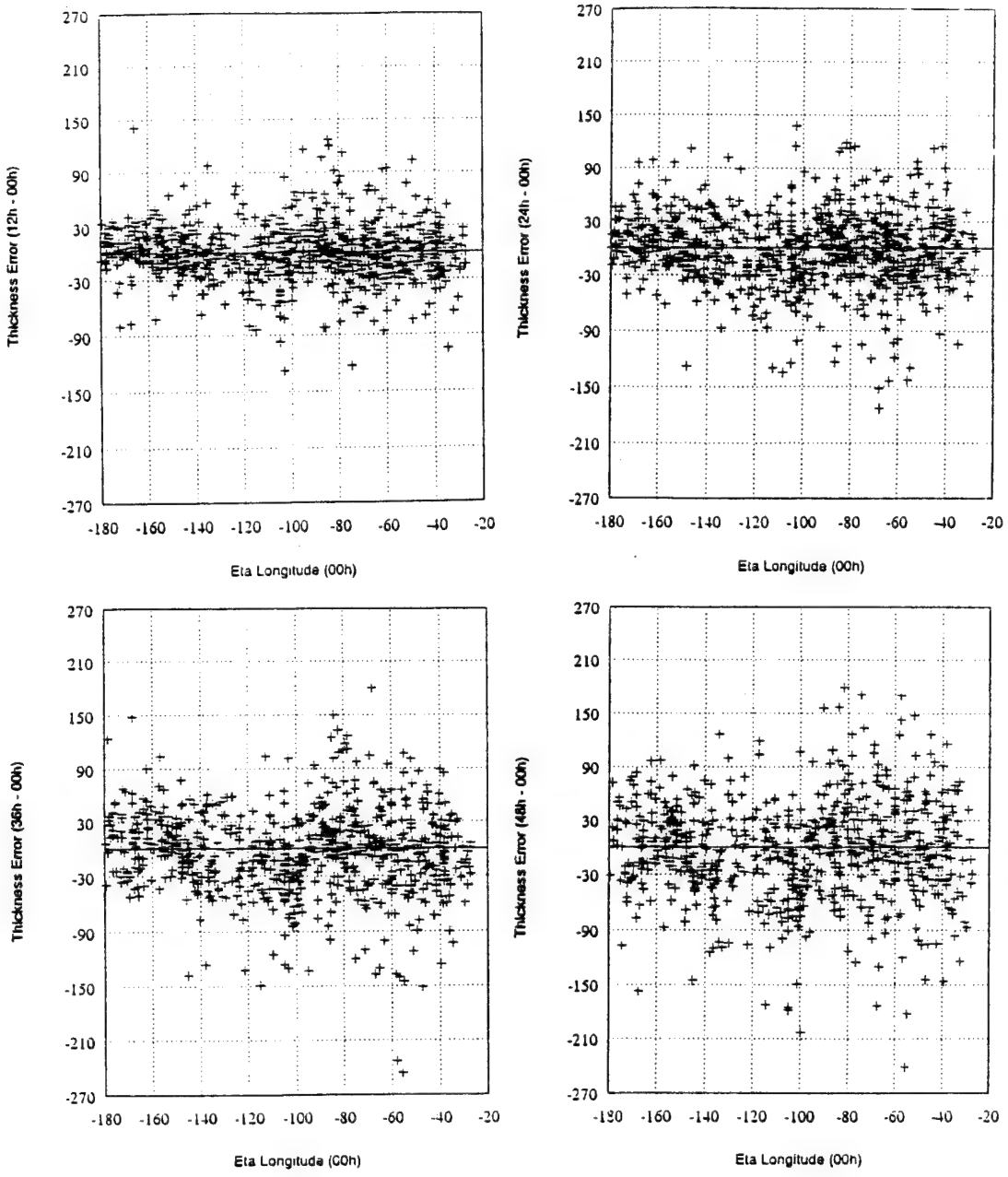

Figures 4.17a-d: As in Figures 4.15a-d, except for the Eta Model.

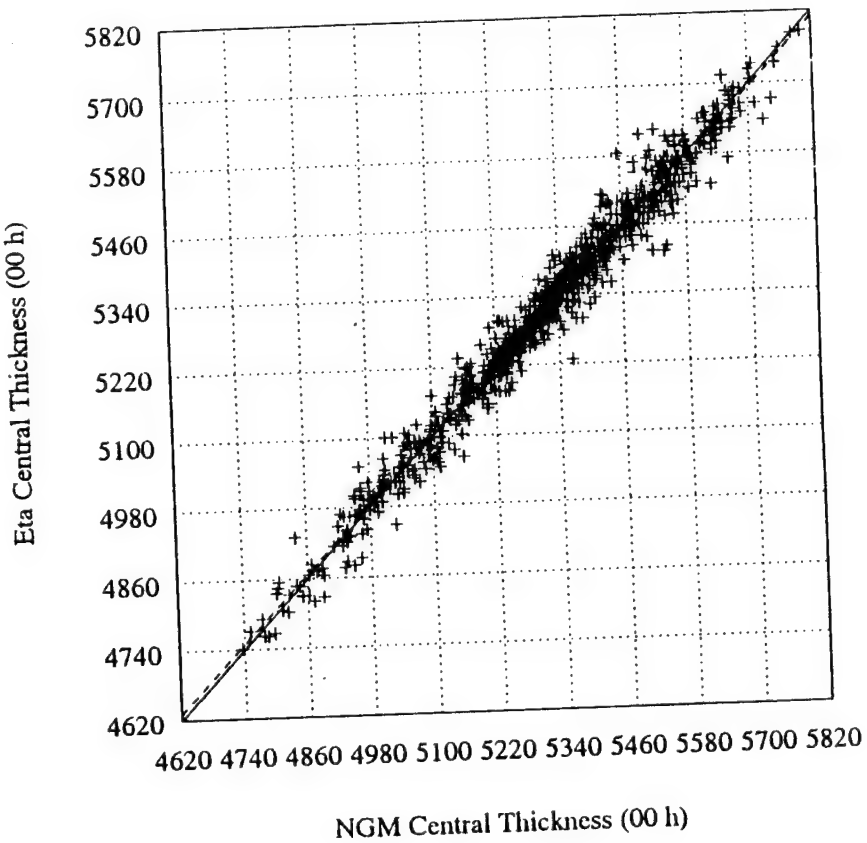

Figure 4.18: Scatter diagrams depicting NGM analyzed cyclone central 1000 - 500 mb thickness values vs Eta Model analyzed cyclone central 1000 - 500 mb thickness values.

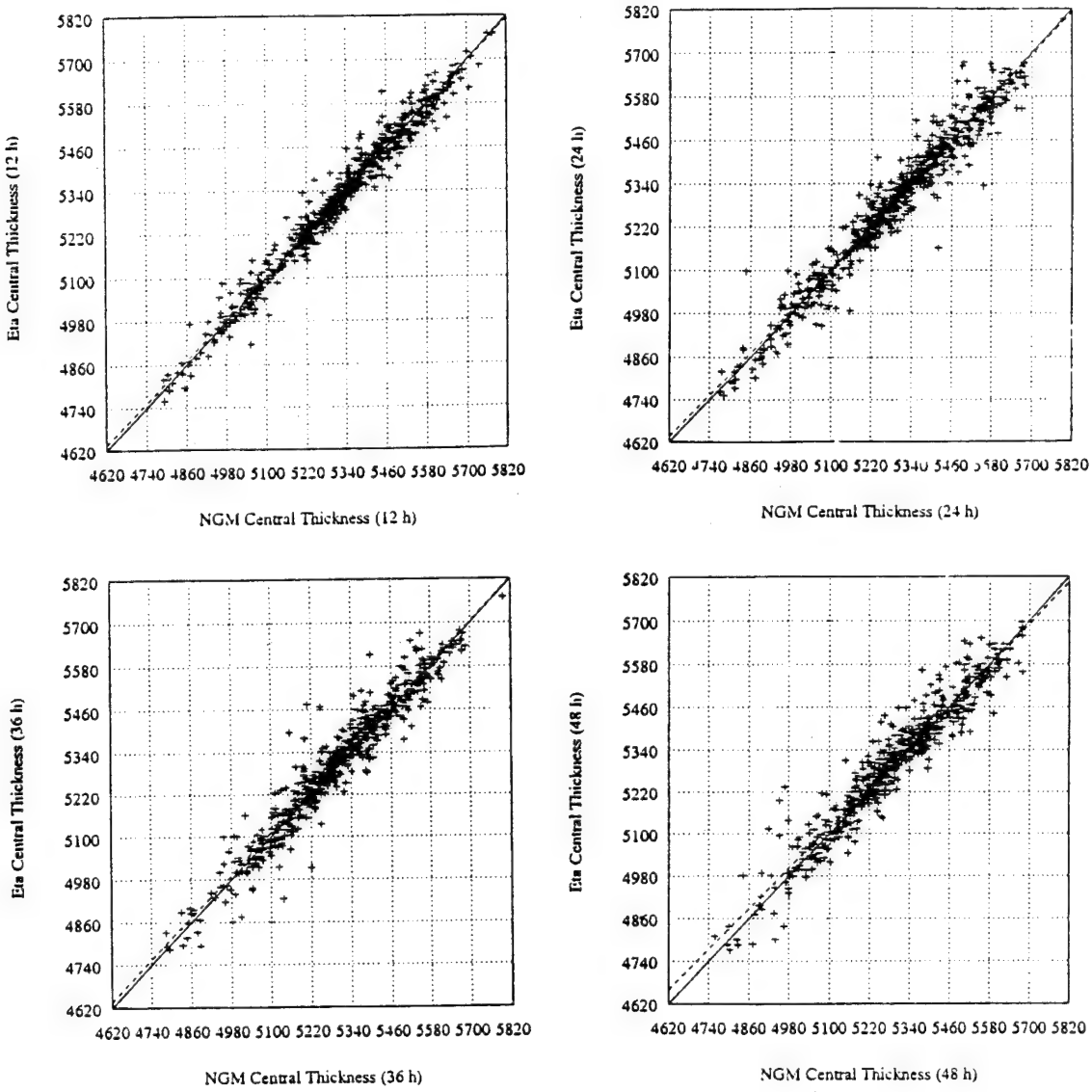

Figures 4.19a-d: As in Figure 4.18, except for forecast ranges 12, 24, 36, and 48h.

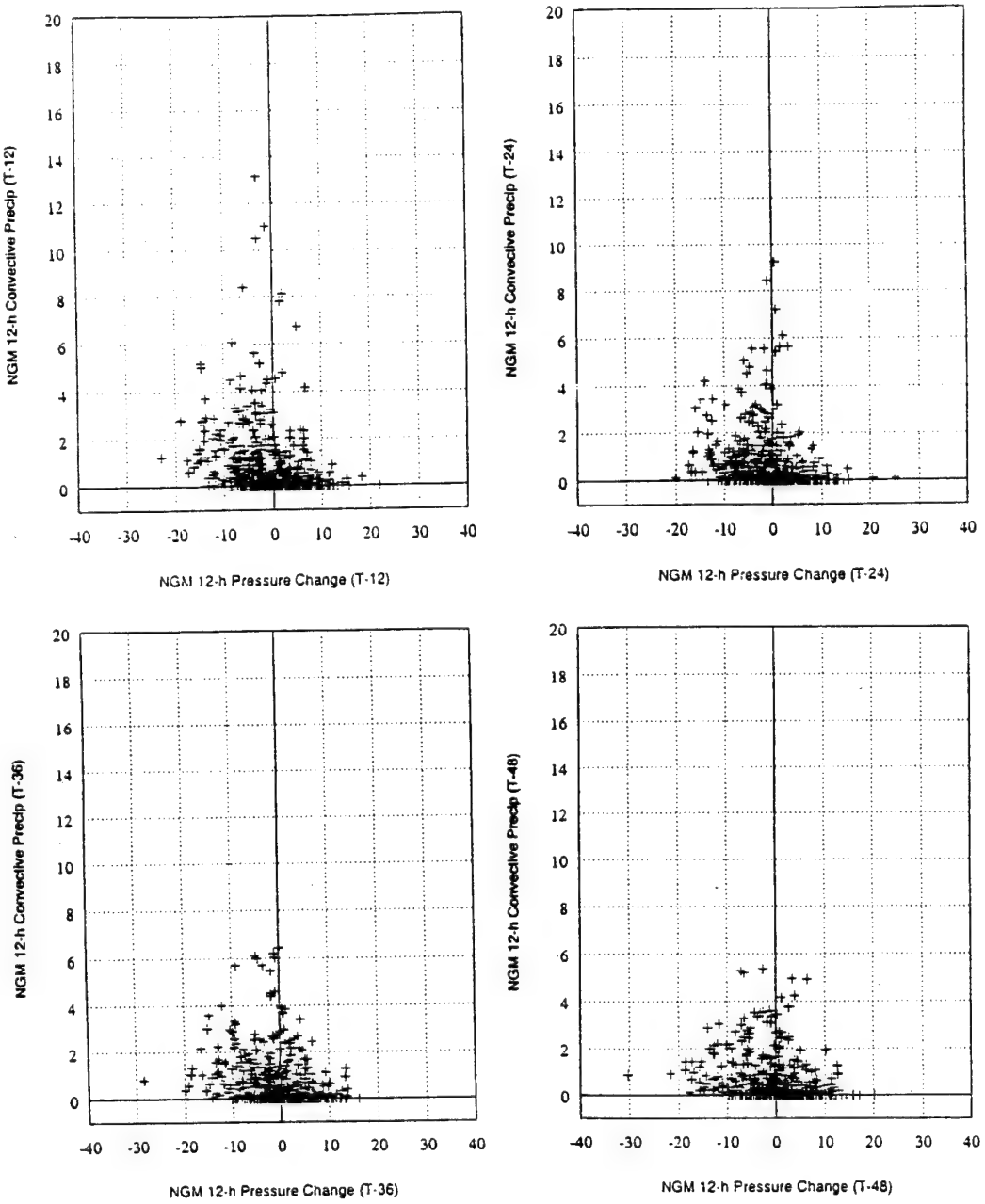

Figures 4.20a-d: Scatter diagrams depicting 12h cyclone central pressure change vs forecast convective precipitation for forecast ranges 12, 24, 36, and 48h for the NGM.

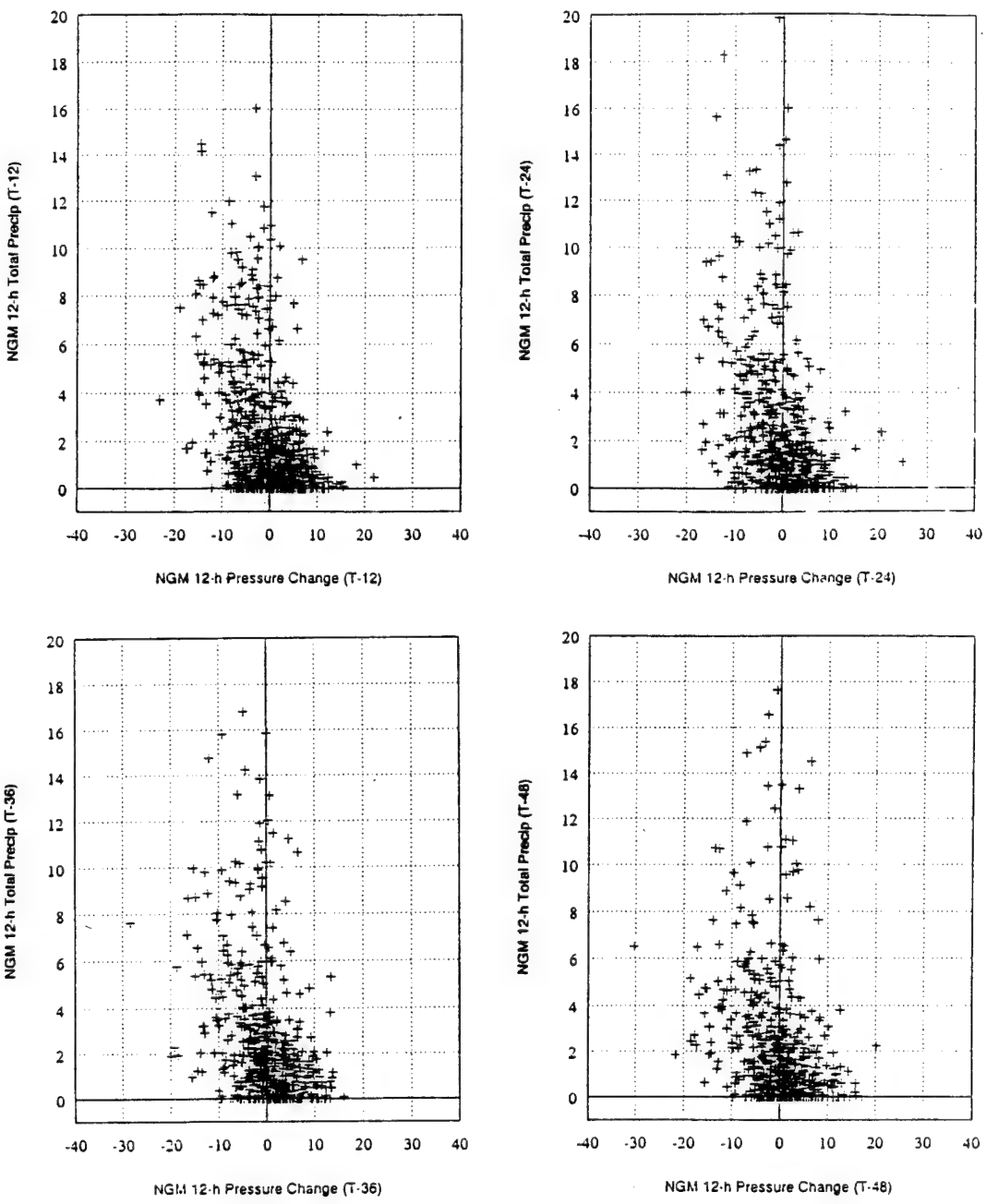

Figures 4.21a-d: As in Figures 4.20a-d, except for total precipitation.

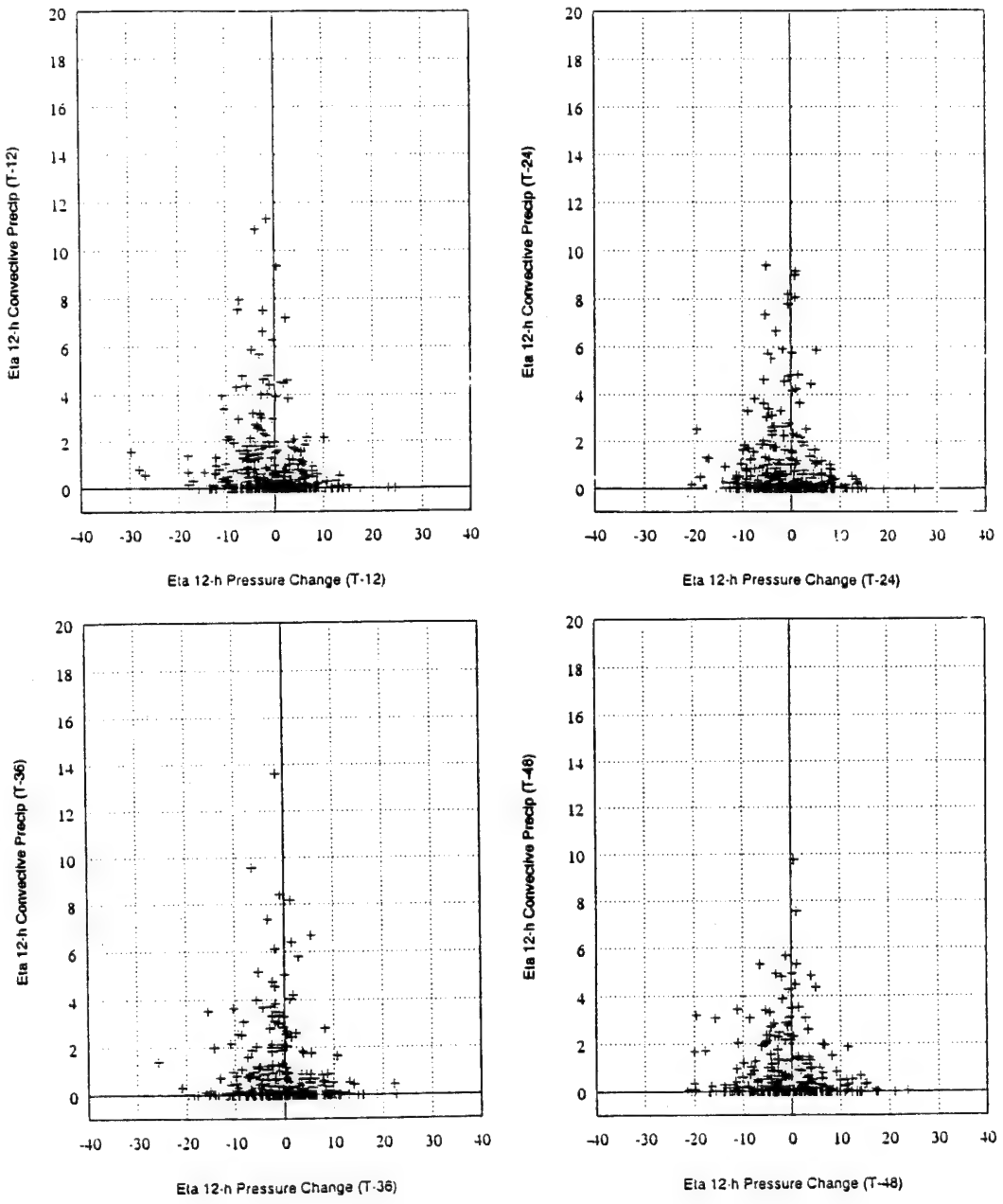

Figures 4.22a-d: As in Figures 4.20a-d, except for the Eta Model.

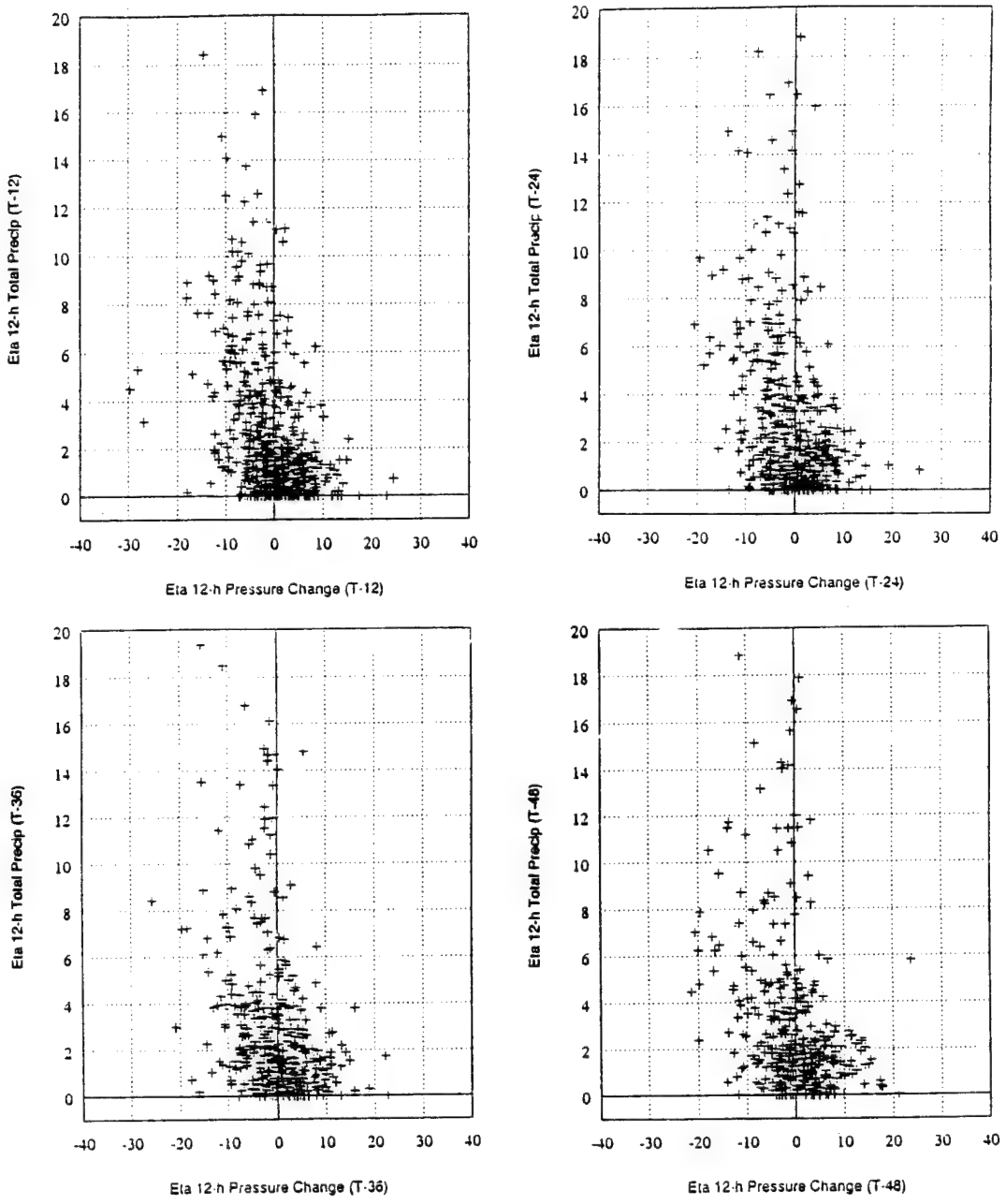

Figures 4.23a-d: As in Figures 4.20a-d, except for total precipitation and for the Eta Model.

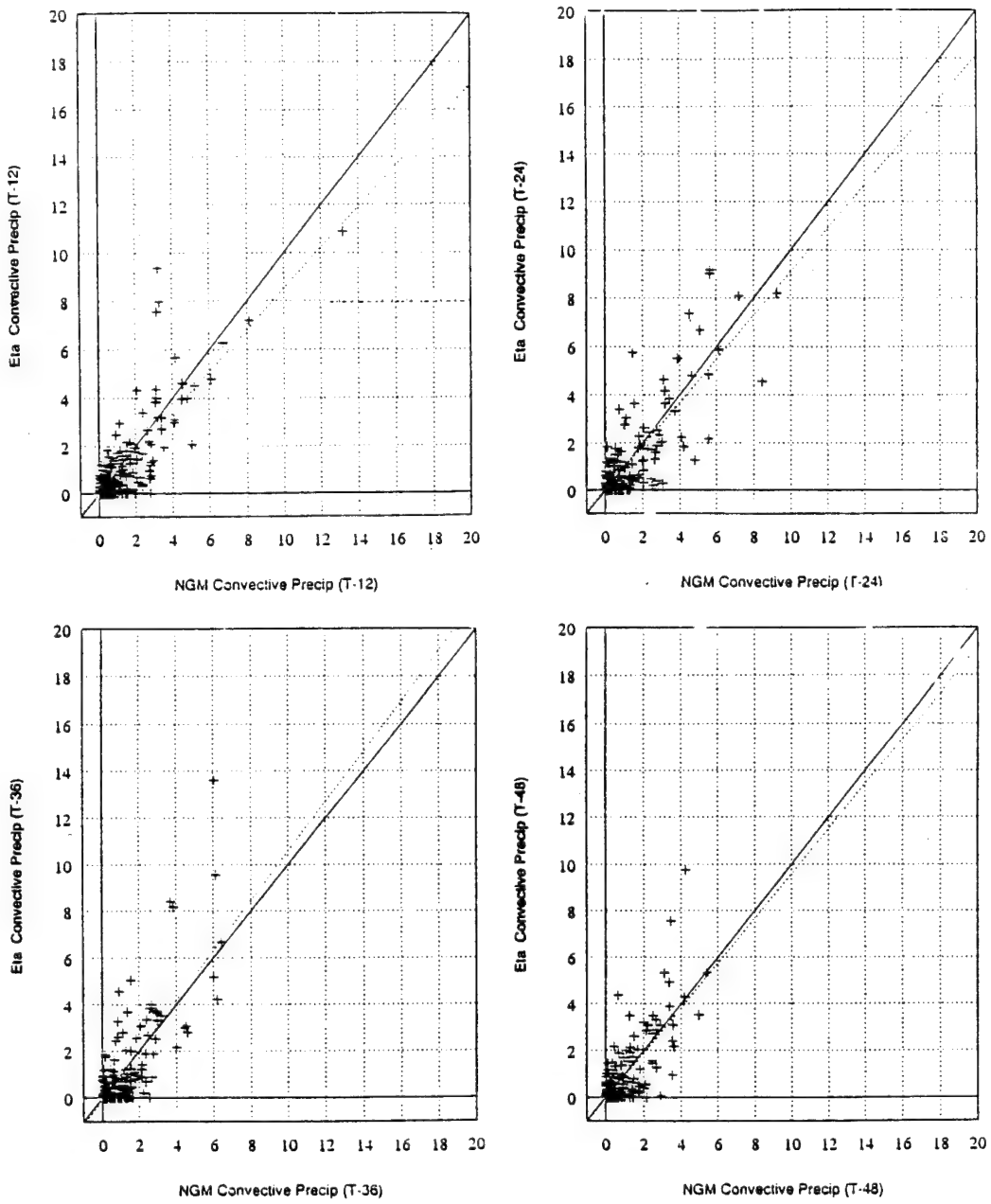

Figures 4.24a-d: Scatter diagrams depicting NGM forecast convective precipitation vs Eta forecast convective precipitation for forecast ranges 12, 24, 36, and 48h.

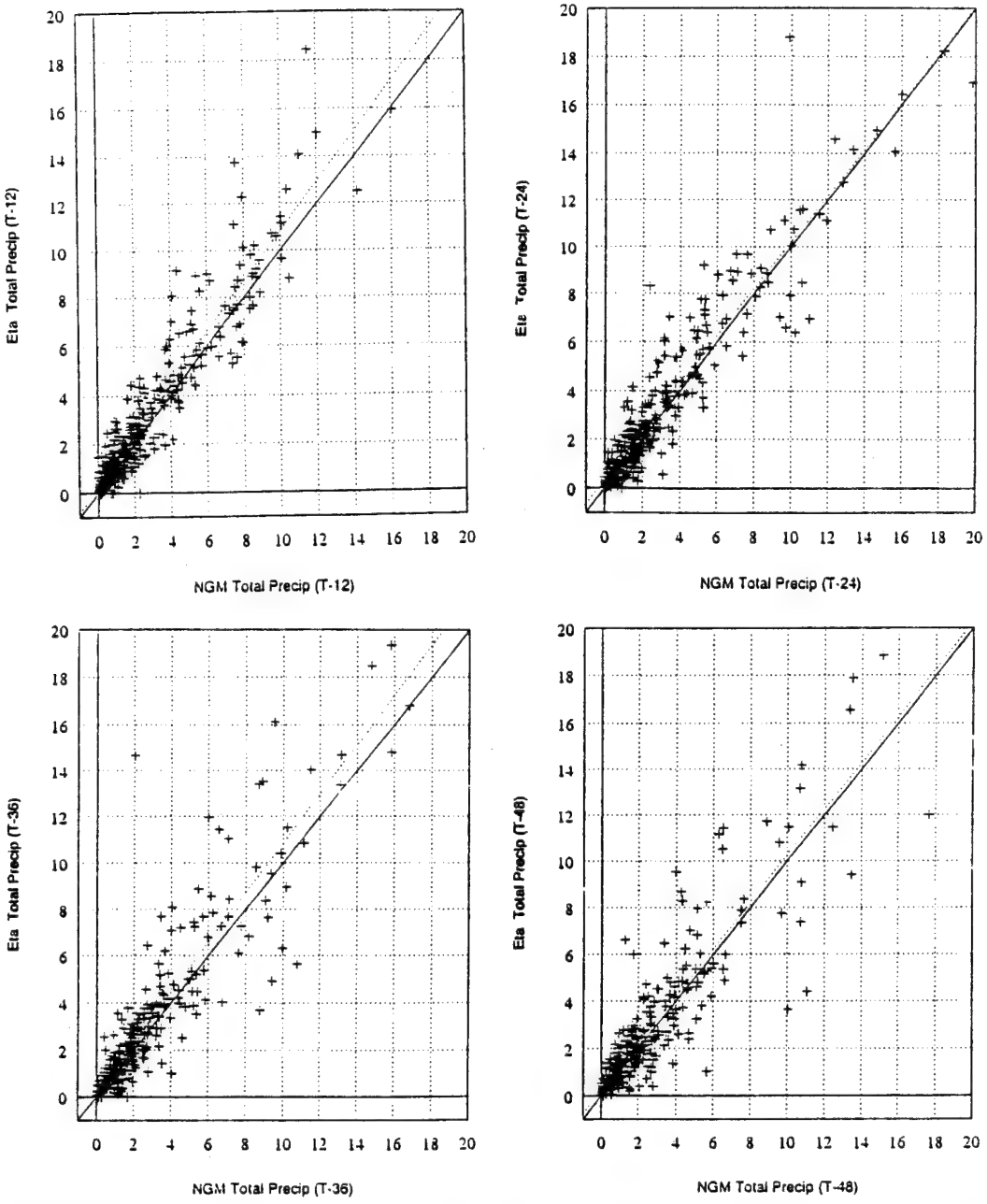

Figures 4.25a-d: As in Figures 4.24a-d, except for total precipitation.

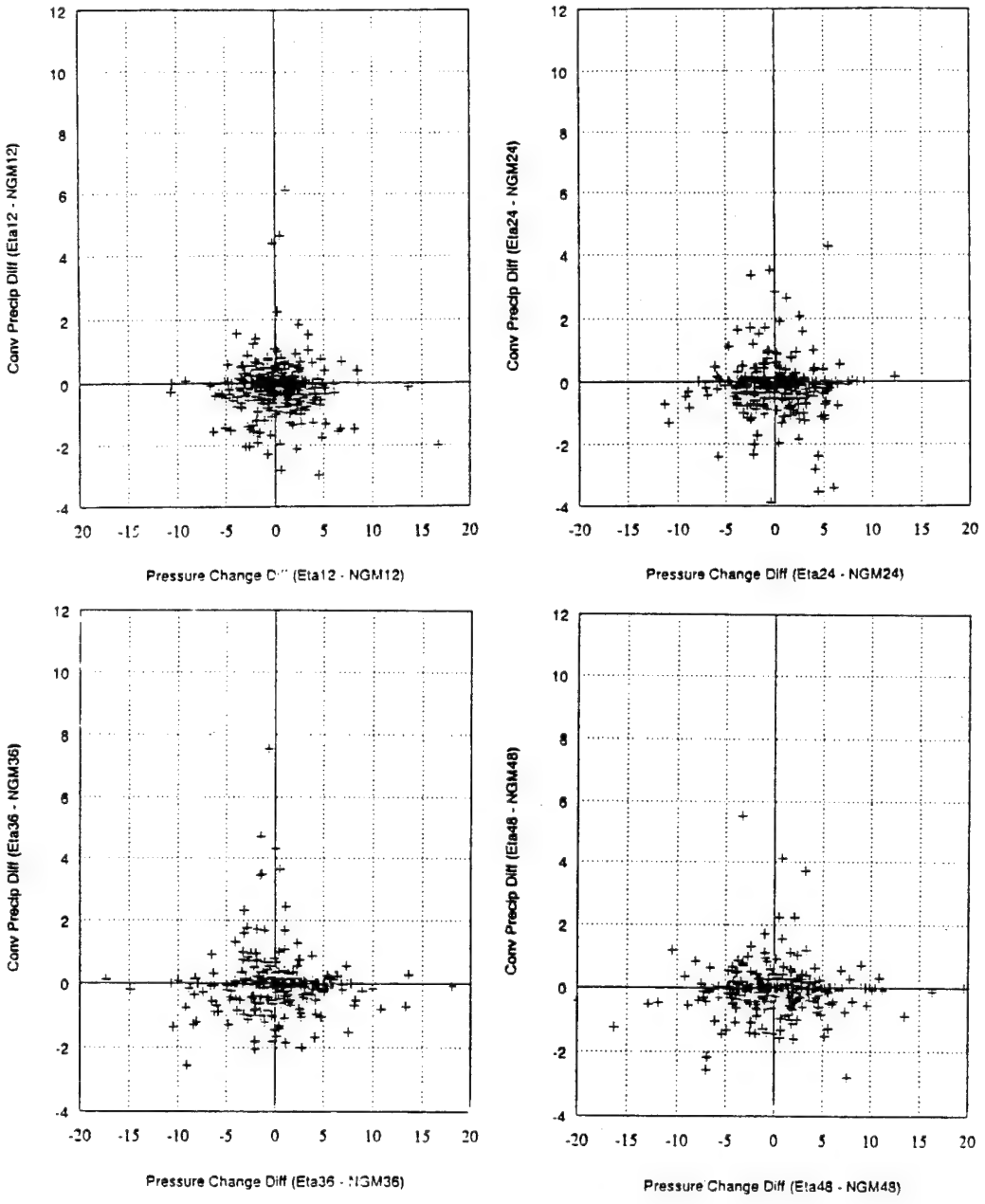

Figures 4.26a-d: Scatter diagrams depicting forecast sea level pressure change differences (Eta - NGM) vs forecast convective precipitation differences (Eta - NGM) for forecast ranges 12, 24, 36, and 48h.

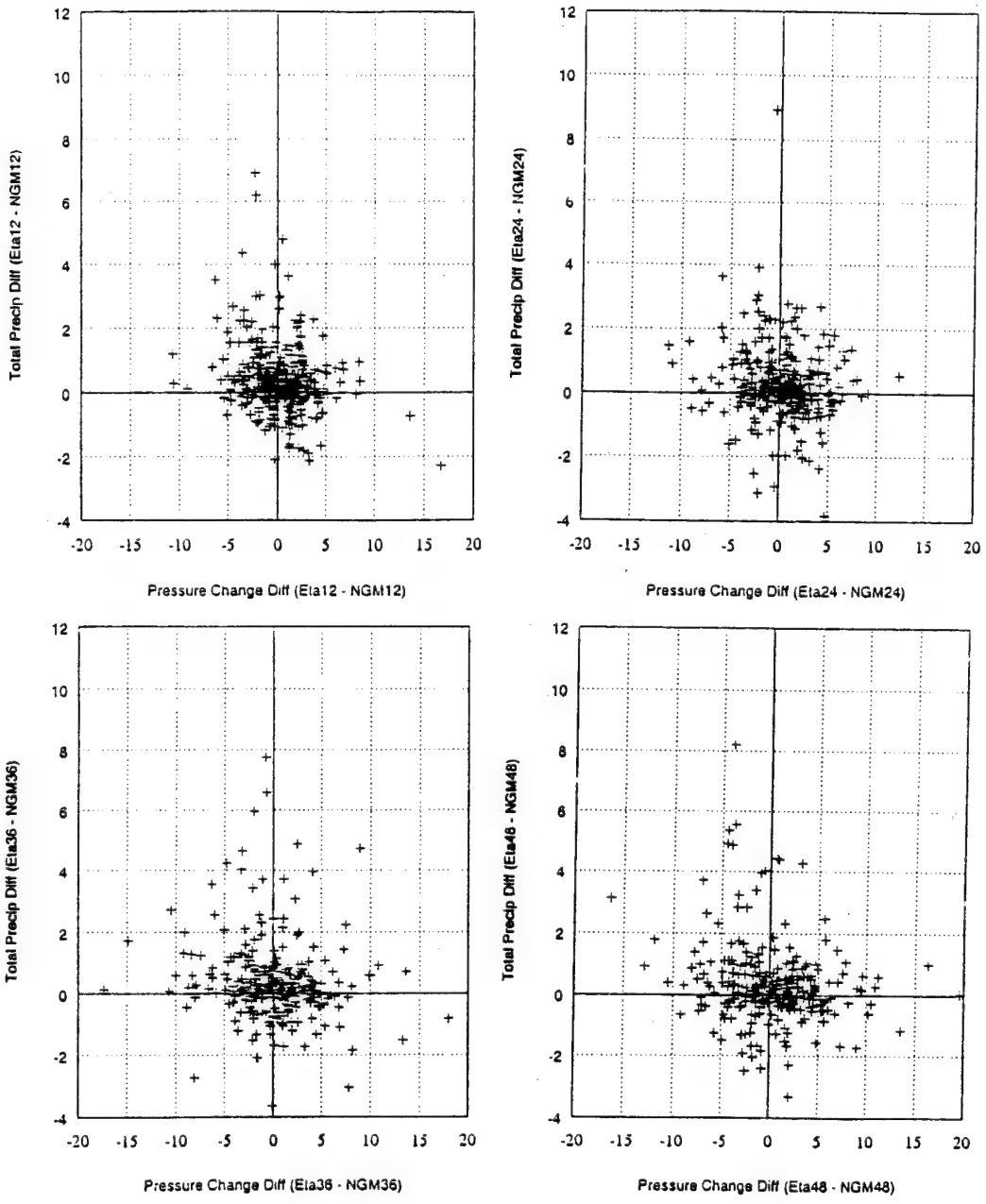

Figures 4.27a-d: As in Figures 4.26a-d, except for total precipitation.

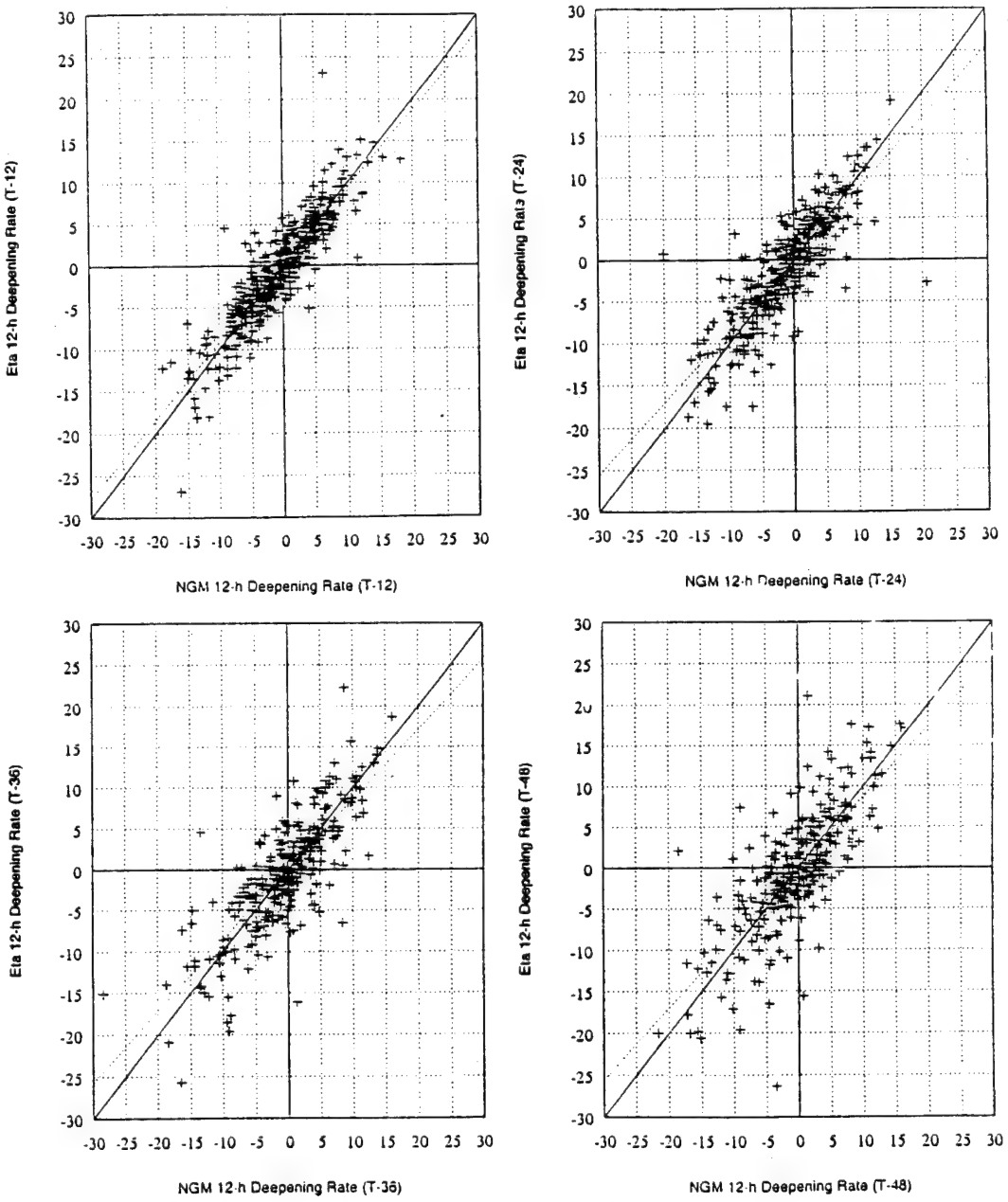

Figures 4.28a-d: Scatter diagrams depicting 12h deepening rates for the NGM vs 12h deepening rates for the Eta Model for forecast ranges of 12, 24, 36, and 48h.

V. SUMMARY AND RECOMMENDATIONS

This study examined the performance of the Eta numerical weather prediction model when compared to the NGM. Model output for the selected forecast ranges of 12h through 48h for each model was evaluated first against its own analysis. Then model output for the two models was compared for the analysis time (00h) through the forecast time 48h for the population of cyclones analyzed and forecast commonly by both models.

Because we are comparing the model forecasts against their own analysis we would tend to get a more favorable comparison than would be obtained from a manual analysis. Part of this difference may be a resolution effect inherent in the models. A manual analysis contains shorter wavelengths than a numerical prediction model can resolve due to smoothing out of shorter wavelengths (Pauley and Bramer 1992).

A. DISCUSSION AND CONCLUSIONS

1. Forecast Sea-Level Pressure Errors

The two models exhibited opposite trends when model forecast cyclone central pressure values were compared. The NGM exhibited a consistent negative forecast central pressure bias which increased almost linearly with time from 12h through 48h, yet remained less than 1 mb in magnitude. Smith and Mullen (1993) also identified a consistent bias toward the NGM over-deepening cyclone central pressure values but with a consistent negative error of about -.70 mb at 24h and 48h. Values at 12h and 36h were not calculated.

The Eta model, exhibited an opposite trend from the NGM, with a consistent positive bias in forecast cyclone central pressures observed. Error magnitudes started out at almost the same as those of the NGM at 12h and then in a non-linear fashion grew to over 1

mb by 24h and remained there with only slight further increases through 48h.

For the population of cyclones commonly analyzed by both models, the Eta Model mean central pressures averaged slightly lower than the NGM by about .5 mb. This trend quickly reversed, as the previous paragraph would imply, with the Eta Model forecasting an average of .4 mb higher than the NGM at 12h and an average of 1.1 mb higher by 24h. This trend continued through 48h. Upon further inspection of graphically compared forecast central pressure values, it becomes apparent that the largest single source of forecast error in central pressure emanates from the deepest few cyclones wherein the Eta Model exhibited the largest magnitudes in departure of forecast central pressure values from the NGM. This trend is significant but does not account completely for the overall positive pressure error in the Eta Model forecast values. In the population of cyclones studied, the most common location of the deepest few cyclones was the oceanic response with a strong bias toward the Western Atlantic. The largest average values of mean forecast pressure error, both positive and negative, was also observed in the case of the deepest few cyclones over oceanic regions, this time with a bias toward the data sparse Pacific Ocean Basin. Smith and Mullen (1993), also identified the largest areas of mean forecast pressure error (MPE), and standard deviation of the pressure error, (SPE), for the NGM and the Aviation Run (AVN) of the Global Spectral Model as data sparse oceanic regions, again with a bias toward the data sparse Pacific Ocean Basin.

2. Forecast Position Errors

Unlike the mean sea-level pressure forecast errors, forecast position errors for both models exhibited no distinct difference in magnitude. Forecast position errors for the two separate models increased nearly in step through 36h with the Eta Model exhibiting a slightly greater degree of error at 48h. Forecast position errors were also compared with forecast mean sea-level pressure

errors with no direct relationship between the sign or magnitude of the pressure errors and sign or magnitude of the position errors apparent. Forecast position errors were also plotted against longitude for both models. Unlike the case of mean forecast sea-level pressure errors (not shown in figures) where the larger magnitude errors occur over oceanic regions, there was little relationship between the magnitude of the cyclone forecast position error and geographical location. Smith and Mullen (1993), compared average displacement errors for the Nested Grid Model and Aviation run of the Global Spectral Model (AVN). Results illustrated overall slightly more accurate position forecasts by the AVN. Mean forecast position differences averaged 14 km at 24h and 31 km at 48h.

3. Forecast Thickness errors

In agreement with the results of Smith and Mullen (1993), the NGM exhibited a distinct cold bias in thickness values which increased proportionately with forecast time. An important observation noted in this net overall cold bias in the NGM is that the largest source of under-forecasting of thickness values lies in the warmer end of the spectrum. A bias toward the NGM over-forecasting the thickness of the coldest few cyclones is also apparent but is not as dramatic. The Eta Model also exhibited an overall cold bias at all but the 12h forecast time-frame where a slight positive value prevailed. It is observed that although the overall error in the Eta Model is negative, it is not as large in magnitude to that of the NGM, with a maximum value of -1.84 m at 48h instead of the -7 m observed in the NGM. The Eta Model ,like the NGM, exhibited a tendency to under-forecast the thickness of the warmest few cyclones, and to over-forecast the thickness of the coldest few cyclones. When the two models are compared there is, as expected from individual model analyses, a notable warm bias in the Eta Model forecast thickness values. The largest source of this

error, through graphical analysis is caused by a more dramatic tendency of the Eta Model to over-forecast the thickness of the deepest few cyclones as compared to the NGM with little forecast thickness difference in the warmest and mid-range thickness valued cyclones noted between the two models.

4. Precipitation and Cyclone Deepening Rate Errors.

Statistics on precipitation quantity within the closest 25 model grid points to the cyclone center for both convective and total categories for both models were generated and evaluated along with mean cyclone central pressure changes. The Eta Model exhibited a distinctly wetter trend for all four forecast periods in both precipitation categories than the NGM with the largest difference in the total precipitation category which mainly results from a large difference in stable precipitation values. As cyclones are separately viewed with progressively higher total precipitation values, a correlation between mean negative pressure change (deepening cyclone central pressures) and higher mean precipitation values becomes apparent for both models. This indicates the distinct probability of a measurable, positive latent heat release feedback mechanism inherent in the deepening of sea-level pressures for both models. This positive feedback mechanism is investigated in a study by Pauley and Smith (1988). The conclusion is reached that latent heat release has direct effects on a cyclone's evolution, as well as indirect effects which lead to a positive feedback mechanism in several other geophysical variables which also lead to greater development of the cyclone.

B. RECOMMENDATIONS FOR FURTHER RESEARCH

The results of this thesis suggest fruitful avenues of future research. First, continued research and analysis of Eta Model forecast tendencies of all major forecast variables will be invaluable as the Eta Model becomes the primary operational

numerical weather prediction model of the National Meteorological Center. Secondly, this thesis focused on only selected variables, with the major emphasis on sea-level pressure, thickness, and precipitation fields.

In future research, analysis could be undertaken on jet-level features with possible correlation to the cyclone statistics presented in this thesis. And finally, an observation of a probable positive feedback mechanism inherent in the correlation of higher precipitation values and deepening cyclone central pressures was observed. This is an area in which additional research, particularly in the area of oceanic and East Coast cyclogenesis would provide great benefits. A statistical comparison on individual cyclone model performance could also be undertaken, with emphasis on selected categories of cyclones such as intense oceanic cyclones or on selected geographical regions.

LIST OF REFERENCES

Black, T., D. Deaven, and G. DiMego, 1993: The Step-Mountain eta Coordinate Model: 80 km 'Early' Version and Objective Verifications. *Technical Procedures Bulletin* **412**. Development Division, National Meteorological Center, World Weather Building, Washington, DC 20233.

Black, T.L., 1994: The New NMC Mesoscale Eta Model: Description and Forecast Examples. *Wea. Forecasting*, **9**, 265-277.

Bonner, W.D., and R.A. Petersen, 1989: Recent Changes to NMC'S Analysis and Forecast System. *Wea. Forecasting*, **4**, 81-82.

Carr, F.H., R.L. Wobus, and R.A. Petersen, 1992: A Synoptic Evaluation of Normal Mode Initialization Experiments with the NMC Nested Grid Model. *Mon. Wea. Rev.*, **117**, 2753-2770.

DiMego, G.J., K.E. Mitchell, R.A. Petersen, J.A. Hoke, and J.P. Gerrity, 1992: Changes to NMC'S Regional Analysis and Forecast System. *Wea. Forecasting*, **7**, 185-198.

Hoke, J.E., N.A. Phillips, G.J. DiMego, J.J. Tucillio, and J.G. Sela, 1989: The Regional Analysis and Forecast System of the National Meteorological Center. *Wea. Forecasting*, **4**, 323-334.

Hoke, J.E., and Juang, H-M.H., 1992: Application of Fourth-Order Finite Differencing to the NMC Nested Grid Model. *Mon. Wea. Rev.*, **120**, 1767-1782.

Kuo, Y-H., and Low-Nam, S., 1990: Prediction of Nine Explosive Cyclones over the Western Atlantic Ocean with a Regional Model. *Mon. Wea. Rev.*, **118**, 3-24.

Pauley, P.M., and Bramer, B.J., 1992: The Effect of Resolution on the Depiction of Central Pressure for an Intense Oceanic Extratropical Cyclone. *Mon. Wea. Rev.*, **120**, 757-769.

Petersen, R.A., G.J. DiMego, J.E. Hoke, K.E. Mitchell, and J.E. Gerrity, 1991: Changes to NMC'S Regional Analysis and Forecast System. *Wea. Forecasting*, **6**, 133-141.

APPENDIX - DATA AVAILABILTY

This appendix lists specific data availability for both models. All data is considered available and usable unless a capital "M" appears in the designated space.

JANUARY 1994

DATE
11TH

FCST TIME	00	06	12	18	24	30	36	42	48
MODEL/RUN									
RGL 00Z									
12Z									
ETA 00Z	M	M	M	M	M	M	M		
12Z									

12TH

FCST TIME	00	06	12	18	24	30	36	42	48
MODEL/RUN									
RGL 00Z									
12Z									
ETA 00Z	M	M	M	M	M	M	M		
12Z									

13TH

FCST TIME	00	06	12	18	24	30	36	42	48
MODEL/RUN									
RGL 00Z									
12Z									
ETA 00Z	M	M	M	M	M	M	M		
12Z									

14TH

FCST TIME	00	06	12	18	24	30	36	42	48
MODEL/RUN									
RGL 00Z									
12Z									
ETA 00Z	M	M	M	M	M	M	M		
12Z									

15TH

FCST TIME	00	06	12	18	24	30	36	42	48
MODEL/RUN									
RGL 00Z									
12Z									
ETA 00Z	M	M	M	M	M	M	M		
12Z									

16TH

FCST TIME	00	06	12	18	24	30	36	42	48
MODEL/RUN									
RGL 00Z	M	M	M	M	M	M	M	M	M
12Z	M	M	M	M	M	M	M	M	M
ETA 00Z	M	M	M	M	M	M	M	M	M
12Z	M	M	M	M	M	M	M	M	M

17TH

FCST TIME	00	06	12	18	24	30	36	42	48
MODEL/RUN									
RGL 00Z									
12Z									
ETA 00Z	M	M	M	M	M	M	M		
12Z									

18TH

FCST TIME	00	06	12	18	24	30	36	42	48
MODEL/RUN									
RGL 00Z									
12Z									
ETA 00Z	M	M	M	M	M	M	M		
12Z									

19TH

FCST TIME	00	06	12	18	24	30	36	42	48
MODEL/RUN									
RGL 00Z									
12Z									
ETA 00Z	M	M	M	M	M	M	M		
12Z									

20TH

FCST TIME	00	06	12	18	24	30	36	42	48
MODEL/RUN									
RGL 00Z									
12Z									
ETA 00Z	M	M	M	M	M	M	M		
12Z									

21ST

FCST TIME	00	06	12	18	24	30	36	42	48
MODEL/RUN									
RGL 00Z									
12Z									
ETA 00Z	M	M	M	M	M	M	M		
12Z									

22ND

FCST TIME	00	06	12	18	24	30	36	42	48
MODEL/RUN									
RGL 00Z									
12Z									
ETA 00Z	M	M	M	M	M	M	M		
12Z									

23RD

FCST TIME	00	06	12	18	24	30	36	42	48
MODEL/RUN									
RGL 00Z									
12Z									
ETA 00Z	M	M	M	M	M	M	M		
12Z									

24TH

FCST TIME	00	06	12	18	24	30	36	42	48
MODEL/RUN									
RGL 00Z									
12Z									
ETA 00Z	M	M	M	M	M	M	M		
12Z									

25TH

FCST TIME	00	06	12	18	24	30	36	42	48
MODEL/RUN									
RGL 00Z									
12Z									
ETA 00Z									
12Z									

26TH

FCST TIME	00	06	12	18	24	30	36	42	48
MODEL/RUN									
RGL 00Z									
12Z									
ETA 00Z									
12Z									

27TH

FCST TIME	00	06	12	18	24	30	36	42	48
MODEL/RUN									
RGL 00Z	M	M	M	M	M	M	M	M	M
12Z	M	M	M	M	M	M	M	M	M
ETA 00Z	M	M	M	M	M	M	M	M	M
12Z	M	M	M	M	M	M	M	M	M

28TH

FCST TIME	00	06	12	18	24	30	36	42	48
MODEL/RUN									
RGL 00Z									
12Z									
ETA 00Z									
12Z									

29TH

FCST TIME	00	06	12	18	24	30	36	42	48
MODEL/RUN									
RGL 00Z									
12Z									
ETA 00Z									
12Z									

30TH

FCST TIME	00	06	12	18	24	30	36	42	48
MODEL/RUN									
RGL 00Z									
12Z									
ETA 00Z									
12Z									

31ST

FCST TIME	00	06	12	18	24	30	36	42	48
MODEL/RUN									
RGL 00Z									
12Z									
ETA 00Z									
12Z									

FEBRUARY

1ST

FCST TIME	00	06	12	18	24	30	36	42	48
MODEL/RUN									
RGL 00Z									
12Z									
ETA 00Z									
12Z									

2ND

FCST TIME	00	06	12	18	24	30	36	42	48
MODEL/RUN									
RGL 00Z									
12Z									
ETA 00Z									
12Z									

3RD

FCST TIME	00	06	12	18	24	30	36	42	48
MODEL/RUN									
RGL 00Z									
12Z									
ETA 00Z									
12Z									

4TH

FCST TIME	00	06	12	18	24	30	36	42	48
MODEL/RUN									
RGL 00Z									
12Z			M	M	M	M	M	M	M
ETA 00Z									
12Z				M					

5TH

FCST TIME	00	06	12	18	24	30	36	42	48
MODEL/RUN									
RGL 00Z	M	M	M	M	M	M	M	M	M
12Z	M	M	M	M	M	M	M	M	M
ETA 00Z	M	M	M	M	M	M	M	M	M
12Z	M	M	M	M	M	M	M	M	M

6TH

FCST TIME__00___06___12___18___24___30___36___42___48__
MODEL/RUN
 RGL 00Z
     12Z
 ETA 00Z
     12Z

7TH

FCST TIME__00___06___12___18___24___30___36___42___48__
MODEL/RUN
 RGL 00Z
     12Z
 ETA 00Z
     12Z

8TH

FCST TIME__00___06___12___18___24___30___36___42___48__
MODEL/RUN
 RGL 00Z
     12Z
 ETA 00Z
     12Z

9TH

FCST TIME__00___06___12___18___24___30___36___42___48__
MODEL/RUN
 RGL 00Z
     12Z
 ETA 00Z
     12Z

10TH

FCST TIME__00___06___12___18___24___30___36___42___48__
MODEL/RUN
 RGL 00Z
     12Z
 ETA 00Z
     12Z

11TH

FCST TIME__00___06___12___18___24___30___36___42___48__
MODEL/RUN
 RGL 00Z
     12Z
 ETA 00Z
     12Z

12TH

FCST TIME__00___06___12___18___24___30___36___42___48__
MODEL/RUN
RGL 00Z
12Z
ETA 00Z
12Z

13TH

FCST TIME__00___06___12___18___24___30___36___42___48__
MODEL/RUN
RGL 00Z
12Z
ETA 00Z
12Z

14TH

FCST TIME__00___06___12___18___24___30___36___42___48__
MODEL/RUN
RGL 00Z
12Z
ETA 00Z
12Z

15TH

FCST TIME__00___06___12___18___24___30___36___42___48__
MODEL/RUN
RGL 00Z
12Z
ETA 00Z
12Z

16TH

FCST TIME__00___06___12___18___24___30___36___42___48__
MODEL/RUN
RGL 00Z
12Z
ETA 00Z
12Z

17TH

FCST TIME__00___06___12___18___24___30___36___42___48__
MODEL/RUN
RGL 00Z
12Z
ETA 00Z
12Z

18TH

FCST TIME__00___06___12___18___24___30___36___42___48__
MODEL/RUN
RGL 00Z
12Z
ETA 00Z
12Z

19TH

FCST TIME__00___06___12___18___24___30___36___42___48__
MODEL/RUN
RGL 00Z
12Z
ETA 00Z
12Z

20TH

FCST TIME__00___06___12___18___24___30___36___42___48__
MODEL/RUN
RGL 00Z
12Z
ETA 00Z
12Z

21ST

FCST TIME__00___06___12___18___24___30___36___42___48__
MODEL/RUN
RGL 00Z
12Z
ETA 00Z
12Z

22ND

FCST TIME__00___06___12___18___24___30___36___42___48__
MODEL/RUN
RGL 00Z
12Z
ETA 00Z
12Z

23RD

FCST TIME__00___06___12___18___24___30___36___42___48__
MODEL/RUN
RGL 00Z
12Z
ETA 00Z
12Z

24TH

FCST TIME__00___06___12___18___24___30___36___42___48__
MODEL/RUN
 RGL 00Z
     12Z
 ETA 00Z
     12Z

25TH

FCST TIME__00___06___12___18___24___30___36___42___48__
MODEL/RUN
 RGL 00Z
     12Z
 ETA 00Z
     12Z

26TH

FCST TIME__00___06___12___18___24___30___36___42___48__
MODEL/RUN
 RGL 00Z
     12Z
 ETA 00Z
     12Z

M

27TH

FCST TIME__00___06___12___18___24___30___36___42___48__
MODEL/RUN
 RGL 00Z
     12Z
 ETA 00Z
     12Z

28TH

FCST TIME__00___06___12___18___24___30___36___42___48__
MODEL/RUN
 RGL 00Z
     12Z
 ETA 00Z
     12Z

MARCH

1ST

FCST TIME	00	06	12	18	24	30	36	42	48
MODEL/RUN									
RGL 00Z									
12Z									
ETA 00Z									
12Z									

2ND

FCST TIME	00	06	12	18	24	30	36	42	48
MODEL/RUN									
RGL 00Z									
12Z									
ETA 00Z									
12Z									

3RD

FCST TIME	00	06	12	18	24	30	36	42	48
MODEL/RUN									
RGL 00Z									
12Z	M	M	M	M	M	M	M	M	M
ETA 00Z									
12Z	M	M	M	M	M	M	M	M	M

4TH

FCST TIME	00	06	12	18	24	30	36	42	48
MODEL/RUN									
RGL 00Z									
12Z									
ETA 00Z									
12Z									

5TH

FCST TIME	00	06	12	18	24	30	36	42	48
MODEL/RUN									
RGL 00Z									
12Z									
ETA 00Z									
12Z									

6TH

FCST TIME__00___06___12___18___24___30___36___42___48__
MODEL/RUN
 RGL 00Z
     12Z
 ETA 00Z
     12Z

7TH

FCST TIME__00___06___12___18___24___30___36___42___48__
MODEL/RUN
 RGL 00Z
     12Z
 ETA 00Z
     12Z

8TH

FCST TIME__00___06___12___18___24___30___36___42___48__
MODEL/RUN
 RGL 00Z
     12Z
 ETA 00Z
     12Z

9TH

FCST TIME__00___06___12___18___24___30___36___42___48__
MODEL/RUN
 RGL 00Z
     12Z
 ETA 00Z
     12Z

10TH

FCST TIME__00___06___12___18___24___30___36___42___48__
MODEL/RUN
 RGL 00Z
     12Z
 ETA 00Z
     12Z

11TH

FCST TIME__00___06___12___18___24___30___36___42___48__
MODEL/RUN
 RGL 00Z
     12Z
 ETA 00Z
     12Z

12TH

FCST TIME__00___06___12___18___24___30___36___42___48__
MODEL/RUN
 RGL 00Z
     12Z
 ETA 00Z
     12Z

13TH

FCST TIME__00___06___12___18___24___30___36___42___48__
MODEL/RUN
 RGL 00Z
     12Z
 ETA 00Z
     12Z

14TH

FCST TIME__00___06___12___18___24___30___36___42___48__
MODEL/RUN
 RGL 00Z
     12Z
 ETA 00Z
     12Z

15TH

FCST TIME__00___06___12___18___24___30___36___42___48__
MODEL/RUN
 RGL 00Z
     12Z
 ETA 00Z
     12Z

16TH

FCST TIME__00___06___12___18___24___30___36___42___48__
MODEL/RUN
 RGL 00Z
     12Z
 ETA 00Z
     12Z

17TH

FCST TIME__00___06___12___18___24___30___36___42___48__
MODEL/RUN
 RGL 00Z
     12Z
 ETA 00Z
     12Z

18TH

FCST TIME	00	06	12	18	24	30	36	42	48
MODEL/RUN									
RGL 00Z									
12Z	M	M	M	M	M	M	M	M	M
ETA 00Z									
12Z	M	M	M	M	M	M	M	M	M

19TH

FCST TIME	00	06	12	18	24	30	36	42	48
MODEL/RUN									
RGL 00Z	M	M	M	M	M	M	M	M	M
12Z	M	M	M	M	M	M	M	M	M
ETA 00Z	M	M	M	M	M	M	M	M	M
12Z	M	M	M	M	M	M	M	M	M

20TH

FCST TIME	00	06	12	18	24	30	36	42	48
MODEL/RUN									
RGL 00Z	M	M	M	M	M	M	M	M	M
12Z	M	M	M	M	M	M	M	M	M
ETA 00Z	M	M	M	M	M	M	M	M	M
12Z	M	M	M	M	M	M	M	M	M

21ST

FCST TIME	00	06	12	18	24	30	36	42	48
MODEL/RUN									
RGL 00Z	M	M	M	M	M	M	M	M	M
12Z	M	M	M	M	M	M	M	M	M
ETA 00Z	M	M	M	M	M	M	M	M	M
12Z	M	M	M	M	M	M	M	M	M

22ND

FCST TIME	00	06	12	18	24	30	36	42	48
MODEL/RUN									
RGL 00Z									
12Z									
ETA 00Z									
12Z									

23RD

FCST TIME	00	06	12	18	24	30	36	42	48
MODEL/RUN									
RGL 00Z									
12Z									
ETA 00Z									
12Z									

24TH

FCST TIME	00	06	12	18	24	30	36	42	48
MODEL/RUN									
RGL 00Z									
12Z									
ETA 00Z									
12Z									

25TH

FCST TIME	00	06	12	18	24	30	36	42	48
MODEL/RUN									
RGL 00Z									
12Z	M	M	M	M	M	M	M	M	M
ETA 00Z									
12Z	M	M	M	M	M	M	M	M	M

26TH

FCST TIME	00	06	12	18	24	30	36	42	48
MODEL/RUN									
RGL 00Z	M	M	M	M	M	M	M	M	M
12Z	M	M	M	M	M	M	M	M	M
ETA 00Z	M	M	M	M	M	M	M	M	M
12Z	M	M	M	M	M	M	M	M	M

27TH

FCST TIME	00	06	12	18	24	30	36	42	48
MODEL/RUN									
RGL 00Z	M	M	M	M	M	M	M	M	M
12Z	M	M	M	M	M	M	M	M	M
ETA 00Z	M	M	M	M	M	M	M	M	M
12Z	M	M	M	M	M	M	M	M	M

28TH

FCST TIME	00	06	12	18	24	30	36	42	48
MODEL/RUN									
RGL 00Z	M	M	M	M	M	M	M	M	M
12Z									
ETA 00Z	M	M	M	M	M	M	M	M	M
12Z									

29TH

FCST TIME	00	06	12	18	24	30	36	42	48
MODEL/RUN									
RGL 00Z									
12Z									
ETA 00Z									
12Z									

30TH

FCST TIME__00___06___12___18___24___30___36___42___48__
MODEL/RUN
 RGL 00Z
     12Z
 ETA 00Z
     12Z

31ST

FCST TIME__00___06___12___18___24___30___36___42___48__
MODEL/RUN
 RGL 00Z
     12Z
 ETA 00Z
     12Z

APRIL

1ST

FCST TIME__00___06___12___18___24___30___36___42___48__
MODEL/RUN
 RGL 00Z
     12Z
 ETA 00Z
     12Z

2ND

FCST TIME__00___06___12___18___24___30___36___42___48__
MODEL/RUN
 RGL 00Z
     12Z
 ETA 00Z
     12Z

3RD

FCST TIME__00___06___12___18___24___30___36___42___48__
MODEL/RUN
 RGL 00Z
     12Z
 ETA 00Z
     12Z

4TH

FCST TIME	00	06	12	18	24	30	36	42	48
MODEL/RUN									
RGL 00Z									
12Z									
ETA 00Z									
12Z									

5TH

FCST TIME	00	06	12	18	24	30	36	42	48
MODEL/RUN									
RGL 00Z									
12Z									
ETA 00Z									
12Z									

6TH

FCST TIME	00	06	12	18	24	30	36	42	48
MODEL/RUN									
RGL 00Z									
12Z									
ETA 00Z									
12Z									

7TH

FCST TIME	00	06	12	18	24	30	36	42	48
MODEL/RUN									
RGL 00Z									
12Z									
ETA 00Z									
12Z									

8TH

FCST TIME	00	06	12	18	24	30	36	42	48
MODEL/RUN									
RGL 00Z									
12Z	M	M	M	M	M	M	M	M	M
ETA 00Z									
12Z	M	M	M	M	M	M	M	M	M

9TH

FCST TIME	00	06	12	18	24	30	36	42	48
MODEL/RUN									
RGL 00Z									
12Z									
ETA 00Z									
12Z									

10TH

FCST TIME__00___06___12___18___24___30___36___42___48__
MODEL/RUN
 RGL 00Z
     12Z
 ETA 00Z
     12Z

11TH

FCST TIME__00___06___12___18___24___30___36___42___48__
MODEL/RUN
 RGL 00Z
     12Z
 ETA 00Z
     12Z

12TH

FCST TIME__00___06___12___18___24___30___36___42___48__
MODEL/RUN
 RGL 00Z
     12Z
 ETA 00Z
     12Z

13TH

FCST TIME__00___06___12___18___24___30___36___42___48__
MODEL/RUN
 RGL 00Z
     12Z
 ETA 00Z
     12Z

14TH

FCST TIME__00___06___12___18___24___30___36___42___48__
MODEL/RUN
 RGL 00Z
     12Z
 ETA 00Z
     12Z

15TH

FCST TIME__00___06___12___18___24___30___36___42___48__
MODEL/RUN
 RGL 00Z
     12Z
 ETA 00Z
     12Z

16TH

FCST TIME	00	06	12	18	24	30	36	42	48
MODEL/RUN									
RGL 00Z									
12Z									
ETA 00Z									
12Z									

17TH

FCST TIME	00	06	12	18	24	30	36	42	48
MODEL/RUN									
RGL 00Z									
12Z									
ETA 00Z									
12Z									

18TH

FCST TIME	00	06	12	18	24	30	36	42	48
MODEL/RUN									
RGL 00Z									
12Z									
ETA 00Z									
12Z									

19TH

FCST TIME	00	06	12	18	24	30	36	42	48
MODEL/RUN									
RGL 00Z									
12Z									
ETA 00Z									
12Z									

20TH

FCST TIME	00	06	12	18	24	30	36	42	48
MODEL/RUN									
RGL 00Z									
12Z									
ETA 00Z									
12Z									

21ST

FCST TIME	00	06	12	18	24	30	36	42	48
MODEL/RUN									
RGL 00Z									
12Z	M	M	M	M	M	M	M	M	M
ETA 00Z									
12Z	M	M	M	M	M	M	M	M	M

22ND

FCST TIME	00	06	12	18	24	30	36	42	48
MODEL/RUN									
RGL 00Z	M	M	M	M	M	M	M	M	M
12Z									
ETA 00Z	M	M	M	M	M	M	M	M	M
12Z									

23RD

FCST TIME	00	06	12	18	24	30	36	42	48
MODEL/RUN									
RGL 00Z									
12Z									
ETA 00Z									
12Z									

24TH

FCST TIME	00	06	12	18	24	30	36	42	48
MODEL/RUN									
RGL 00Z									
12Z									
ETA 00Z									
12Z									

25TH

FCST TIME	00	06	12	18	24	30	36	42	48
MODEL/RUN									
RGL 00Z									
12Z									
ETA 00Z									
12Z									

26TH

FCST TIME	00	06	12	18	24	30	36	42	48
MODEL/RUN									
RGL 00Z	M	M	M	M	M	M	M	M	M
12Z									
ETA 00Z	M	M	M	M	M	M	M	M	M
12Z			M						

27TH

FCST TIME	00	06	12	18	24	30	36	42	48
MODEL/RUN									
RGL 00Z									
12Z									
ETA 00Z									
12Z									

28TH

FCST TIME	00	06	12	18	24	30	36	42	48
MODEL/RUN									
RGL 00Z	M	M	M	M	M	M	M	M	
12Z									
ETA 00Z	M	M	M	M	M	M	M	M	M
12Z									

29TH

FCST TIME	00	06	12	18	24	30	36	42	48
MODEL/RUN									
RGL 00Z	M	M	M	M	M	M	M	M	M
12Z									
ETA 00Z	M	M	M	M	M	M	M	M	M
12Z									

30TH

FCST TIME	00	06	12	18	24	30	36	42	48
MODEL/RUN									
RGL 00Z									
12Z									
ETA 00Z									
12Z									

MAY

1ST

FCST TIME	00	06	12	18	24	30	36	42	48
MODEL/RUN									
RGL 00Z									
12Z	M	M	M	M	M	M	M	M	M
ETA 00Z									
12Z	M	M	M	M	M	M	M	M	M

2ND

FCST TIME	00	06	12	18	24	30	36	42	48
MODEL/RUN									
RGL 00Z	M	M	M	M	M	M	M	M	M
12Z									
ETA 00Z	M	M	M	M	M	M	M	M	M
12Z									

3RD

FCST TIME	00	06	12	18	24	30	36	42	48
MODEL/RUN									
RGL 00Z									
12Z	M	M	M	M	M	M	M	M	M
ETA 00Z									
12Z	M	M	M	M	M	M	M	M	M

4TH

FCST TIME	00	06	12	18	24	30	36	42	48
MODEL/RUN									
RGL 00Z	M	M	M	M	M	M	M	M	M
12Z	M	M	M	M	M	M	M	M	M
ETA 00Z	M	M	M	M	M	M	M	M	M
12Z	M	M	M	M	M	M	M	M	M

5TH

FCST TIME	00	06	12	18	24	30	36	42	48
MODEL/RUN									
RGL 00Z	M	M	M	M	M	M	M	M	M
12Z	M	M	M	M	M	M	M	M	M
ETA 00Z	M	M	M	M	M	M	M	M	M
12Z	M	M	M	M	M	M	M	M	M

6TH

FCST TIME	00	06	12	18	24	30	36	42	48
MODEL/RUN									
RGL 00Z	M	M	M	M	M	M	M	M	M
12Z									
ETA 00Z	M	M	M	M	M	M	M	M	M
12Z									

7TH

FCST TIME	00	06	12	18	24	30	36	42	48
MODEL/RUN									
RGL 00Z									
12Z									
ETA 00Z									
12Z									

8TH

FCST TIME	00	06	12	18	24	30	36	42	48
MODEL/RUN									
RGL 00Z									
12Z									
ETA 00Z									
12Z									

9TH

FCST TIME__00___06___12___18___24___30___36___42___48__
MODEL/RUN
 RGL 00Z
     12Z
 ETA 00Z
     12Z

10TH

FCST TIME__00___06___12___18___24___30___36___42___48__
MODEL/RUN
 RGL 00Z
     12Z
 ETA 00Z
     12Z

11TH

FCST TIME__00___06___12___18___24___30___36___42___48__
MODEL/RUN
 RGL 00Z
     12Z
 ETA 00Z
     12Z

INITIAL DISTRIBUTION LIST

		No.Copies
1.	Defense Technical Information Center Cameron Station Alexandria, VA 22304-6145	2
2.	Librarian, Code 052 Naval Postgraduate School 411 Dyer Rd Rm 104 Monterey, CA 93943-5101	2
3.	Oceanography Department Code OC/BF Naval Postgraduate School 833 Dyer Rd Rm 331 Monterey, CA 93943-5122	1
4.	Meteorology Department Code MR/HY Naval Postgraduate School 589 Dyer Rd Rm 254 Monterey, CA 93943-5114	1
5.	Dr. Patricia M. Pauley Code MR/PA Department of Meteorology Naval Postgraduate School 589 Dyer Rd RM 254 Monterey, CA 93943-5114	4
6.	Dr. Wendell A. Nuss Code MR/NU Department of Meteorology Naval Postgraduate School 589 Dyer Rd RM 254 Monterey, CA 93943-5114	1
7.	LT Jay W. Colucci, USN 4 Deerfield Lane Monroe, CT 06468	1
8.	Commander Saul A. Beres, USN (Ret) 1106 Monroe Tpke Monroe, CT 06468	1
9.	Commander Naval Meteorology and Oceanography Command 1020 Balch Boulevard Stennis Space Center MS 39529-5005	1

10. Commanding Officer — 1
Naval Oceanographic Office
Stennis Space Center
MS 39529-5001

11. Commanding Officer — 1
FLENUMMETOCCEN
7 Grace Hopper Ave Stop 4
Monterey, CA 93943-5501

12. Commanding Officer — 1
Naval Oceanographic and Atmospheric
Research Laboratory
Stennis Space Center
MS 39529-5004

13. Superintendent — 1
Naval Research Laboratory
7 Grace Hopper Ave. Stop 2
Monterey, CA 93943-5502

14. Chairman — 1
Oceanography Department
U.S. Naval Academy
Annapolis, MD 21402

15. Chief of Naval Research — 1
800 N. Quincy Street
Arlington, VA 22217

16. Office of Naval Research (Code 420) — 1
Naval Ocean Research and Development
Activity
800 N. Quincy Street
Arlington, VA 22217

17. Library — 1
Scripps Institution of Oceanography
P.O. Box 2367
La Jolla, CA 92037

18. Library — 1
Department of Atmospheric Science
University of Washington
Seattle, WA 98105

19. Library — 1
Cicese
P.O. Box 4803
San Ysidro, CA 92072

20.	Library College of Oceanography Oregon State University Corvallis, OR 97331	1
21.	Director, Pacific Marine Center (N/MOP) National Ocean Service, NOAA 1801 Fairview Avenue East Seattle, WS 98102	1
22.	Director, Atlantic Marine Center (N/MOA) National Ocean Service, NOAA 439 W. York Street Norfolk, VA 23510	1
23.	Commander (Air-370) Naval Air Systems Command Washington, DC 20360	1
24.	Commander, International Ice Patrol Avery Point Groton, CT 06340-6096	1
25.	Commanding Officer U.S. Coast Guard Research and Development Center Avery Point Groton, CT 06340-6096	1
26.	NOAA Library 7600 Sand Point Way NE Building 3 Seattle, WA 98115	1